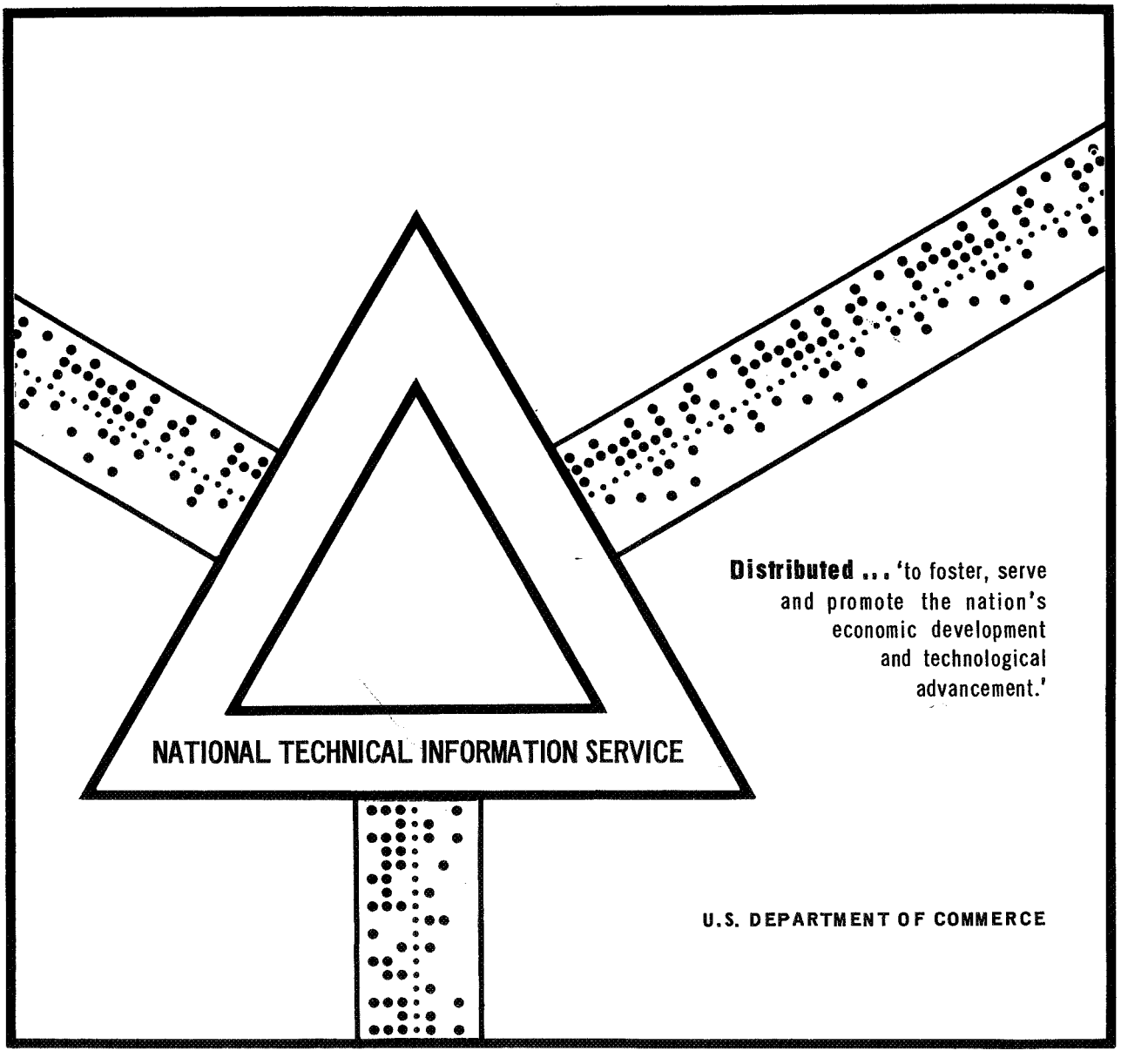

Differential Scattering with Charge Transfer to the 2s State of Hydrogen from $H^+ \rightarrow He$ and $H^+ \rightarrow Ar$ Collisions

D. H. CRANDALL

D. H. JAECKS

AUGUST, 1970

UNIVERSITY OF NEBRASKA
LINCOLN, NEBRASKA

DIFFERENTIAL SCATTERING WITH CHARGE TRANSFER TO THE 2s STATE OF HYDROGEN FROM H^+-He AND H^+-Ar COLLISIONS

by

David H. Crandall

A THESIS

Presented to the Faculty of

The Graduate College in the University of Nebraska

In Partial Fulfillment of Requirements

For the Degree of Doctor of Philosophy

Department of Physics

Under the Supervision of Professor Duane H. Jaecks

Lincoln, Nebraska

August , 1970

DIFFERENTIAL SCATTERING WITH CHARGE TRANSFER TO THE 2s STATE OF HYDROGEN FROM H^+ - He AND H^+ - Ar COLLISIONS

David H. Crandall, Ph.D.

University of Nebraska, 1970

Adviser: Duane H. Jaecks

For collisions of protons with helium and argon target gases; the differential cross sections for total scattering, the probabilities of charge transfer forming a hydrogen atom, and the probabilities of charge transfer forming a hydrogen atom in the 2s states were measured. The measurements were differential in the angle to which the incident particle was scattered. Scattering angles between 1^0 and 7^0 were used. The measurements were made for the range of incident proton energies between 3 and 20 keV.

A beam of protons, magnetically selected from the output of a duoplasmatron type ion source, was brought into a scattering chamber. The pressure of the gas in the chamber was held sufficiently low that collisions of incident protons with more than one target gas atom were negligible. The fast, scattered particles (either protons or hydrogen atoms) were detected by a bare electron multiplier set at an angle to the original proton direction. With knowledge of the target gas density, the total number

of incident protons, the efficiency of the particle detector, and the scattered particle acceptance geometry; the differential cross section for total scattering was obtained from the number of scattered particles for each angle and incident proton energy used. These measurements of differential scattering cross sections are compared to the predictions of classical scattering theory.

By deflecting the positively charged protons and detecting only the fast hydrogen atoms, the probability of charge transfer forming a hydrogen atom was obtained for each angle, energy, and target species. The probability is the ratio of hydrogen atoms detected to the number of total particles (hydrogen atoms and protons) detected for the same experimental conditions. These measurements are compared to the previous measurements of Everhart, et al and the available coupled state calculations for charge transfer.

If the hydrogen atom formed by charge transfer is formed in the 2s state, it will remain in that state until after detection unless the atom is in an electric field. In a strong electric field the 2s state is coupled to the 2p state and the atom will then decay to the ground state emitting a characteristic photon. A portion of the photons induced by establishing an electric field in the path of the scattered particles were counted using a photodetector. With knowledge of what fraction of the total number of

induced photons were counted; the probability, defined as the ratio of hydrogen atoms in the 2s state to total scattered particles at a particular angle and energy, was obtained. These probability measurements are compared to the coupled state impact parameter calculations of Sin Fai Lam and the previous probability measurements at one fixed angle by Dose.

TABLE OF CONTENTS

LIST OF FIGURES

I. INTRODUCTION

The process of exchange of electrons, or charge exchange, during collisions of atoms and ions has been widely studied. Processes of the type $A^+ + B \rightarrow A + B^+$ where A and B may or may not be the same atomic species, have received considerable attention, experimentally and theoretically. This process has been investigated with interest in the total charge transfer, in transfer during close collisions with scattering to particular angles, and in collisions where one of the colliding partners is left in an excited state.

Several quantum mechanical techniques for calculating and understanding the physical properties of charge transfer processes have been advanced. These techniques will be discussed briefly in section II, but no attempt will be made to undertake a complete discussion of these theories or to catalogue all of the calculations which have been done.

Recent experimental work on charge transfer has been directed beyond measurement of quantities for direct practical applications, toward testing the range of validity of the various theoretical calculations. For this reason much of the recent work has been with the simplest atoms and ions available. There has been recent experimental interest in charge transfer with scattering to particular angles (differential charge transfer) and on transfer to

excited states, as these provide the most critical tests of the theoretical thechniques.

In this spirit, an experiment to measure cross sections and probabilities for charge transfer to the n=2 state of hydrogen from collisions of protons with various rare gases as a function of impact energy and scattering angle has been undertaken in this laboratory. It will be the function of this thesis to present results for transfer to the 2s state of hydrogen from collisions of protons with helium and argon over the range of impact energies from 3 to 20 keV and scattering angles from 1^{o} to 7^{o}. These results will be compared with the available theoretical calculations and similar experimental results (section V).

In order to make these measurements it was necessary to measure related quantities, some of which have received previous attention. The total transfer cross sections (all angles) to the 2s state of hydrogen for collision of protons with helium and argon were measured in order to obtain a calibration of the efficiency of a photodetector used. These results are presented and compared to previous work in section IV. As a part of the experiment the total differential scattering cross sections, including elastic and inelastic and charge changing processes, in collisions of protons with helium and argon were measured. Some appropriate classical theory related to total differential

scattering is presented in section II and compared to the present experimental results in section V. Finally, the differential charge transfer probabilities for forming hydrogen in any state were measured. Comparisons with earlier results are found in section V.

II. THEORIES

A. Classical Theory of Differential Scattering.

The interaction energy, V, of two charge particles with charges Q_1 and Q_2 is well understood classically and is represented by $V = \frac{Q_1 Q_2}{r}$ where r is the separation of the charges. Bohr[1] has discussed the potential

$$V = \frac{Z_1 Z_2 e^2}{r} \exp(-r/a)$$

for representing the interaction between two colliding atoms of nuclear charge Z_1 and Z_2 times the electronic charge "e". The exponential factor expresses the effect of the electrons in shielding or screening the nuclear charge. Bohr[1] proposed a screening length, a, of the form $a = a_o / (Z_1^{2/3} + Z_2^{2/3})^{1/2}$ where a_o is the radius of the first Bohr orbit. Bohr arrived at this form by considering the screening of a single atom, given by the Thomas-Fermi statistical model[2] to be $a = 0.885\, a_o (\frac{1}{Z^{1/3}})$. Bohr ignored the 0.885 factor and took the reciprocal square of the total screening length for two atoms to be the sum of the reciprocal squares of the screening lengths of the individual atoms. Lindhard, et al[3] found that this estimate agreed well with more exact numberical estimates. Firsov[4] has also considered this potential in developing more detailed Thomas-Fermi screening parameters.

Several authors have considered the range of validity

of calculations using such a classical potential[1,3,5]. For classical approximations to hold two conditions must be satisfied: (a) the orbit must be well defined, and (b) the uncertainty principle must not be violated. The first condition requires that any dimension of the scattering field be large compared to the deBroglie wavelength of the incident particle, that is $a \gg \lambda$. This first requirement also leads to an upper limit on the relative velocity of $v \ll Z_1 Z_2 e^2/h$. A requirement on the deflection angle, θ, produced by the collision can be obtained from the second condition, namely that $\theta \gg \frac{\lambda}{2\pi a}$. Dimensions of the scatterer other than "a" are often used in discussion of classical collisions, such as the minimum or "head-on" collision diameter $b = \frac{Z_1 Z_2 e^2}{1/2mv^2}$ (where m is the reduced mass and v is the relative velocity) and the impact parameter, ρ (see Fig. 1). All of the experimental situations in this thesis fall within these classical limitations so that classical approximations may be applied for the total scattering.

For a known central potential, V(r), the deflection of an incident charged particle in the center of mass coordinates is calculated classically from

$$\theta = \pi - 2 \int_{r_o}^{\infty} \frac{(\rho/r^2)\, dr}{\left[1 - \frac{\rho 2}{r^2} - \frac{v(r)}{1/2mv^2} \right]^{1/2}}$$

(derived in many standard textbooks, e.g. reference 9),

Fig. 1

SCHEMATIC OF A COLLISION

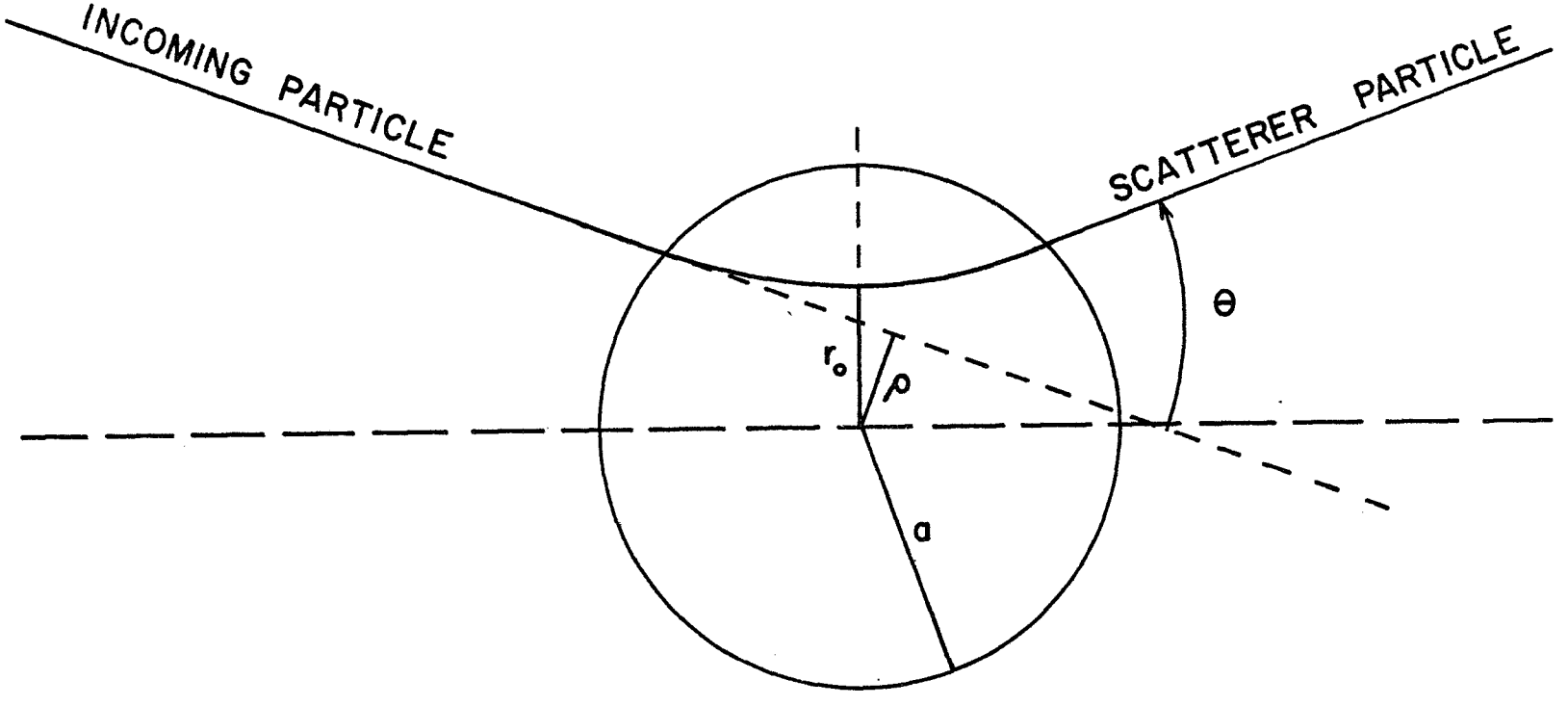

where Θ is the deflection angle, r_o is the distance of closest approach, and ρ is the impact parameter.

For scattering of a beam of particles it is customary to define the effective scattering cross section, $\frac{d\sigma}{d\Omega}(\Theta)$, as the ratio of the number of particles scattered per unit time into solid angle $d\Omega$ (between Θ and $\Theta + d\Theta$) to the number of incident particles per unit time. The relation between the cross section and the scattering angle is

$$\frac{d\sigma}{d\Omega}(\Theta) = \frac{\rho}{\sin\Theta} \left| \frac{d\rho}{d\theta} \right| .$$

Tables giving the differential cross section and distance of closest approach for various values of b/a for scattering described classically by the above expressions and the Bohr potential have been calculated by Everhart, et al[6] and by Bingham[7]. Bingham's tables are more detailed and have been used to obtain calculated cross sections for comparison to experimental results in section IV. A.

More recently, other forms of screening have been employed which more accurately describe the distribution of electronic charge in atoms. F. T. Smith[8] has suggested a potential of the form $V(r) = (\frac{e}{r}) \sum_\nu \alpha_\nu \exp(-r/a_\nu)$ where $\alpha_\nu = 2,8,8...$ for K, L, M shells respectively and $a_\nu = a_o (I_H/I_\nu)^{1/2}$, I_H being the ionization potential of

hydrogen and I_ν being the closed shell ionization potential for the respective shells of the particular atom considered. The form indicated for the screening lengths, a_ν, is obtained from a simple hydrogenic model of the charge distribution.

The classical expression for the deflection angle can be put into the form $$\Theta = \frac{\rho}{1/2mv^2} \int_\rho^\infty \frac{dV(r)}{dr} \frac{dr}{(r^2-\rho^2)1/2}$$ if the assumption $r_o = \rho$ is used for the lower limit of the integral. If a potential of the form $V(r) = Z_{eff}/r$ is used the integral reduces to $\Theta T = Z_{eff}/\rho$[9], where $T = 1/2mv^2$. Dose[10] has taken the potential suggested by Smith and used it with the expressions given above. By equating $$\Theta T = \rho \int_\rho^\infty \frac{dV(r)}{dr} \frac{dr}{(r^2-\rho^2)1/2} = Z_{eff}/\rho$$ and evaluating the integral with the potential suggested by Smith, he obtains values of Z_{eff} as a function of impact parameter, ρ, for protons and hydrogen atoms incident on helium, neon, and argon. Using his values of Z_{eff}, the cross section can be determined directly from the familiar Rutherford formula $$\frac{d\sigma}{d\Omega}(\Theta) = 1/4 \left(\frac{Z\ Z_{eff}\ e^2}{2T}\right)^2 \frac{1}{\sin^4\ \Theta/2}$$ where Z is the charge of the incident particle (for protons Z = 1) and T is the energy as before. At least for helium, the values of Z_{eff} obtained by Dose are in good agreement with values of Z_{eff} obtained from a Hartree-Fock calculation[11].

Comparisons of cross sections from Bingham's tables and those obtained from Dose's values of Z_{eff} and the present experimental results are found in section V.

B. Charge Transfer Theories.

1. Born Approximation.

First consider charge transfer between one initial state of atom A and one final state of atom B, i.e. $A^+ + B_i \rightarrow A_j + B^+$. The most easily applied approximation is the two state Born approximation, in which the charge transfer amplitude is given by[12]

$$g_{ij}(\theta,\phi) = -\frac{M}{2\pi}\iint \phi_i^B(r_B)\phi_j^{A*}(r_A)\exp\left\{i(k_i\hat{n}_i - k_j\hat{n}_j)\cdot\vec{R} - i\vec{v}\cdot\vec{r}\right\}\cdot[V^B(r_B) + W(R)]\, d^3r_A d^3R$$

where:

(1) $\phi_i^B(r_B)$ and $\phi_j^A(r_A)$ are the electronic eigenfunctions describing the initial state, i, of atom B and the final state, j, of atom A respectively. (2) The exponential expression describes incoming and outgoing plane waves, $\hat{n}_j$ is a unit vector in the direction of scattering (θ,ϕ). (3) $V^B(r_B)$ is the potential for the electron with atom B. (4) W(R) describes the interaction of nuclei A and B. (5) r_A, r_B are the position vectors of the electron to atom A and B respectively and r is the electron vector to the center of mass of A and B. (6) R is the inter-

nuclear separation. (Examples of useful discussions of this and other approximations are Bates and McCarrol, reference 12, and reference 13, 14, 15, and 16.)

The total charge transfer cross section, σ_{ij}, between any two states can be obtained from the above expression by integrating the square of the absolute value of the amplitude over scattering angles θ,ϕ.

There are several limitations on the range of validity of this result. A weak interaction, W(R), is assumed. Many cases of charge transfer are not weak interactions so that this approximation is always suspect. Beyond this, the weak interaction criterion is violated in close collisions resulting in scattering to large angles. Also, the relative velocity of the colliding atoms must be sufficiently fast that the description of the target by undistorted atomic wave functions remains valid and that the velocity is constant during the collision. In general, the perturbation of the interaction potential, W(R), on the wave description of the atomic states must be much greater than the perturbation on these states due to the relative motion. This condition is best satisfied at high velocities. The limits of validity are made clear only by comparison to experiment.

Total charge transfer cross sections for $H^+ + He \rightarrow H + He^+$

have been calculated in this approximation, by Mapleton[17]. The results are in fair agreement with experiment[28] for energies above 50 keV. This agreement may be partly due to the large contribution of distant collisions (weak interaction) to the total charge transfer. (Fig. 4 shows the results of Mapleton's calculation for the total cross section for transfer to the 2s state in H^+ + He collisions.)

If it is desired to calculate charge transfer probabilities to a final state which may be influenced by other nearby states or some intermediate state, for example in an exchange such as, $H^+ + He \rightarrow H(n=2 \text{ states}) + He^+$; then direct application of the above two state approximation should not be expected to give accurate results. It is appropriate, in this case, to use an approximation where the effects of these other states can be included more directly.

The comparison of this theory with experiment clearly shows that transfer to the 2s state of hydrogen in the energy range 3 - 20 keV will not be accurately described by the two-state Born approximation.

2. Impact Parameter Method.

An alternative formulation which also relies on the validity of classical trajectories, but which can be

constructed to allow for some distortion (change of energy levels) during collision, and to allow for the influence of intermediate states, is the coupled state impact parameter formulation.

In the impact parameter formulation the wave function for the system $A^+ + B \rightarrow A + B^+$ is expanded in terms of a finite number of the atomic eigenfunctions of the separated atoms. Generally, the eigenfunctions used include the ground state, $\chi_p(r_B)$, of the target atom, B, and a few of the eigenfunctions, $\phi_m(r_A)$, of the atom formed from projectile, A^+, when it receives an electron. That is,

$$\Psi(r_B,t) = a_p(t)\ \chi_p(r_B)\ \exp\left[\frac{imvZ_B}{\hbar} - \frac{i}{\hbar}\ (E_p + 1/2mv^2)t\right]$$

$$+\sum_m b_{pm}(t)\phi_m(r_A)\ \exp\left[\frac{imvZ_B}{\hbar} - \frac{i}{\hbar}\ (E_m + 1/smv^2)t\right]$$

where $Z_B = \vec{r}_B \cdot \vec{V}$, Ep and Em are the eigenenergies of the respective eigenfunctions, (see references 14 and 33).

The expansion coefficients, $b_{pm}(t)$, for a given v, depend on ρ and ϕ as well as t. If the charge transfer from state p of atom B to state j of atom A is required, then it is necessary to solve for $b_{pj}(\infty)$. The probability of transfer to the state j is then $P_{pj}(\rho,\phi) = |b_{pj}(\infty)|^2$ at a particular impact parameter. (For classical

trajectories there is a one-to-one correspondence between ρ and θ.) The coupled equations for these coefficients are obtained from substitution of the constructed wave function, $\Psi_p(r_B,t)$, into the electronic wave equation $H_e \Psi (r_B,t) = i \frac{\partial}{\partial t} \Psi_p(r_B,t)$ where $H_e = - \frac{\hbar^2}{2m} \nabla^2 + V^A + V^B +$ electron-electron interactions, and V^A and V^B are the potentials between the electron and A and B respectively.

The probability, P_{pj}, is the most direct quantity predicted by this theory. The most critical comparisons between experiment and theory thus are obtained from measured values of $P_{pj}(\rho)$. However, the quantity desired for most applications, and which is frequently measured, is the total cross section. This cross section can be obtained from the theory by

$$\sigma_{pj} = \int_0^{\infty}\int_0^{2\pi} P_{pj}(\rho,\phi)\rho d\rho d\phi$$

which usually can be simplified to

$$\sigma_{pj} = 2\pi \int_0^{\infty} P_{pj}(\rho)\rho d\rho.$$

The comparison of experimental total cross sections to those predicted by theory is not as critical as comparisons of probabilities because of the averaging effects of the integration and the large contribution for

large values of ρ.

A two-state impact parameter solution of this type is known to be equivalent to the Born formulation[14], so that additional states must be included in the expansion and effects such as distortion included before the impact parameter technique can be expected to improve on Born results.

In practice the calculations may be tedious and the accuracy will depend on how well the system is described by the wave function chosen and how accurate the potential terms in the Hamiltonian are.

Distortion is quite important at lower velocities. To first order, distortion is included by generalizing the expansion coefficients in such a way that the unperturbed eigenenergies, E_m, are replaced by $N_m=E_m+V_{mm}$ where

$$V_{mm} = \int \phi_m^*(r_B)\ V^A\ \phi_m(r_B) d^3 r_B$$

(for details see reference 14). Here, as in the original impact parameter formulation, well defined stationary states are assumed to exsist. For small impact parameter, violent collisions, the transitions within the quasi-molecule formed during the collision may not be adiabatic and well defined states may not exsist even in reasonably slow collisions.

For sufficiently low velocities the impact parameter method may fail even with many eigenfunctions included in the wave function expansion and distortion accounted for. Then it is necessary to find new wave function expansions which more adequately represent the system, such as the eigenfunctions of the quasi-molecule formed by the colliding partners.

Again, the range of validity of these impact parameter calculations is best established by comparison of theory and experiment.

The impact parameter method has been applied successfully to several charge transfer problems. The simplest system for charge exchange is $H^+ + H \rightarrow H + H^+$. This exchange has been treated by several authors in the impact parameter formalism. Among the more successful calculations, Wilets and Gallaher[18] and Lovell and McElroy[19], have calculated the total (all angles) transfer to the 1s state and 2s and 2p states of hydrogen and have shown results for the probability P_{pj} for ground state transfer at a particular scattering angle (Fig. 2). Wilets and Gallaher expand the wave function in terms of the eigenfunctions of 1s, 2s, $2p_o$, $2p_{\pm 1}$, centered about both nuclei. For the total cross section for transfer to H(1s) their results are in reasonable agreement with the measurements of McClure[20] (all above 2 keV). For cross

sections of transfer to the n=2 states they are in good agreement with the 2s measurements by Bayfield[21] and in fair agreement with the 2s measurements of Colli, et al[22], and in fair agreement with measurements for the 2p state by Stebbings, et al[23].

The measurements of the probability of transfer to any state by Everhart, et al[24], at a constant scattering angle for $H^+ + H$ collisions, show an interesting oscillating structure as a function of collision time, sometimes referred to as resonance (to be discussed in the next section). This oscillation is due to interference between transfer amplitudes of the lowest symmetric and antisymmetric states of the H_2^+ system. The Wilets and Gallaher calculation reproduces the measured oscillations of Everhart, et al except that the calculated oscillations are out of phase by about one fourth cycle (Fig. 2).

An impact parameter calculation by Cheshire[25] for $H^+ + H$ collisions has included the effect of screening of the nuclear charge of the target hydrogen atom by the electron. Only slight improvement in the agreement with experiment by Everhart, et al is obtained, but the technique may be important to other systems where screening is more important.

Of more direct interest to this report are the

Fig. 2

CHARGE TRANSFER PROBABILITY FROM PROTONS ON HYDROGEN
(at 3° laboratory)

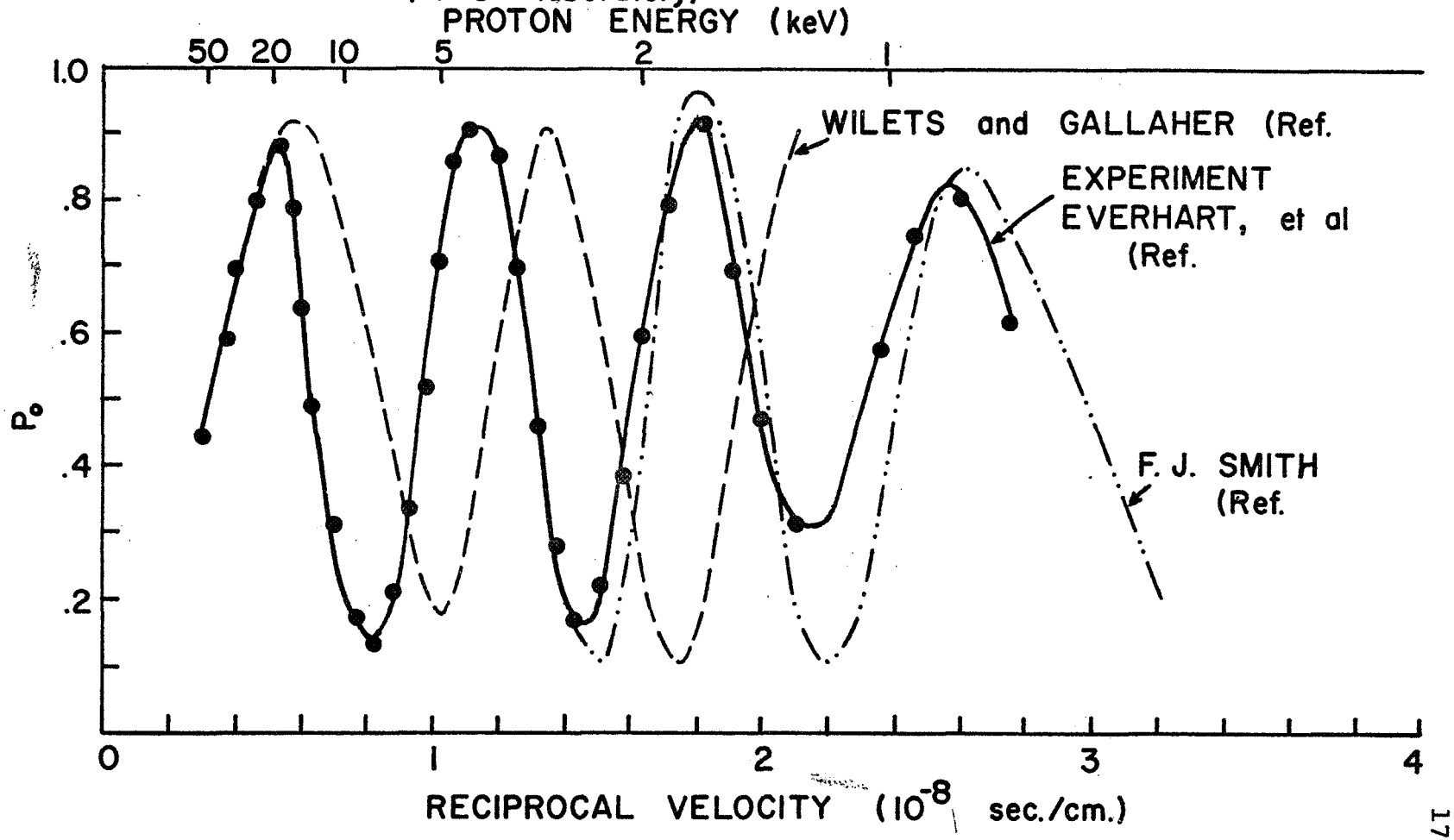

calculations of charge transfer for the system $H^+ + He \rightarrow He^+ + H$. Several impact parameter calculations of total transfer cross sections to the ground state of hydrogen have been done in a two state approximation, for example by Green, et al[26,27]. In the range 6 to 100 keV the calculations of the total cross section for transfer to H(1s) by Green, et al are in good agreement with experiment[28], which includes capture to higher states of hydrogen. In the range, 6 - 40 keV, the calculations by Green, et al, agree better with experiment than similar previous calculations. This may be because of inclusion of distortion affects in the collision.

Green[27] also published calculation of the transfer probability for capture into H(1s) at particular impact parameters for comparison to the experiment of Helbig and Everhart[29] who measured probability for capture into all states of hydrogen at small impact parameters in the collision $H^+ + He \rightarrow He^+ + H$ at energies between 1 and 100 keV (see Fig. 3). In this application the theory correctly predicted the positions of the observed oscillation peaks, but failed to obtain satisfactory agreement with the observed magnitudes of the peaks. (In Fig. 3 the distance of closest approach, R_o, has been related to the product of scattering angle and incident energy, θT. This relationship, using the impact parameter, ρ, rather than R_o, has been discussed in section II.)

Fig. 3

CHARGE TRANSFER PROBABILITY
AT FIXED IMPACT PARAMETER

$H^+ + He(1s^2) \rightarrow H + He^+(1s)$

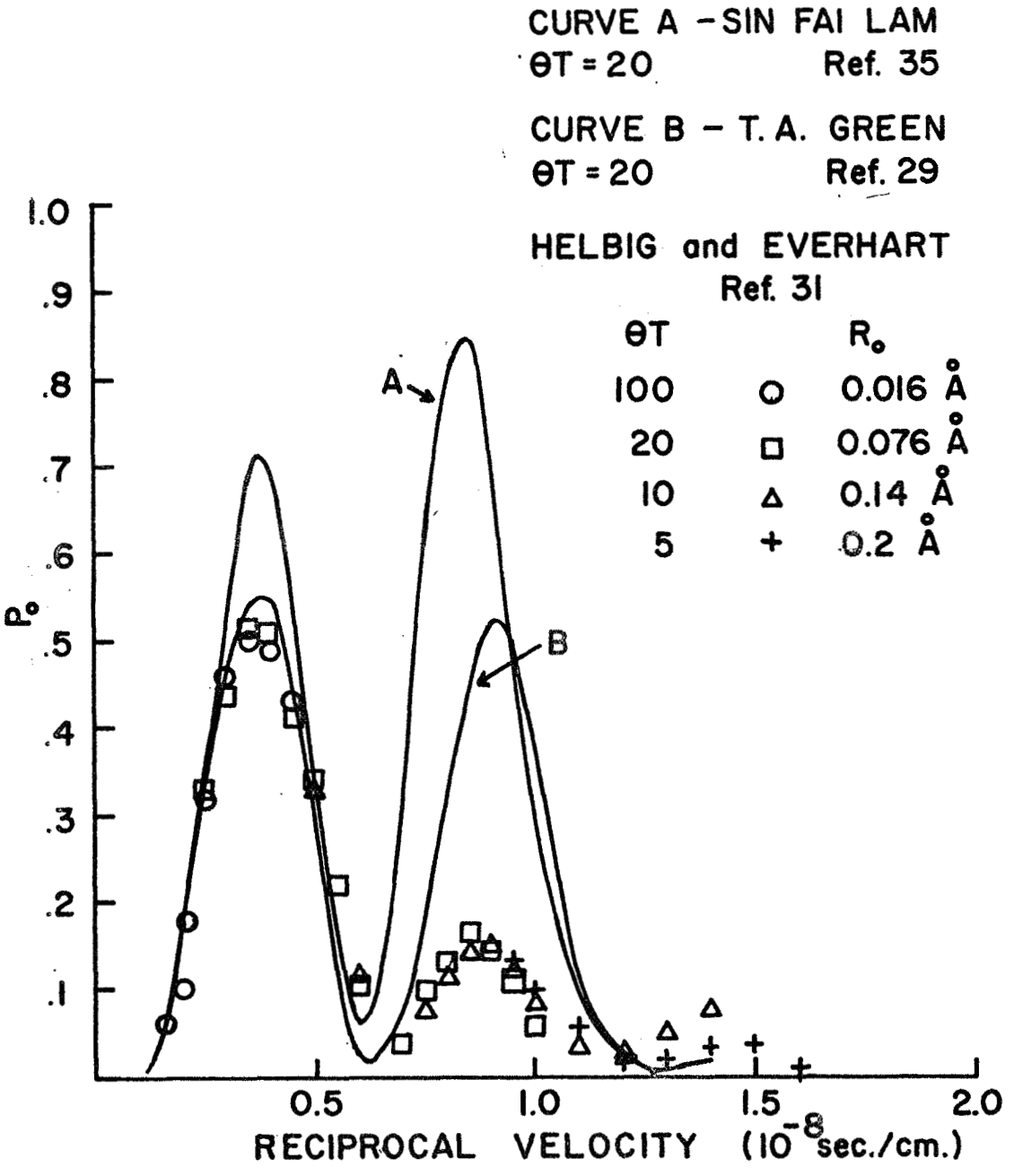

Two-state impact parameter calculations have been used by Polvetkov and Presnyakov[30] to obtain some understanding of observed total (all angles) charge transfer to the 2p state of hydrogen in $H^+ + He \rightarrow H(2p) + He^+$ and $H^+ + Ne \rightarrow H(2p) + He^+$. This investigation (6-40 keV) added the direct transfer to H(2p) and transfer through the rival ground state to the 2p state. Jaecks, et al[31] had suggested that the observed double maxima in these cross sections could be interpreted as arising separately from the direct transfer and transfer through the ground state. The qualitative agreement between the two state calculations and the experiments of Pretzer, et al[31, 32] and Andreev, et al[33] supports the suggestion of coupling through the ground state.

More recently L. T. Sin Fai Lam[34] has published impact parameter calculations for the $H^+ + He$ system with a direct bearing on this report. This calculation employs expansion of the wave function in terms of the four atomic eigenfunctions of 1s, 2s, $2p_o$, $2p_{\pm 1}$ states of hydrogen (with ground state of He^+), and the initial ground state of helium. Calculation of the total charge transfer cross sections (including transfer to all 4 hydrogen states) yielded nearly the same results as obtained by Green for transfer to the 1s state. The calculation of the total transfer cross section to the 2s state of hydrogen gave quantitative agreement with experiment from

3 to 100 keV (where data is available) except for a shoulder seen by all observers around 12 keV. The comparison is illustrated by Fig. 4, reproduced from ref. 35, where some of the data has been renormalized.

Of greatest importance to this report, Sin Fai Lam calculated the charge transfer probabilities to the 2s and 2p states as a function of impact parameter for a few energies and as a function of energy at a fixed small impact parameter. These results will be compared to present experimental measurements for the 2s state in section V.

Sin Fai Lam's prediction of the total charge transfer fraction at a fixed impact parameter was similar to that of Green, showing the same relationship to the measurements of Everhart, et al (Fig. 3).

C. The Quasi-Molecule Approach

1. Resonance

The application of quantum mechanics to the H_2^+ molecule led to development of the concept of the electron oscillating between the two nuclei. Heisenberg[36] introduced the term resonance in the quantum description of excited states of helium because the behavior of two degenerate states was analogous to the classical system of two coupled oscillators customarily described as exchanging energy by resonance. The concept was applied to the

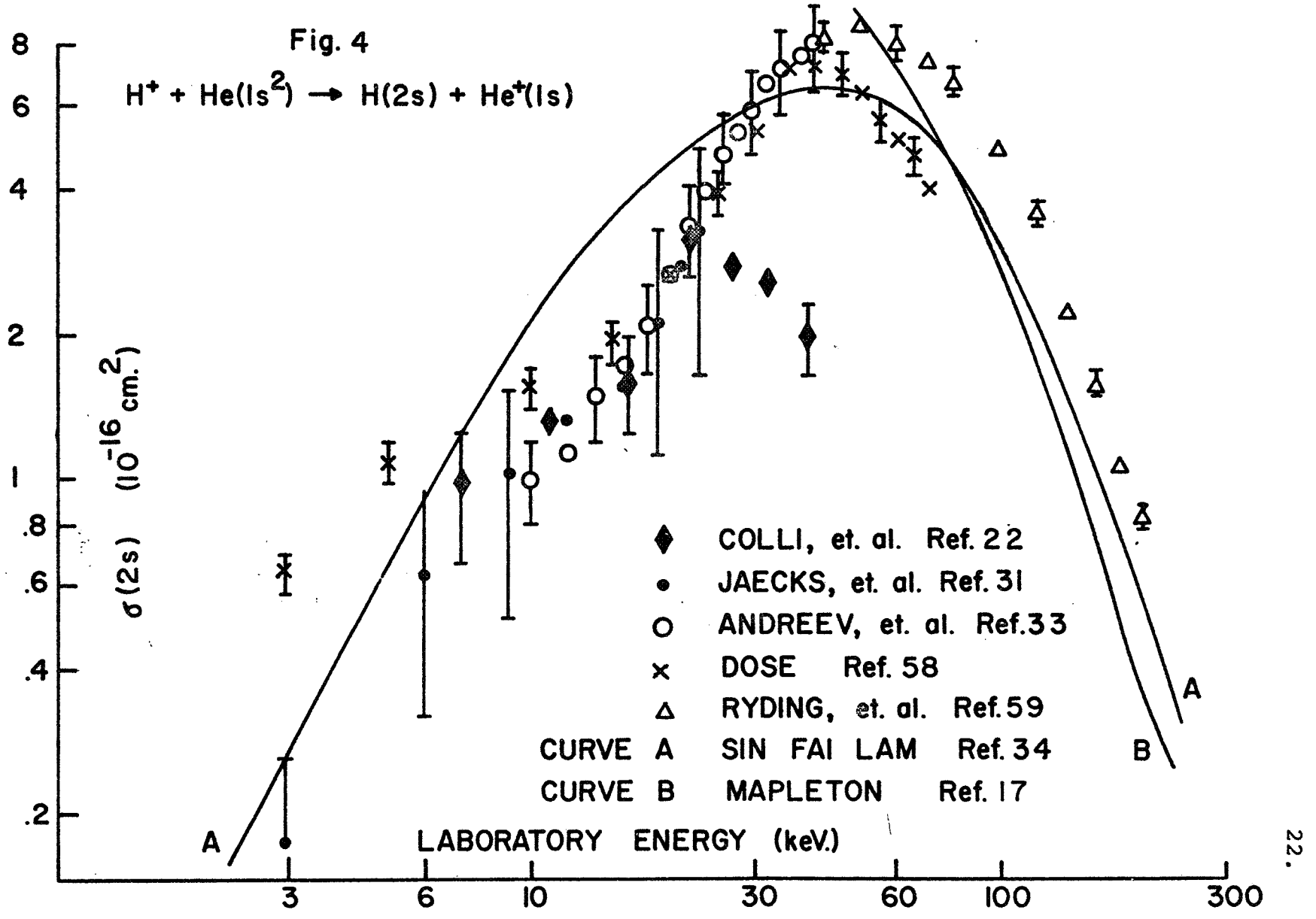
Fig. 4
$H^+ + He(1s^2) \rightarrow H(2s) + He^+(1s)$
$\sigma(2s)$ $(10^{-16}\ cm.^2)$
8
6
4
2
1
.8
.6
.4
.2
3
6
10
30
60
100
300
LABORATORY ENERGY (keV.)
COLLI, et. al. Ref. 22
JAECKS, et. al. Ref. 31
ANDREEV, et. al. Ref. 33
DOSE Ref. 58
RYDING, et. al. Ref. 59
CURVE A SIN FAI LAM Ref. 34
CURVE B MAPLETON Ref. 17
A
B

H_2^+ molecule by Pauling[37] and others[38]. At finite nuclear separation, the two lowest stationary states of this molecule are symmetric and antisymmetric states constructed from the sum of states of $H_A(1s)\ H_B^+$ and $H_A^+\ H_B(1s)$. In the construction of the symmetric and antisymmetric states, a resonance exchange of the electron between $H_A(1s)\ H_B^+$ and $H_A^+ H_B(1s)$ arises, with the charge exchange frequency E/h where E is the energy separation between the symmetric and antisymmetric states.

It is this resonance in the quasi-molecule of H_2^+ formed during the $H^+ + H$ collision which causes the oscillation in charge transfer probability observed by Everhart, et al[24] (Fig. 2). During the collision the electron is oscillating between the target and the projectile as described for the H_2^+ molecule. As the relative velocity of the collision is increased the electron is left alternately on the target and the projectile, resulting in regular oscillation of the charge transfer probability with collision time.

2. Perturbed Stationary States.

The resonance concept, arising in the description of the H_2^+ molecule, relates most directly to the charge exchange during collisions when the velocity of the colliding atoms is sufficiently slow that the system is most accurately described by molecular eigenstates. In

this case, the system wave function is expanded in two-center, bound state eigenfunctions rather than in terms of single-center eigenfunctions of the individual atoms.

The original procedure for such a perturbed stationary state expansion was given by Mott[39]. Again, for the system $A^+ + B \rightarrow A + B^+$, require that the system wave function, $\Psi(r,R)$, satisfy the wave equation

$$[-\frac{\hbar^2}{2M} \nabla_R^2 - \frac{\hbar^2}{2m} \nabla_r^2 + V^B(r_B) + V^A(r_A) + W(R)]\Psi = E\Psi$$

where M is the reduced nuclear mass, m is the electron mass, r is the electron coordinate relative to the center of mass of A and B, and R is the separation of nuclei A and B.

It is assumed that there exist molecular electronic eigenstates, $\chi(r,R)$, for which

$$[\frac{\hbar^2}{2m} \nabla_r^2 + E_B(R) - V^B(r_B) - V^A(r_A)] \chi(r,R) = 0$$

is satisfied. It is necessary to distinguish two forms of electronic eigenfunctions, $\chi(r,R)$; those which tend to atom A as $R \rightarrow \infty$ and those which tend to atom B. That is,

$$\chi_p^B (r,R) \xrightarrow[R\rightarrow\infty]{} \phi_p^B(r_B) \quad \text{and} \quad \chi_q^A(r,R) \xrightarrow[R\rightarrow\infty]{} \phi_q^A(r_A)$$

where the ϕ_p^B and ϕ_q^A are atomic eigenfunctions of atoms B and A respectively.

The system wave function $\Psi(r,R)$ is now expanded as a linear combination of the molecular eigenfunctions

$$\Psi = \sum_p a_p(R)\ \chi_p{}^B(r,R) + \sum_q b_q(R)\ \chi_q{}^A(r,R).$$

When this wave function is substituted into the first wave equation, which it must satisfy, coupled equations for $b_q{}^{(\infty)}$ can be obtained and the probability of the electron ending in state $\phi_q{}^A$ of atom A is thus obtained in a manner similar to the impact parameter treatment. The cross sections are then obtained as in the impact parameter method.

Unfortunately, several difficulties arise with this approach. This original formulation has not included any effects of the translation motion. Bates (see reference 14) has shown that this omission leads to serious error because the rotation of the internuclear line gives rise to coupling terms for any states which are not spherically symmetric. In fact the original formulated theory had taken into account only matrix elements joining the states of the quasi-molecule which tend to the initial and final states of interest, i.e. coupling between various states of the quasi-molecule had not been included. In addition to the coupling introduced by the rotation, it is necessary to include coupling between any molecular states which have potential energy curves which lie close to the state of interest, especially for small impact parameter collisions where electronic energies are not precisely defined. The equations resulting from inclusion of such

coupling are complicated, thus calculations have been successfully performed only for cases where such coupling can be ignored.

Coupling terms can be ignored in cases where only spherically symmetric initial and final states enter and for which no other molecular eigenstates lie close to the eigenstate connecting the initial and final states of interest. The only cases where these criteria are found to be well obeyed are resonance transfer (when final electronic energy is unchanged by transfer) between spherically symmetric states, such as $H^+ + H(1s) \rightarrow H(1s)+H^+$ or $He^+(1s) + He(1s)^2 \rightarrow He(1s)^2 + He^+(1s)$.

An application of the resonance concept through perturbed stationary state calculation of collisions of $H^+ + H$ was made by Bates, et al[40] in 1953. For close collisions, the charge transfer probability was predicted to oscillate between 0 and 1. The experimental work of Everhart, et al showed such oscillations, but the amplitude was damped (not reaching 0 or 1). The observed oscillations, as a function of inverse velocity (collision time), were out of phase with the calculated oscillations by about $\pi/4$ (as was the case for the similar impact parameter calculation[18]). A p.s.s. calculation by F. J. Smith[41] showed that even for the simple $H^+ + H$ case, coupling between 2p σ_u and 2p π_u states of the quasi-

molecule had to be included before quantitative agreement between theory and experiment could be obtained (see Fig.2).

The prospect of carrying out adequate perturbed state calculations for systems such as $H^+ + He$ is apparently poor. In the situation of interest in this thesis, where the hydrogen atom is formed in the 2s state from collision of $H^+ + He$, there are several nearby molecular states tending to different atomic configurations in separated atom limit (see Fig. 5).

3. Semi Empirical Approach.

Lockwood and Everhart[42] observed that their results for resonant capture, $H^+ + H \rightarrow H + H^+$, could be represented empirically by the equation

$$P_o = K_1(1/v) + K_2(1/v) \sin^2 \left[\frac{\pi \langle Ea \rangle}{vh} - B \right]$$

where "a" is the distance over which the collision takes place, E is the energy, and K_1 and K_2 are slowly varying functions of 1/v. With $K_1 = 0$, $B = 0$ and $K_2 = 1$, this result is equivalent to perturbed stationary state results of Bates, et al[40]. The quantity $\langle Ea \rangle$ is determined from the data. The oscillations of transfer probability are observed to be quite regular as a function of 1/v. The period of oscillation is $T = \frac{a}{v_n} - \frac{a}{v_{n+2}} = \frac{h}{E}$

from which $\langle Ea \rangle_n = \frac{h}{1/v_{n+2} - 1/v_n)}$ where n denotes

a particular peak or valley in the observed oscillation. Using the value of <Ea> from the data and adjusting the phase, B, the equation given provides an excellent fit to Lockwood and Everhart's data. The value of B obtained is near $\pi/4$.

Lichten[43] discusses these results and the equation given by Lockwood and Everhart. He points out that oscillations in the charge transfer probability arise from interference between symmetric and antisymmetric electronic states which tend to the same separated atom configuration. Competition from nearby states will cause damping of the oscillations (as already seen from perturbed stationary state calculations) and may even destroy them. Further, for oscillations in charge transfer to occur, the electronic energy levels of symmetric and antisymmetric states must be sufficiently separated in energy to allow many oscillations of the charge probability during the collision. Thus Lichten concludes that oscillating charge exchange occurs most favorably when the ratio of energy splitting between symmetric and antisymmetric state to the width of the band of competing states is large. He also discusses theoretical determination of the quantity <Ea>.

The total charge transfer probabilities for close collisions of $H^+ + He \rightarrow H + He^+$, measured by Helbig and

Everhart[29], are of more direct interest to the present work. The observed probability oscillates with considerable damping (Fig. 3). Again the empirical equation given above was found to provide a good description of these oscillations.

Lichten[44] has also discussed these results, calling the oscillations quasi-resonant. The term quasi-resonant is applied because the measured probabilities exhibit oscillations which are regular as a function of collision time, following the resonance concept developed for $H^+ + H$ collisions. However, the $H^+ + He \rightarrow H + He^+$ transfer is not resonant with respect to electronic energies in that the initial and final electronic energies are different. This energy difference contributes to the damping.

Lichten points out that the empirical equation can be put into form identical with that for a damped harmonic oscillator,

$$P_o = e^{-T/T_o} \sin^2 \left[\frac{\langle Ea \rangle}{4\lambda} T - B\right]$$

where T is the period of oscillation and λ is the effective range of the interaction. He also establishes criteria for oscillations to exist. One condition is that $\Delta E\tau << 1$ (in atomic units) so that transitions will take place in spite of the difference, ΔE, in initial and final electron energy (τ is the collision time). Further, as mentioned in the resonant case, the energy levels

during the collision must be widely separated in order that many changes of charge occur. For close collisions this is $[E_2(0) - E_1(0)]\tau >> 1$ (where E_2 and E_1 are the energy levels of the states between which charge transfer occurs, the (0) denoting that the distance of approach of the nuclei is approximately zero.) These two conditions together are

$$E_2(0) - E_1(0) >> \frac{1}{\tau} > E_2(\infty) - E_1(\infty) .$$

For the $H^+ + He$ system, the united atom limit is L_i^+. A correlation diagram is shown in Fig. 5 and demonstrates that Lichten's criterion is satisfied for charge transfer to the ground state of hydrogen in close collisions.

Quantitative understanding of these charge transfer oscillations requires detailed knowledge of the electronic energy levels at all distances of nuclear separation. Some of this knowledge can be supplied without exact wave functions and without calculations describing the entire collision. The energy levels of the quasimolecule at various nuclear separations can be obtained by self consistent energy calculations employing linear combinations of atomic orbitals or molecular orbitals. In this way an energy level diagram showing the behavior of various states of the system for changing internuclear distance is obtained. Some of this work, for the system of interest, $(H + He)^+$, has been carried out by H. H.

CORRELATION DIAGRAM FOR

Fig 5

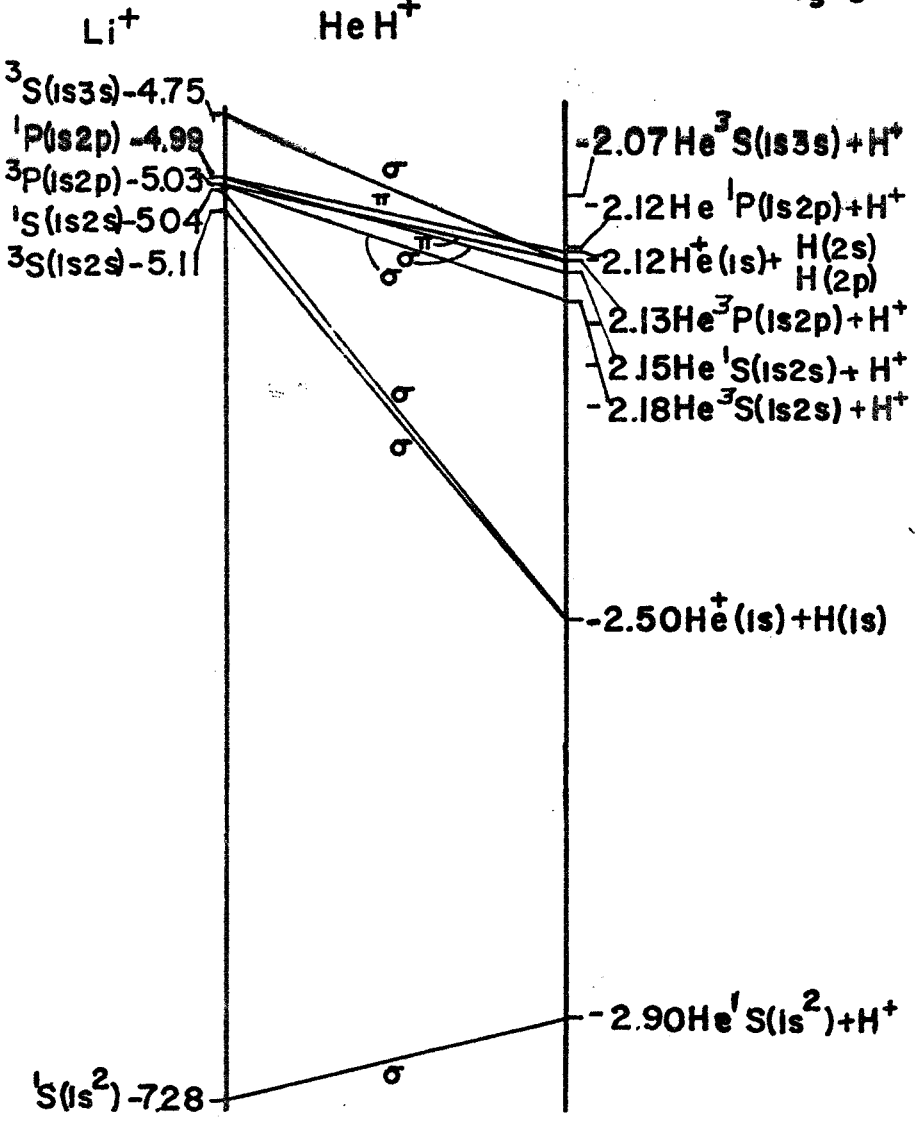

POTENTIAL ENERGY CURVES
for Low Lying Singlet States
of HeH+

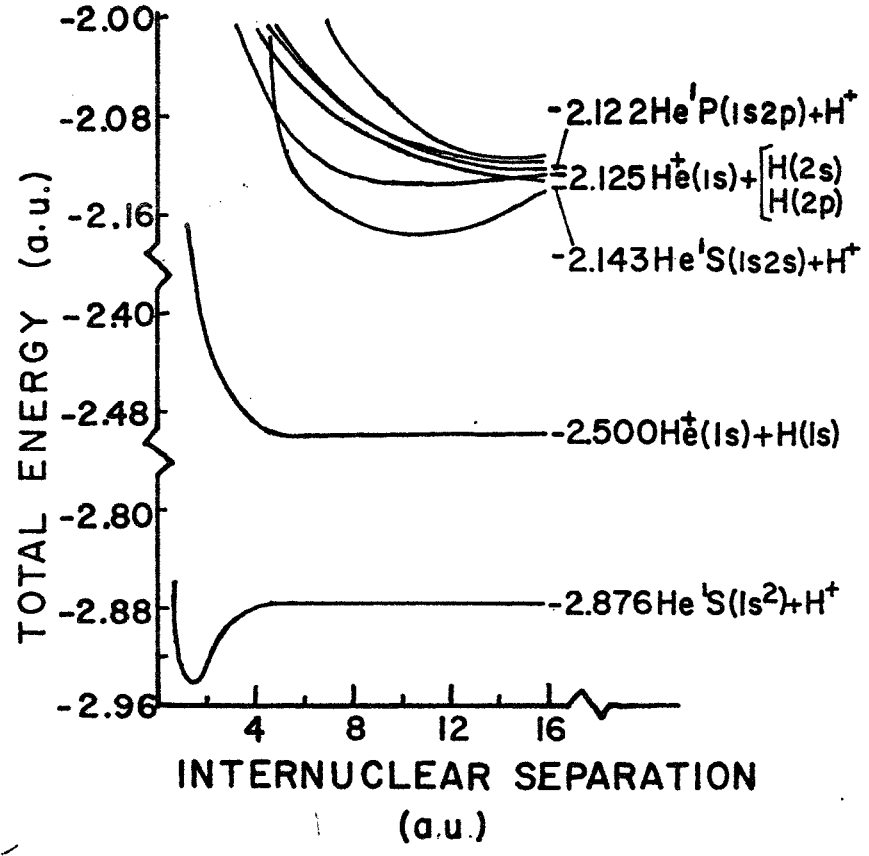

Michels[45], and is represented by Fig. 5. Even though the nuclear repulsion is included in this diagram, the complication for transfer to H(2s) arising from competition of several nearby states is demonstrated.

Some application of the Everhart formula and Lichten criterion to the present results for transfer to the 2s state in H^+ + He collisions will be attempted when these results are presented in section V.

III. THE EXPERIMENT

A. Experimental Arrangement

1. Schematic of the Apparatus.

The experiment was conceived to measure the fraction of the charge transfer which ended in the 2s state of hydrogen from collisions of protons with rare gas target atoms. A schematic of the experimental arrangement is shown in figure 6. A conceptual description of the experiment is given below; but the apparatus will be described in detail in section III. B.

Protons are selected from the output of the ion source by the analyzing magnet and enter the scattering chamber through two beam defining apertures. The scattering chamber is filled with target gas at sufficiently low pressures that only single collision processes are important.

Protons and hydrogen atoms (charge transfer), which are scattered to a particular angle, enter an assembly containing particle and photon detectors. This externally rotatable assembly opens to the scattering chamber only through the first of two slits defining the spread of angles from which the detector assembly will accept scattered particles. The detector assembly is pumped by a 4 inch diffusion pump so that the pressure inside the detector assembly is below that in the scattering chamber.

Fig. 6

EXPERIMENTAL ARRANGEMENT

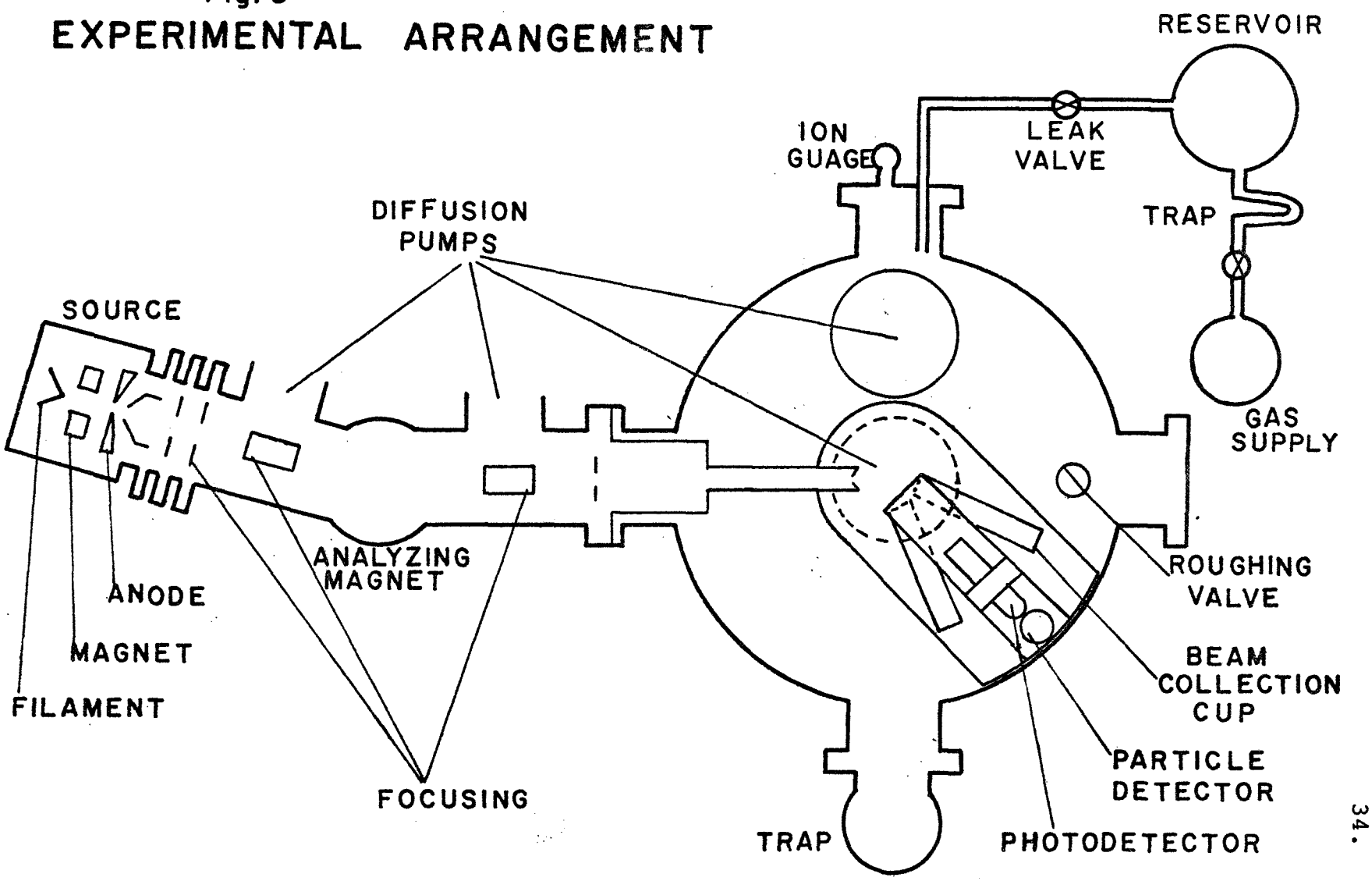

The second slit defining the scattering acceptance angle is a hole in a plate located inside the assembly; this plate serves also as the grounded side of a capacitor.

When voltage is applied, the capacitor presents an electric field parallel to the direction of motion of particles scattered into the acceptance angle defined by the two slits. If the scattered particles have undergone charge transfer to the 2s state of hydrogen, they should remain in that state until they enter the capacitor region. The lifetime of the 2s state in a field free region is 0.14 seconds, but in an electric field of 600 volts/cm the lifetime decreases to about 4×10^{-9} seconds due to stark mixing of the 2s and 2p states. In such a field hydrogen atoms of a few keV energy will travel less than the 2 cm length of the capacitor before decaying through the 2p states to the ground state emitting Lyman alpha photons of 1216 A wavelength.

A detector to count these emitted photons views the capacitor region from above. The fraction of the total emitted photons which are counted by this detector will depend on the detector efficiency, the solid angle subtended by this detector, and the fraction of the excited atoms decaying within the path length viewed by the detector.

The scattered particles pass through a small hole (which is large enough not to affect the scattering

geometry definition) in the high voltage end of the quenching capacitor. Beyond the capacitor all the particles which entered the scattering acceptance geometry are incident on a bare electron multiplier which counts a percentage of them depending on its efficiency.

Data collection is controlled by a current integrator. This device is connected to the beam collection cup which is receiving the direct beam. The integrator monitors the current and stores it on a capacitor, discharging the capacitor when it is fully charged and then recharging it. The integrator continues until a preset amount of charge has been collected. The scalers collecting photon and particle counts are started when the integrator is started and are stopped automatically by the integrator when the preset charge has been collected.

2. Quantities to be Measured.

The primary quantity of interest is the ratio of hydrogen atoms in the 2s state to the total particles (protons plus hydrogen atoms in any state) scattered into a particular angle defined by the detector geometry. This quantity is referred to as P_{2s} in this report and is defined by

$$P_{2s} = \left.\frac{H(2s)}{H^+ + H}\right|_{\substack{\text{at detector} \\ \text{angle}}} = \frac{S_{2s}\ /\varepsilon_p \cdot f}{S\ /\varepsilon_m}$$

where: 1. S_{2s} is the number of detected 2s photons and S is the total number of counted particles. 2. ε_M is the efficiency for detection of protons and hydrogen atoms by the multiplier. 3. ε_p is the efficiency for detection of L_α photons by the photodetector times the fraction of the total 4π solid angle viewed by this detector. 5. f is the fraction of H(2s) decaying within the path length viewed by the photodetector. The measurements of ε_M and ε_p are described in section IV.,and the technique for calculating f is described in appendix A.

In actual measurements, the number of detected photons from the 2s state was determined from two consecutive data collections. Photons were counted with voltage applied to the quench capacitor and with the capacitor grounded, but with all other parameters held constant. The difference between these two is the number of photons from the 2s state. The tube noise and any photons from excitation of background gas within the capacitor are thus subtracted. This whole process was generally repeated with gas removed from the scattering chamber. If these background signals were found to be appreciable (5% or more) they were appropriately subtracted.

If a minor addition to the apparatus is made, the quantity P_o, defined as

$$P_o = \left.\frac{H \text{ (all states)}}{H^+ + H}\right|_{\text{at detector angle}}$$

can also be measured. The required modification is the addition of a device to deflect the protons after scattering so that only the hydrogen atoms reach the multiplier. To accomplish this, a set of curved deflection plates was placed before the quenching capacitor. The top plate was made with a slot to pass the undeflected hydrogen atoms. A biased collector cup was used to collect the deflected protons. With no voltage on the deflector plates all particles pass through the quenching capacitor to the particle detector and the L_α photons can be detected simultaneously by using the quenching capacitor. When voltage is applied to the deflection plates, only hydrogen atoms are passed, but for most deflection voltages the 2s state is quenched in the deflection plates so that $L_\alpha$photons from this state cannot then be detected in the quenching capacitor region.

If it is assumed that the particle detector efficiency is identical for protons and hydrogen atoms of the same velocity (to be substantiated in section IV), then the quantity P_o is independent of the particle detector efficiency. In fact,

$$P_o = \frac{H \text{ (all particles detected with deflection)}}{H^+ + H \text{ (all particles detected with no deflection)}}$$

provided the target pressure and total number of incident protons, which determine how many particles are scattered

into the detector geometry, are the same during deflection-on and deflection-off data collections.

Everhart, et al[29,63] have measured P_o for most of the experimental configurations used in the present work and comparison of results is made in section V.

If the detector assembly is set at zero degrees, that is, so that the incident beam passes directly through the detector geometry, the total cross section (integrated over angles) for charge transfer to the 2s state can be measured directly. Of course, this assumes that any particle undergoing charge transfer to the 2s state and scattered by a larger amount than the detector acceptance angle can be accounted for or neglected. In fact these can be neglected as will be demonstrated, indicating that the particles detected at angles where no direct beam enters the detector geometry are a negligible portion of the total scattering.

In practice, most manageable proton beams for the apparatus used, were too intense for the direct beam individual particles to be counted. Therefore, the total 2s cross sections were measured with a Faraday cup in place of the particle multiplier.

Assuming single collision conditions, the cross section for total charge transfer to the 2s state, σ_{2s}, is defined from $N_{2s} = N_o \rho L \sigma_{2s}$ where; N_{2s} is the number

of hydrogen atoms formed in the 2s state for N_o total incident protons, ρ is the target gas density, and L is the length of target gas traversed by the beam.

In actual data collection, N_o, was determined by integrating the total charge collected by the collection cup at the end of the detector assembly. The total integrated charge, Q (in coulombs), is equal to $e \cdot N_o$ where e is the charge on each proton, 1.602×10^{-19} coulombs.

At the low pressures used, the ideal gas law can be used to relate the density of the target gas to the pressure. The relationship is

$$\rho = 3.535 \times 10^{16} \left(\frac{273}{T}\right) P; \quad \left(\text{let } 3.535 \times 10^{16} \left(\frac{273}{T}\right) \equiv \alpha_T\right)$$

where ρ is in units of cm^{-3} if P is in mm of Hg and T is in degrees Kelvin. The temperature was taken to be room temperature which was always within a few degrees of 300^oK, so that $T = 300^oK$ was used for all data.

As in the previously defined probability, the quantity N_{2s} was determined by counting the L_α photons during consecutive data runs with all parameters held constant, within experimental limits, except that one run was with quenching voltage applied and one was with quenching capacitor grounded. This process was then repeated with target gas removed from the chamber, and this background was subtracted unless it was found to be negligible. We thus have, for target gas in the chamber

$$N_{2s} = [\, S_{2s}\ (\text{quench-on}) - S_{2s}(\text{quench-off})\,]\ [\frac{1}{\varepsilon_p \cdot f}\,]$$

Where the S_{2s} quantities are actual photon counts and ε_p and f are as previously defined.

The background (or gas-out) pressure reading was always less than 1% of the gas-in target pressure as measured by an ion guage, and the difference pressure was thus taken to be the pressure measured with target gas in the chamber.

With these experimental quantities the cross section definition becomes

$$\sigma_{2s} = \frac{[S_{2s}(\text{quench on}) - S_{2s}(\text{quench off})]e}{\alpha_T\ PLQ\varepsilon_p f}$$

No attempt was made to measure absolute total 2s cross sections, rather, the relative measurements of this quantity were normalized to published values in order to obtain a measurement of the photodetector efficiency, ε_p (see section IV. D.).

Finally, the differential cross sections for total scattering and scattering with charge transfer to all states and to the 2s state only were measured at various angles. In fact, the ratios P_{2s} and P_o can alternatively be defined as differential cross section ratios, i.e.

$$P_{2s} = \frac{d\sigma_{2s}}{d\Omega} \Big/ \frac{d\sigma_{\text{total}}}{d\Omega} \quad \text{and} \quad P_o = \frac{d\sigma_{\text{charge exchg.}}}{d\Omega} \Big/ \frac{d\sigma_{\text{total}}}{d\Omega}$$

Since the measured quantities for P_{2s} and $\frac{d\sigma_{2s}}{d\Omega}$ and $\frac{d\sigma_{total}}{d\Omega}$ are determined simultaneously it is only necessary to determine P_{2s} and $\frac{d\sigma_{total}}{d\Omega}$, then $\frac{d\sigma_{2s}}{d\Omega}$ is given by

$$\frac{d\sigma_{2s}}{d\Omega} \equiv P_{2s} \frac{d\sigma_{total}}{d\Omega} ,$$

where the identity holds for this experimental data because of the simultaneous collection of data and the identical geometry that defines the scattering angles and solid angles. The cross section $\frac{d\sigma_{2s}}{d\Omega}$ can be obtained directly, without measuring $\frac{d\sigma_{total}}{d\Omega}$, as well as from the above identity.

The differential cross section for scattering of any particle (proton or hydrogen atom) into the solid angle element defined by the detector geometry is given from

$$N = N_o \rho \frac{d\sigma_{total}}{d\Omega} \ell \Delta\Omega$$

where N is the number of particles (neutral plus positive) scattered into the detector solid angle $\Delta\Omega$ for N_o incident protons and ρ is target gas density. The quantity ℓ is the length of the primary beam in the target gas which is viewed by the detector geometry. In general the quantity $\ell\Delta\Omega$ is a function of the apparatus and of the varied scattering angle, θ. The evaluation of $\ell\Delta\Omega$ is most easily carried out for the product and is referred to as $\ell d\Omega$ or $(\ell\Delta\Omega)_{eff}$. This evaluation will be made in the next section

Using the experimental quantities defined in the discussion of σ_{2s} with those just discussed, we have

$$\frac{d\sigma_{total}}{d\Omega} = \frac{[S]e}{\alpha_T PQ \cdot d\Omega \cdot \epsilon_M}$$

where S again represents the actual number of counts recorded, in this case by the particle detector.

As mentioned, the quantity, S, was measured simultaneously with the quantities S_{2s} (quench-on) and S_{2s} (quench-off). S was obtained during both the quench-on and quench-off data collections and the average was used in the determination of $\frac{d\sigma_{total}}{d\Omega}$. These two determinations of S typically differed by 2%, indicating the extent to which the pressure and number of incident protons remained constant between quench-on and quench-off collections, and indicating that the quenching field did not appreciably alter the path of the scattered particles (some are protons) through the detector assembly.

B. Apparatus

1. Accelerator.

The ion source, analyzing magnet, high voltage supply, and control console were produced commercially.

The ion source, shown schematically in Fig. 6, is a Von Ardenne[46] duoplasmatron type modified so that H^- ions may be extracted[47], as well as positive ions. With hydrogen gas supplying the source, the total positive ion

yield at the analyzing magnet was observed to be near one milliamp, but, after selecting only protons and restricting entrance into the scattering chamber with two 0.040 inch apertures, typical proton beams used for the experiment were 10-50 nanoamps. Transportation of the beam from the ion source to the scattering chamber is aided by three lenses, an einzel lens at the source, an electrostatic quadrupole doublet lens before the analyzing magnet, and another einzel lens between the analyzing magnet and the chamber.

The ion source and all of the associated control electronics are raised to the accelerating potential. The extraction electrode is grounded so that the accelerating potential is applied between the anode and the extraction electrode. The high voltage is specified by the manufacturer of the supply to be ±1% of the selected value and is continuously variable between 0.5 and 21.0 kilovolts.

The spread of energies of ions extracted from the source was not measured in this experiment. In general the spread of energies from duo-plasmatron type sources is less than 10 to 20 ev[46,48]. It is expected that ions passed by the analyzing magnet and entering the scattering chamber through the beam defining apertures do not have a larger energy spread than 10 to 20 ev.

2. Scattering Chamber and Vacuum.

The differential scattering assembly and detectors are enclosed by a circular stainless steel scattering chamber as indicated by Fig. 6. The inside diameter of the chamber is 18 inches with 1/2 inch thick walls. The chamber is made in two sections. The 7 inch deep lower half bolts directly to a 1 inch thick stainless base plate with the vacuum seal made by compression of an aluminum o-ring. This lower section has 4 entrance ports of 4 inches diameter each at 90^{o} intervals. The top half of the chamber, which is 6 1/2 inches deep, bolts to the lower half with the vacuum seal again made by compression of an aluminum o-ring. This upper section has one entrance port in the center of the top, through which all of the electrical connections are made by means of ceramic to metal insulated vacuum feed-throughs.

The base plate has three holes, two 5 inches in diameter, the third 2 inches in diameter. The center 5 inch hole is below the rotatable detector assembly and opens into the chamber only through the 0.0202 inch by 1.25 inch slit formed by the two stainless steel beam collection cups. The other 5 inch hole opens directly into the chamber. Each of these holes leads from the chamber to a gate valve, liquid nitrogen baffle, water baffle, and standard 4 inch diffusion pump in that order.

A small valve beneath the 2 inch hole provides access to the chamber for initial rough pumping and for a McLeod guage used as an absolute pressure standard.

One of the four side ports opens to a small liquid nitrogen cold trap. This trap is to help in removal of pump oil, water, or any other condensable material which might contaminate the target gas. Since it presents only a relatively small surface area to the target gas, its effect on the target gas temperature has been ignored.

The next side port, moving clockwise around the chamber, opens to the drift tube connecting the chamber and the accelerator. The proton beam enters the chamber through two .040 inch circular aperatures which are 10.2 inches apart. The outer aperture is a circular hole in a thin plate of tungsten. The plate is mounted on three ceramic insulators, leaving space between it and the walls for pumping of the region between the apertures. The current on this plate can be monitored externally, but during data collection the plate was always directly grounded. The second aperture is a .040 inch circular hole at the end of a stainless steel tube extending to within 1.70 inches of the center of the chamber. The accelerator drift tube opens to the chamber only through this aperture so that differential pressures can be maintained between the chamber and the drift tube.

When data were being collected the side pump (opening directly into the chamber) was closed and the chamber was filled with gas. The pump under the detector assembly maintained a pressure in the rotatable assembly approximately 1/100 of that in the chamber, as measured by two ion guages, one in the valve below the center hole and the other opening to the chamber. The pump on the drift tube maintained a pressure there of about 1/500 of that in the chamber when target gas was in the chamber.

The third side port provides a target gas inlet to the chamber and supports the ion guage used to measure target gas pressures. The target gas used was "high purity" grade specified by the manufacturer to be 99.995% pure. Gas from the supply bottle was admitted through a regulator and liquid nitrogen cold trap into a gas storage reservoir. This reservoir feeds the chamber through a commercially produced leak valve which controls flow through a Monel to silver seat. Through this valve the pressure in the chamber could be manually set to any desired ion guage reading. After reaching equilibrium, without further adjustment, the leak would maintain a constant chamber pressure within 2 - 5% over a period of several hours.

During the period when most of the data in this report were collected, the vacuum system was maintained intact for several months. Under these conditions, the ion guage

indication of pressure (not absolute) with target gas in the chamber was typically 5 x 10^{-5}mm of Hg. When the leak valve was closed this indicated pressure dropped within two to five minutes to approximately 6 x 10^{-8}mm of Hg. When the side pump (opening directly into the chamber) was also opened the indicated pressure would drop to 1 - 2 x 10^{-8}mm of Hg.

3. Detector Arrangement and Geometry

The external rotation, support, and pumping of the detector platform is illustrated in Fig. 7. The cylinder connecting chamber and pump was constructed to accept a vacuum feed-through rotator which employed a stainless steel bellows seal. This rotator allowed rotation of an external crank to drive the detector assembly as indicated.

The external crank was fitted with a divided circle marked into one hundred parts and a counter to count full turns. Calibration of the rotation gear in degrees was accomplished by placing a 90° prism on top of the assembly, reflecting a laser beam off one face of the prism, then rotating the assembly until the laser spot was reflected to the same point by the other face of the prism. The angle rotated through was then the prism angle. The relationship was found to be 1 turn = 2.571°.

The zero angle position of the detector assembly was determined using the ion beam by finding the maximum

ROTATING DETECTOR ASSEMBLY

Fig. 7

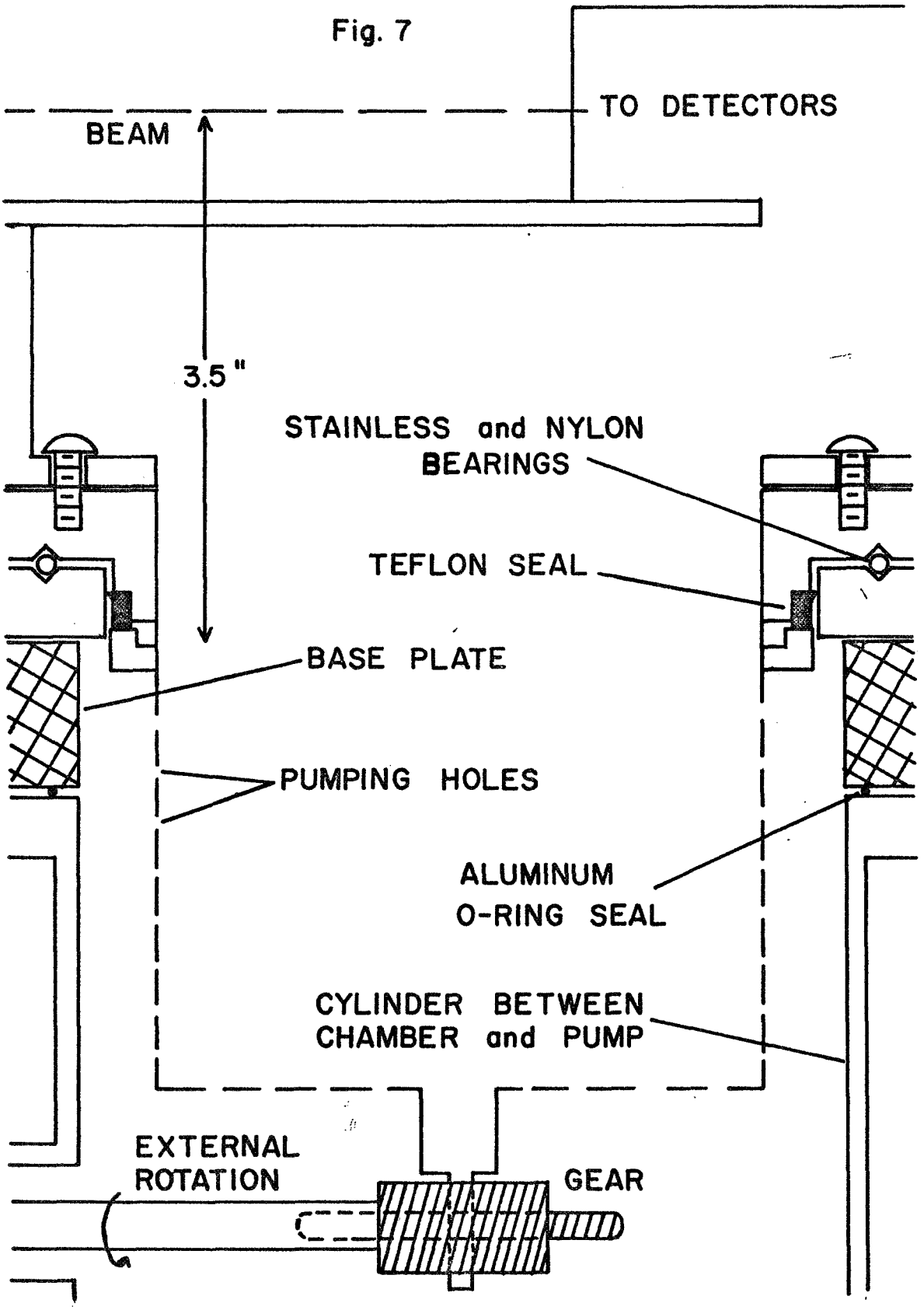

particle count rate with the chamber evacuated and the protons deflected. That is, the zero position was taken to be the position for maximum neutral atoms formed by charge exchange with background gas. Counting these atoms with a count rate meter, this position could be determined to within ±.01 turns (.03°). The zero position was checked frequently and never spontaneously varied during the experiment. The reproducibility of any angle setting has been taken to be ±.01 turns or ±.03°.

The details of detector placement are shown in Fig. 8. A platform supporting the proton deflection plates, deflector collection cup, quenching capacitor, and particle detector supports is anchored directly to the base of the rotating assembly.

The assembly housing has two cover plates. With both plates removed only the base of the housing and the side walls remain. The first plate covers much of the assembly below the beam level and supports the beam collection cups. It has a hole and sides the proper shape to surround the deflection plates, quench capacitor and particle multiplier which extend through this first cover to beam height. The top view in Fig. 8 shows this first cover plate in place, but the top cover plate removed. The top cover bolts to the extended sides of the first cover. This top cover has a hole through which the

Fig. 8 DIFFERENTIAL SCATTERING DETECTOR ARRANGEMENT

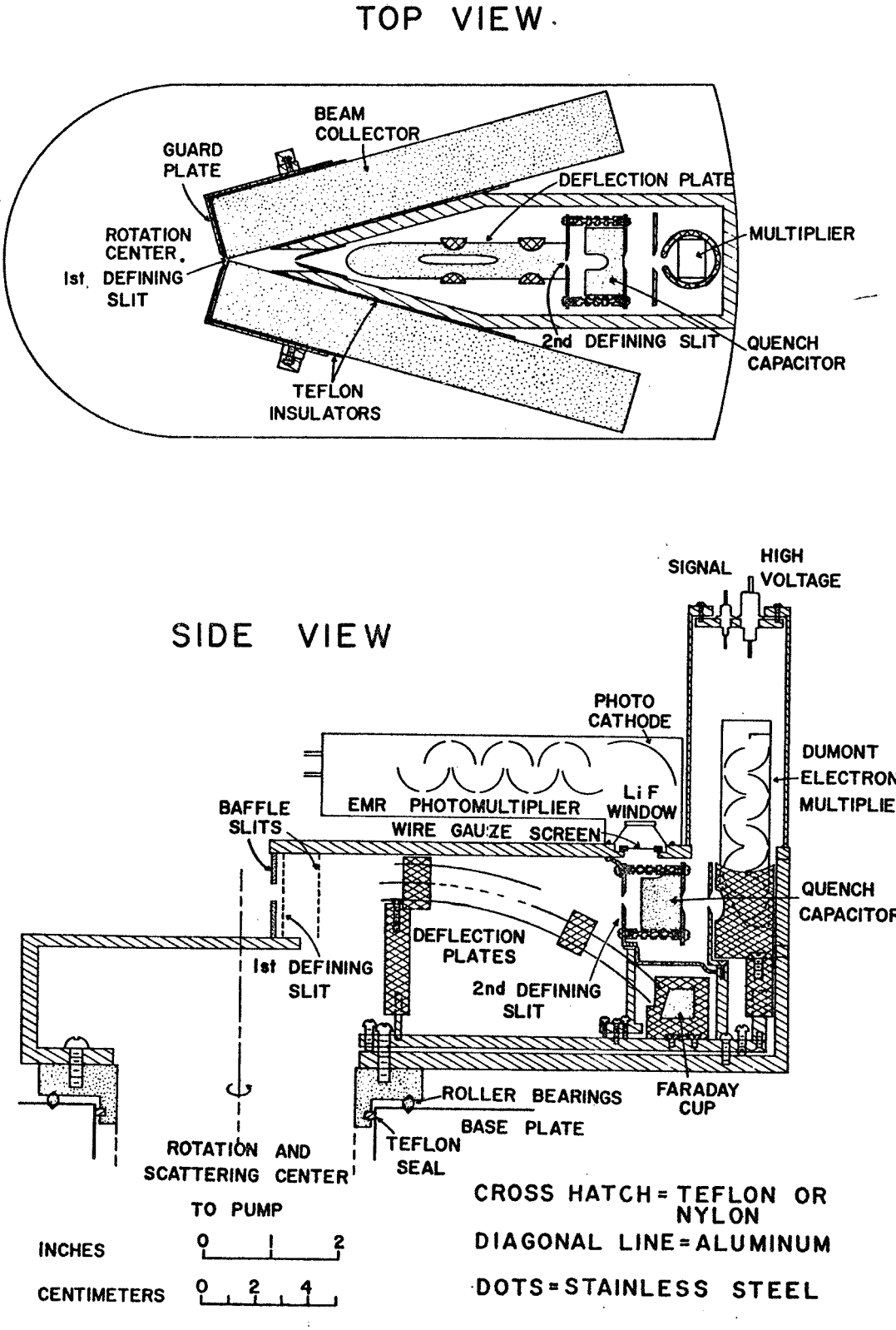

photodetector views the quenching region. Both detectors are attached to this top cover plate, the photodetector by means of a saddle and clamp. The particle multiplier is attached through its voltage divider resistors and signal lead to the top of the tower built on the top plate as a housing for the multiplier.

The plates for deflecting charged particles are located between the geometry defining slits. Baffle slits before the deflection plates prevent direct beam from reaching the deflection plate spacers when the assembly is set at angles less than 2^{o}, where some direct beam passes the first defining slit.

The deflection plates were made from 1/16 inch thick stainless steel strips 9/16 inch wide tapered at the front to fit the available space. These strips were bent on circular radii of 5 inches and 5 1/4 inches. They are held separated at 1/4 inch by the nylon spacers. As illustrated in Fig. 8, a slot in the upper plate is necessary in order to pass scattered particles which are not deflected. This slot is 3/16 inch wide and 1 3/8 inch long. A third plate was placed above this slot to prevent weakening of the deflecting field due to the slot. When deflection is desired, a negative potential is applied to the lower plate, while the center plate is grounded. Originally, a positive potential, equal in

magnitude to the negative potential on the lower plate, was applied to the slot cover plate. However, no difference in operation of the deflection system could be detected when this cover plate was grounded, so data was taken with the cover plate grounded inside the chamber.

The potential required to deflect protons of various energies into the collection cup was determined experimentally. Fig. 9 shows the results of this determination.

The hole in the top plate of the rotating assembly, through which the photodetector views the quenching region, is restricted by a 3/8 inch inside diameter washer. The washer supports a tungsten wire screen which helps to prevent penetration into the photocathode region of the electric field from the capacitor. The transmission of this screen for white light in the visible region is .88 ±.01 as measured with a photo cell.

The photodetector is EMR model 641J. The response of this detector as a function of wavelength is limited by the LiF window to 1050A at one extreme and by the photocathode material to about 1800A at the other extreme, with maximum response near the 1216A line to be detected. The physical shape of this detector is as shown in Fig. 8.

The photodetector effective opening is specified by the manufacturer to be 3/8 inch and is approximately 3/8 inch above the washer opening. This geometry, defining the portion of the quenching region viewed by the photo-

Fig. 9

DEFLECTION PLATE CALIBRATION

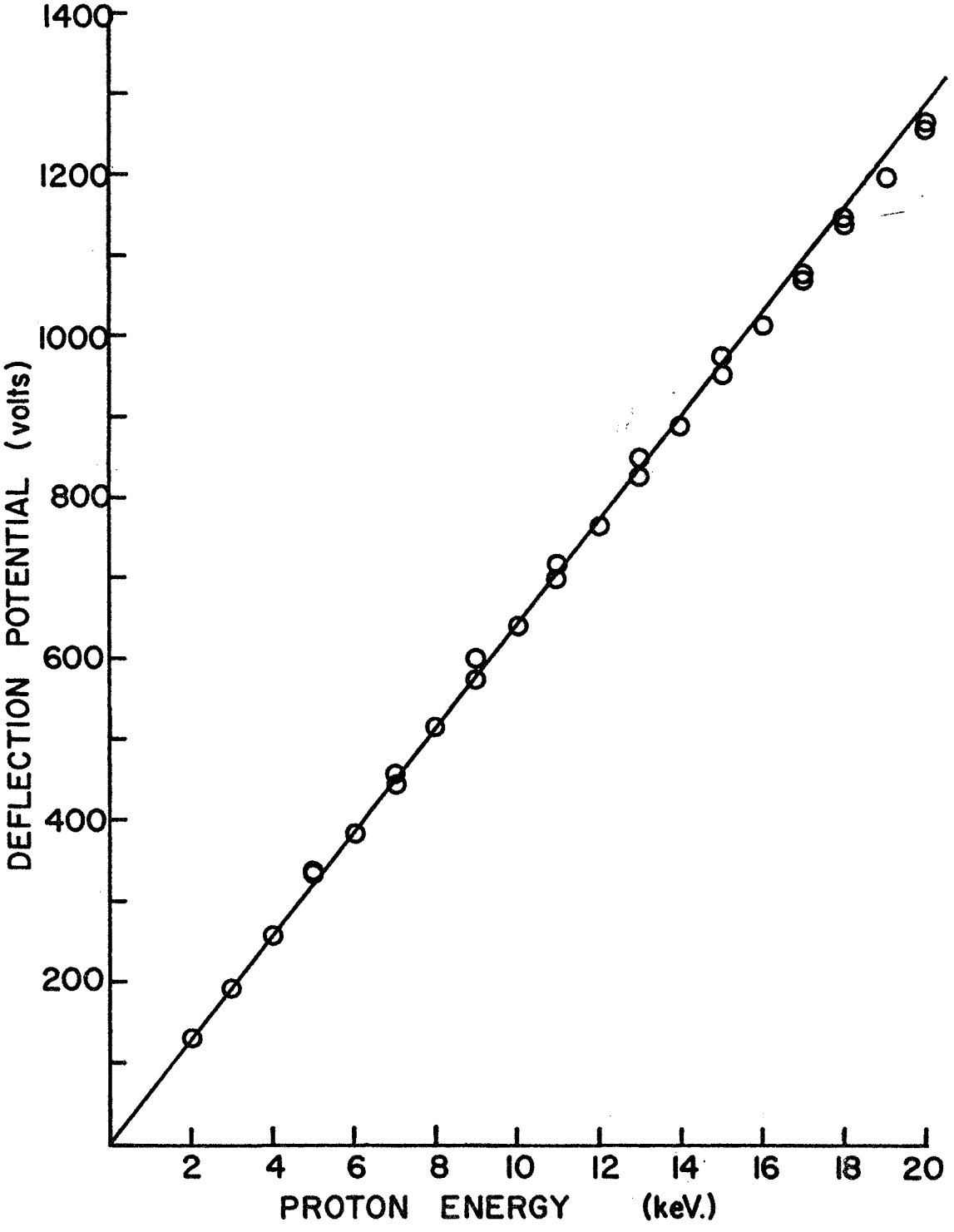

detector is not restrictive, implying that the acceptance angle for receiving photons from the quenching region is not well defined. This construction was deliberate in order to obtain as large a photon signal as possible. The shape of the quenching capacitor, electric field strength, and radiation of photons along the axis of the capacitor are discussed in Appendix A.

The particle detector is a modified 14 stage Fairchild-Dumont electron multiplier with Cu-Be dynode surfaces. The modification is the removal of the target dynode, using the first multiplication dynode as the target. This modification allows the orientation of the multiplier to be at right angles to the direction of motion of the particles detected, rather than along this direction as originally required. This modification was necessitated by the limit of space in the rotatable assembly.

The scattered particle acceptance geometry is defined by two slits. The first slit is formed by the edges of the stainless steel beam collection cups which are milled to a knife edge. These cups ride on teflon strip insulators and slide along the extended sides of the first cover plate. They are slid forward until nearly touching and are then clamped in place. The slit width was measured after each assembly with a traveling microscope. All of

the differential (in angle) data in this report were taken with this slit at .0202±.0002 inches.

The collection cups could not be directly biased because the electric field would cause quenching decay of the 2s state to be detected. However, at the small angles used the direct beam strikes a cup near the front, generating secondary electrons. In order to collect as many of these secondary electrons as possible, a plate was isolated inside each collection cup and biased at 67 1/2 volts. Current on this plate was added to that on the cup. A baffle plate was extended across the opening of each cup. These grounded baffle plates allowed entrance of the direct beam, but helped prevent secondary electrons from escaping into the chamber and helped to contain the electric field of the bias plates in the cups.

The second scattered particle geometry defining element is a rectangular aperture. This aperture was formed by drilling a 0.150 inch hole in the front plate of the quenching capacitor, then masking the hole with two thin pieces of stainless steel. The masking pieces were set nominally at .040 inches separation and were measured to be separated .0398 ±.0001 inches. The resulting aperture is nearly rectangular with the height of the rectangle being taken to be the height which would give a rectangular aperture of the same area as the true hole. This height is 0.1467 ±.0005 inches.

The resulting scattering geometry is illustrated in Fig. 10. The total spread of acceptance angle, $2\Delta\theta$, is .67 degrees. The product of beam length and solid angle must be evaluated. A small length of beam, d, is subtended by the entire area of the rectangular aperture. However, additional parts of the beam length are subtended by only a portion of this second defining element, due to the first slit obstructing the second aperture.

A simple formula was obtained by Jordan and Brode[49] for evaluating the effective product, $(\ell\Delta\Omega)_{eff}$ for such geometry. This formula counts approximately half of the beam length which is viewed by only part of the rectangular aperture. Referring to Fig. 10, the total solid angle subtended by the rectangular aperture is $\Delta\Omega = W_2h_2/R^2$. If only one of the partially viewed beam segments is counted, take $\ell_{eff}=L'$. By similar triangles, with the triangle base approximated as $L' \sin\theta$,

$$\frac{W_1}{Y} = \frac{L' \sin\theta}{R} \quad \text{giving} \quad L' = \frac{RW_1}{Y \sin\theta}$$

where R and θ are approximate. (These approximations are satisfactory only for $Y>>W_1$, and W_2.) With similar approximations this same result can be obtained by including only the other partially viewed beam segment. Finally,

$$(\ell\Delta\Omega)_{eff} = L'\Delta\Omega = \frac{W_1W_2h_2}{YR \sin\theta}$$

is identical to the formula obtained by Jordan and Brode.

Fig. 10
SCATTERED PARTICLE
ACCEPTANCE GEOMETRY

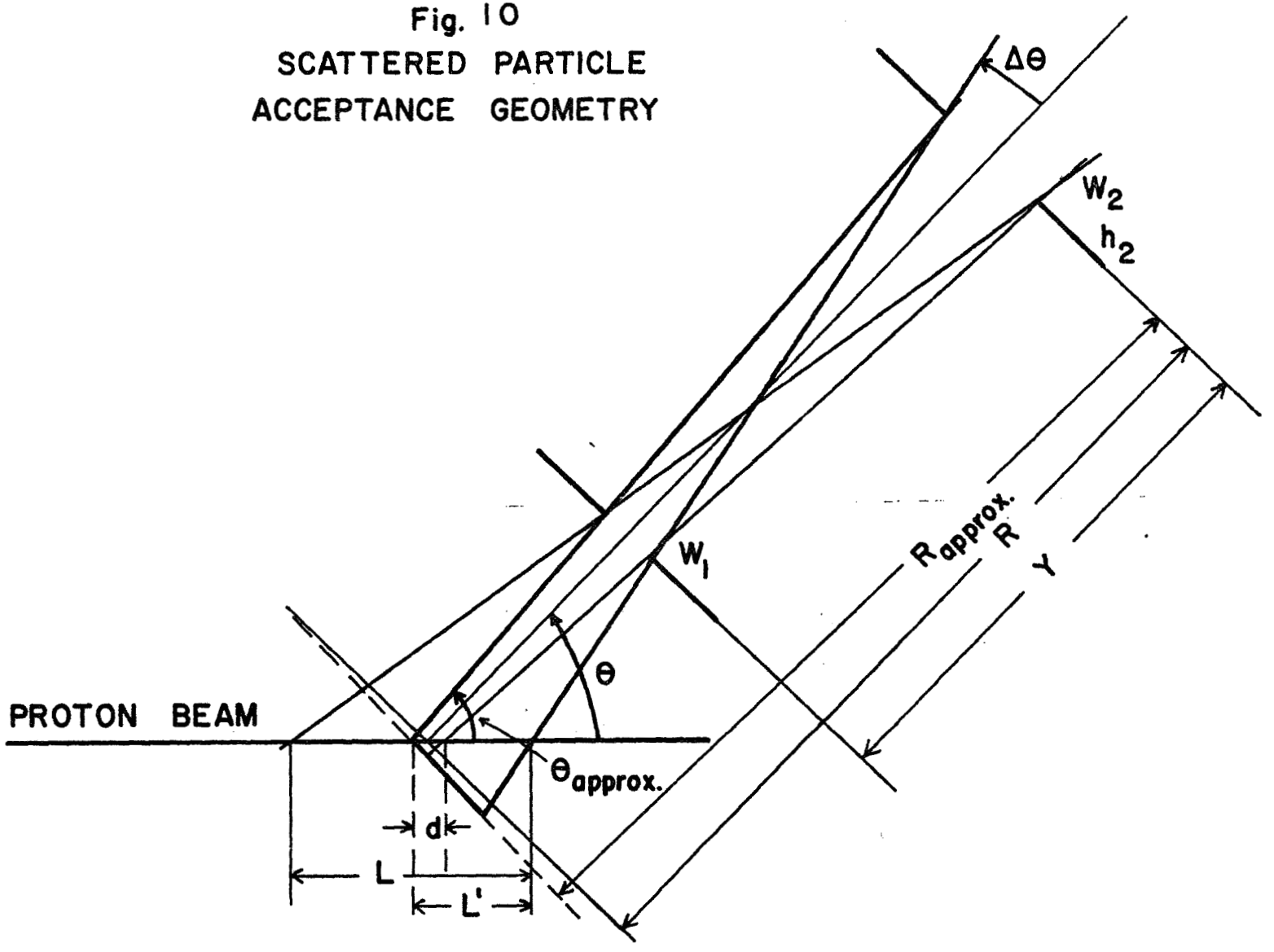

This formula will be least accurate at small angles (θ). A numerical evaluation of $(\ell\Delta\Omega)_{eff}$, for this same geometry by R. H. McKnight[50] shows that the above formula agrees with more exact evaluation to within 1.5% at 1^{o}. (The numerical evaluation is for a beam of no thickness.) Because of this good agreement the simple formula was used throughout.

For the geometry used:

$Y = 4.985 \pm .016$ inches (12.66 cm)
$R = 5.625 \pm .020$ inches (14.29 cm)
$W_1 = 0.0202 \pm .0002$ inches (.0513 cm)
$W_2 = 0.0398 \pm .0001$ inches (.1010 cm)
$h_2 = 0.1476 \pm .0005$ inches (.3727 cm)

so that

$$(\ell\Delta\Omega)_{eff} = \frac{1.066 \times 10^{-5} cm}{\sin \theta} .$$

According to the quoted errors in the measured quantities, the product $(\ell\Delta\Omega)_{eff}$ should be accurate to about 2 - 3%. However, a critical factor has not yet been mentioned. It is important that the first geometry defining slit be centered on the line from the center of the rectangular aperture to the center of rotation of the assembly.

This alignment of the geometry was accomplished by directing a laser light beam down the drift tube into the chamber through the circular beam defining apertures. It was readily verified that this laser beam did pass over the

rotation center. The rotating assembly was set so that the laser spot fell on the center of the rectangular aperture serving as the second scattered particle defining aperture. The first defining slit was then set by movement of the collector cups as described. This first slit was as nearly as possible centered on the laser beam. However, the uncertainty in the lateral placement of this slit relative to the laser beam was about ±.004 inches. This error was determined by moving the rotatable assembly and attempting to reset it with the first slit centered on the laser beam. The angular error in this resetting, times the distance from the scattering center to the first slit, gives the error in the lateral placement of the slit.

A slit placement error of .004 inch corresponds to an error in the angle, θ, of approximately $.05^{o}$ at 1^{o}, and a smaller error in θ at larger angles. This error is slightly larger than the estimated reproducibility of any angular setting. Further, it is a systematic error rather than random. An error of $.05^{o}$ at 1^{o} would give an error in a Rutherford cross section (the angular dependence is $1/\sin^{4}(\theta/2)$) of about 20% at this angle.

Since this error is positive on one side of zero and negative on the other, it should be observed as a systematic difference in the observed cross sections measured at positive and negative scattering angles.

Indeed such a systematic difference was observed (see Fig. 20.) This systematic difference was not well established due to scatter in the data and failure of one collection cup to maintain stable collection efficiency at small angles. However, using the right (negative angle) and left (positive angle) observations of $\frac{d\sigma_{total}}{d\Omega}$ and $\frac{d\sigma_{2s}}{d\Omega}$ for protons on argon at $\theta T = 20$ keV·deg., a correction factor was constructed. Since one collection cup was more stable at low angles than the other, all of the remaining data was taken to the left of zero and corrected by the constructed correction factor which varied linearly from 11% at 1.0^{o} to 3% at 2.0^{o}, being neglected for higher angles.

Another problem arises in the measurement of differential cross sections with apparatus having a finite acceptance angle such as just defined. The cross sections to be measured behave basically as a Rutherford cross section, that is the dependence on angles is $1/(\sin^4 \theta/2)$. This is a very rapidly varying dependence so that at small angles the acceptance of a finite spread of angles implies that the observed cross section is averaged over a region where the contribution from the lower part of the acceptance angle will be significantly greater than the contribution from the higher angle portion. The problem is to unfold the apparatus function and the true cross

section.

This deconvolution has not been performed for the present data. The difference between the real cross section and observed cross section is expected to be significant only at the smallest angles. R. H. McKnight[50] has numerically evaluated $\int_{\Delta\Omega} \frac{\ell\, d\Omega}{\sin^4 \theta/2}$ for the geometry of the present apparatus. This includes the angular dependence of the cross section in the evaluation of the apparatus geometry function. The results indicate that the observed cross section may be as much as 25% higher than the true cross section at 1^o, but that the discrepancy has reduced to about 4% by 2^o.

A thorough deconvolution of apparatus function and cross section may not be justified due to additional problems at low angles. At angles less than 2.0^o part of the primary beam misses the collector cup edge and enters the detector assembly (as mentioned previously). This allows for the possibility of primary beam particles deflecting from the first defining slit edge through the second aperture onto the particle detector. In practice, for angles near 1^o, the apparent magnitude of the scattered particle cross section could be changed by almost a factor of two by deliverately focusing the beam for maximum apparent scattering. This difficulty probably arises from the combination of beam profile distortion

and reflections from the first defining slit. Some of the apparent increase could be subtracted out as background since it remained after gas was removed from the chamber.

In order to minimize geometrical difficulties, data were taken in the following manner. The beam was focused for maximum current with the detector assembly at a large angle where the beam went deep into the cup. The ratio between this true intensity and the intensity at the particular angle of interest (where some beam might pass into the detector or appear diminished by loss of secondaries) was measured. Without refocusing, data was collected for gas-in the chamber and for backgound or gas-out of the chamber. The beam intensity ratio (or collection efficiency) was remeasured. (This collection efficiency ratio was observed to vary by as much as 5% between post and prior measurements.) Data taken in this manner was reproducible to better than ±15% even at the lowest angles (near 1^{o}).

The quantities P_{2s} and P_{o} are not affected by the preceding geometrical problems since the geometry factors are identical for the numerator and denominator of these fractions.

IV. AUXILIARY MEASUREMENTS

A. Pressure

The pressure in the scattering chamber was monitored throughout the experiment by a Bayard-Alpert type ionization gauge. A Consolidated Vacuum Corporation model GIC-017 gauge and model GIC-110B control circuit were used. The emission of ionizing electrons from the filament was controlled at 2 milliamps (well below the manufacturer's standard of about 7 milliamps). The original gauge failed before completion of the experiment, so that two different gauges were used.

The ionization gauge was considered to be an adequate and stable indicator of the relative pressure, but was calibrated against a McLeod gauge to obtain absolute pressure values. The McLeod gauge employs Boyles law to measure low gas pressures by compressing a known volume (at the pressure to be measured) into a small capillary and measuring the pressure in the capillary. The pressure in the capillary is determined from comparison of heights of columns of mercury, one compressing the gas in the capillary and the other in an identical capillary open to the system at low pressure. The particular gauge used was a commercial model produced by Consolidated Electrodynamics Corporation. It operated in the pressure range 1×10^{-7} to 2×10^{-3}mm of Hg by compressing a volume of 2210 cm^3

into a capillary of .0533 cm diameter.

The gauge was connected to the system through a liquid nitrogen cold trap by 1/2 inch copper tubing and glass tubing of approximately the same diameter. The total length from the gauge bulb to the chamber was about 5 feet.

Such gauges are subject to a number of systematic errors. The most significant is the Gaede[51] (or Iishi[52]) effect. Mercury from the reservoir streaming toward the cold trap between the gauge and the system carries gas of which the partial pressure is to be measured with it. There are two established techniques for reducing this effect. One is to restrict communication of the mercury reservoir with the vacuum system with an orfice. This requires modification of the gauge and was not attempted. The other technique is to cool the mercury reservoir thus reducing the vapor pressure of the mercury.

For the present measurements the mercury reservoir was cooled to approximately -15^{o}C by dry ice. The observed pressure difference between the cooled and uncooled McLeod Gauge for Argon gas was approximately 16%. This was found to be in reasonable agreement with the measurement and calculation of deVries and Rol[53]. It is assumed that not more than about 2% error remained due to this effect. For helium gas the Gaede effect is much less significant.

Thermal transpiration can cause systematic errors when a cold trap is used or when the mercury resevoir is cooled[53,54]. This source of error is dependent on the dimensions of the cold trap, as well as the temperature difference between gauge bulb and chamber. The dimensions of the cold trap were such as to minimize any error due to the presence of a trap. The bulb of the gauge was partially cooled indirectly when the mercury resevoir was cooled. Assuming a bulb temperature of 0°C, chamber temperature of 23°C, and the law of thermal transpiration, $\frac{P_1}{P_2} = \sqrt{\frac{T_1}{T_2}}$, the error in the pressure would be 3.5%. The law of thermal transpiration is not always obeyed[53]. The correction estimated represents a maximum. Since this error is not exactly known, but is estimated to be less than 3.5%, it has been ignored in the present work.

A further source of error is a possible difference in the depression of the mercury in the two capillaries due to surface forces. There are techniques for reducing this "sticking" of the mercury in the capillaries, such as roughening the capillary surfaces with acid. According to the manufacturer the gauge used has been treated to reduce sticking. Some authors report "tapping" the capillaries to overcome sticking. We found that such

tapping was necessary for the gauge used in order to reduce random errors. The relative depression of the capillaries can be checked experimentally as described by Carr[54]. If very low vacuums are attained the capillaries can be compared directly. No systematic difference in the capillary depression was found for the gauge used, but several attempts at measuring it reveal that the sticking of the mercury in the capillaries may be the main source of random error in the measurements.

An example of the data for calibration of the ion gauge to the McLeod gauge is shown in Fig. 11. The ion gauge, as operated, gave values about a factor of 30 lower than the true pressure for helium, and about a factor of 8 low for argon.

The overall systematic errors in the pressure measurement should be less than ±7%. Adding to this the random errors and possible changes in the ion gauge, the measured pressures may be as inaccurate as ±10%, in spite of the considerable care taken in these measurements.

Fig. 11

ION GAUGE CALIBRATION

HELIUM GAS

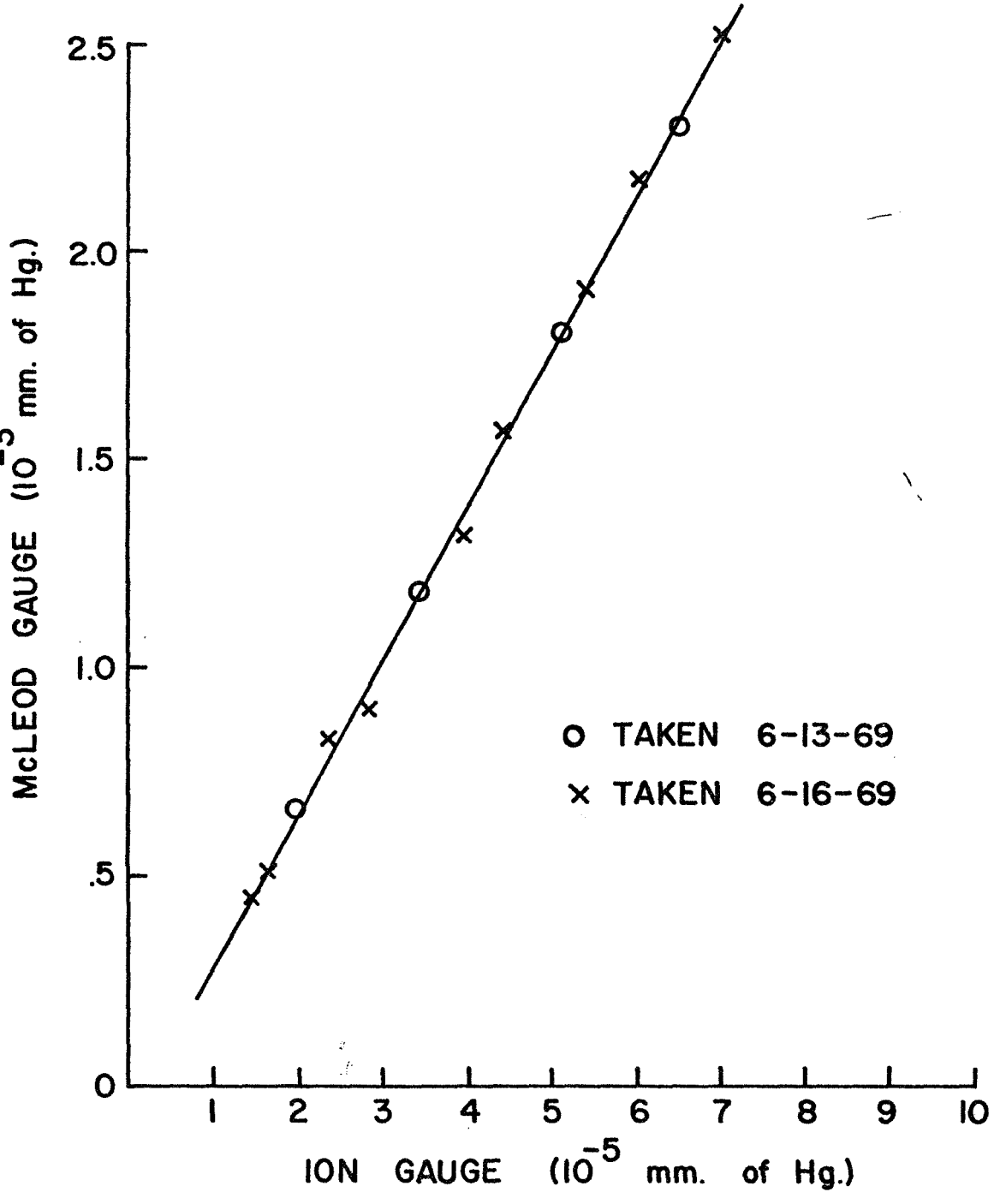

B. Beam Profile.

An attempt was made to check the profile of a beam of 4 keV protons by counting particles and 2s photons as a function of angle near zero degrees detector setting. A reasonably steady beam of 6×10^{-11} amps was obtained. The number of 2s photons, neutral hydrogen atoms, and total particles (protons and hydrogen atoms) were counted for gas in the chamber and with the chamber evacuated (see Fig. 12).

With the chamber evacuated, the beam (total particles) was very well defined, cutting off at detector positions 41.58 and 41.92, corresponding to $\theta = 0.46^{o}$ and $\theta = -0.45^{o}$, if zero angle is taken to be 41.76 as previously measured. The counting rate inside these limits quickly rose above the response of the electronics. With the chamber evacuated some small reproducible peaks were found in the 2s photon, and neutral intensity. For the photon case, these results for gas out of the chamber are shown in Fig. 12. These small irregularities are probably due to reflections from the first scattered particle defining slit edges.

With argon gas at a pressure of 3.4×10^{-4}mm of Hg in the chamber, these small irregularities could not be seen. The 2s photon signal (derived from the difference of quench-on and quench-off time integrations) is shown for gas in the chamber. The shaded extremities of the peak represent

the photons from atoms which have undergone charge transfer and have been scattered out of the direct beam. These represent only about 7% of the total. This information will be used in the photodetector calibration. The fraction of atoms formed by charge transfer and scattered out of the beam should decrease with increasing energy due to the necessity of imparting greater lateral momentum for the same angular displacement. The differential cross section varies as $1/T^2$ where T is kinetic energy. At energies above 4 keV fewer atoms will be scattered out of the beam.

From Fig. 12, the zero position of the detector assembly is seen to be 41.76 ±.01. The beam defining geometry and calibration of angular position to reading of the crank position have been mentioned. The beam defining apertures allow the maximum angular divergence, $\pm\Delta\theta$, of the beam to be $\pm 1/4^{o}$. This would allow a beam width of 0.105 inches at the second scattered particle acceptance geometry defining aperture. Since the beam incident on the beam defining apertures is nearly parallel, it is expected that the true beam width would be smaller. Fig. 12 illustrates that the full beam width (with chamber evacuated) is 0.35 turns (0.83 degrees) which is a beam width of .049 inch at this second scattered particle defining slit. The minimum beam width expected is the .040 inch diameter of the beam defining apertures.

Fig. 12

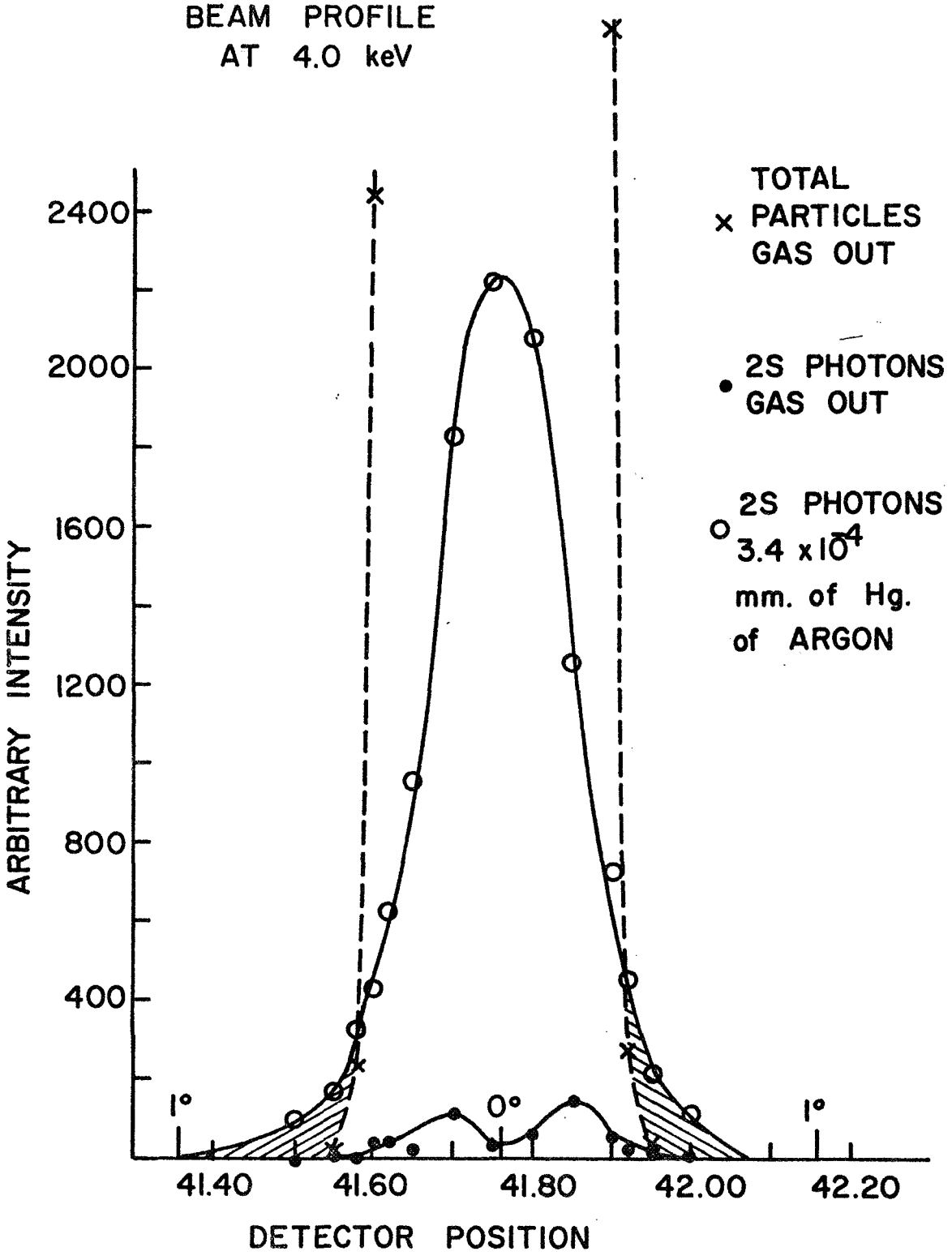
BEAM PROFILE
AT 4.0 keV
TOTAL
PARTICLES
GAS OUT
2S PHOTONS
GAS OUT
2S PHOTONS
3.4 x 10⁻⁴
mm. of Hg.
of ARGON
ARBITRARY INTENSITY
2400
2000
1600
1200
800
400
1°
0°
1°
41.40
41.60
41.80
42.00
42.20
DETECTOR POSITION

C. Photodetector.

1. General Operation.

Both the photodetector and the particle detector were electronically connected as pulse counting devices. In the case of the photodetector, the photocathode was held at ground potential while the anode of the multiplier was at positive high voltage (see Fig. 13). Pulses of charge at the anode generated a transient voltage in a 10 megohm resistor (outside the vacuum system) between the high voltage supply and anode. These voltages pulses were passed by a blocking capacitor (blocking the high voltage) to a preamplifier of the type described by Edwards[55] and referred to here as the nuvistor preamp. The only modification of the original preamplifier design being the addition of by-passing capacitors between the preamplifier bias voltage and ground, to reduce electronic noise arising from the coupling of the preamplifier to the preamplifier bias voltage supply. The output of the preamp was processed by a Hammer model NA-15 amplifier-discriminator and recorded on a scaler.

The photodetector was operated with 3000 volts applied between the photocathode and the anode. This applied voltage results in a gain for the multiplier of about 6×10^6.

Electronic noise from preamplifier operation, line

Fig. 13

SCHEMATIC OPERATION OF PHOTODETECTOR

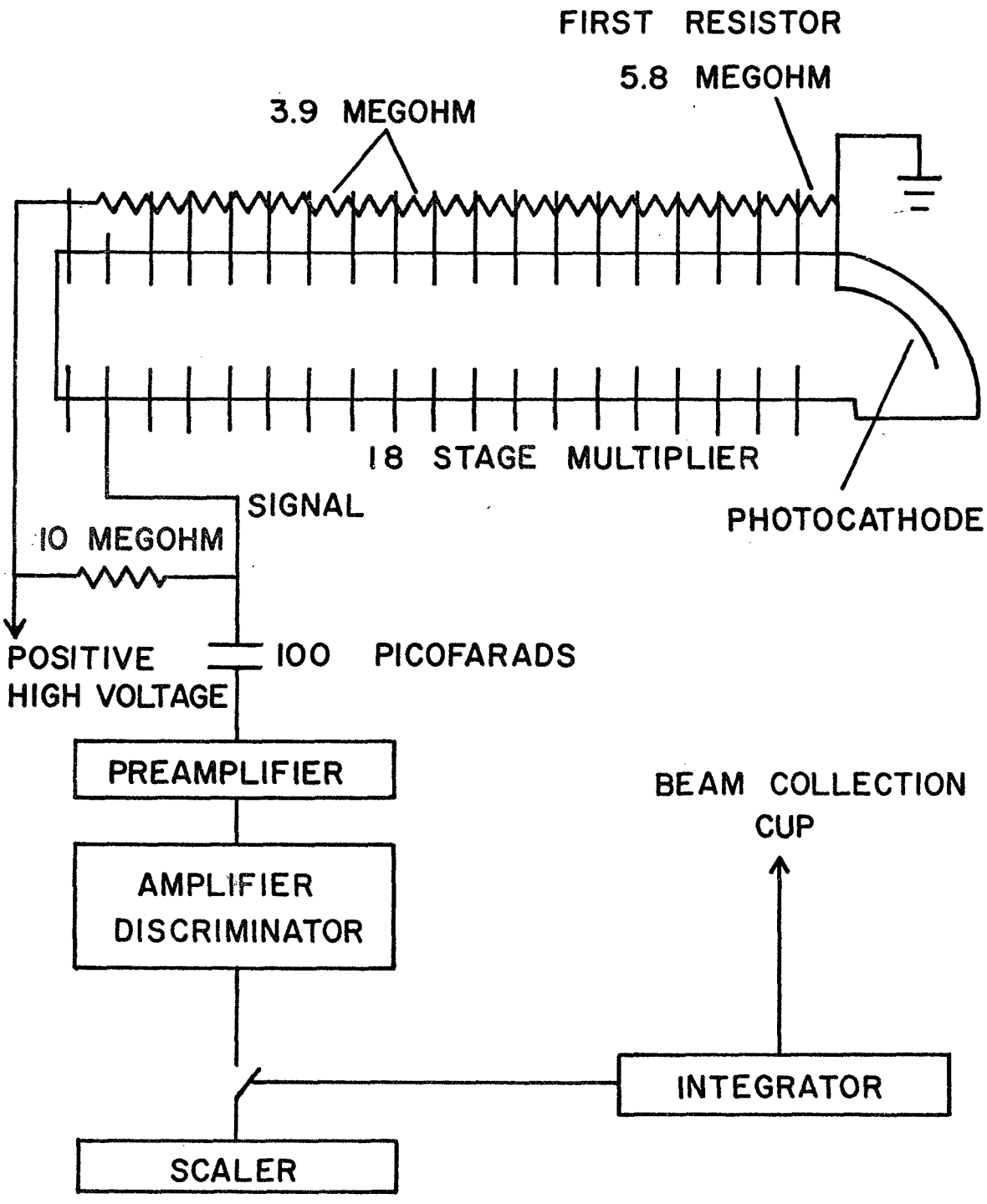

voltage transients, and other sources had to be minimized and discriminated against. In the angularly differential measurements, frequently only a few photon signal counts per minute were received. Therefore electronic noise from operation of other equipment in the laboratory had to be eliminated. To minimize these noise problems, amplification and discrimination were selected for most noise free operation rather than maximum transmission of pulses.

Fig. 14 shows the distribution of photon pulse heights after amplification. This measurement was made with 10 keV protons incident on argon target gas. The pressure in the chamber was held constant and a constant total beam charge was collected for each data point. The discrimination setting indicates the minimum pulse height (approximately in volts) which is passed by the electronics and counted. For a stable and noise free operation the amplification chosen in the NA-15 amplifier was the lower value (coarse gain 1/8, fine gain 1.0). The discriminator setting used throughout the data collection was 1.0. For this operation, the detector dark current was about 15 - 20 counts per minute being distributed in pulse height similar to signal pulses.

From Fig. 14 it is seen that for the selected operating conditions only about 2,700 of approximately 4,200 available signal counts are transmitted by the electronics.

Fig. 14

PULSE HEIGHT DISTRIBUTION
of EMR 641J PHOTODETECTOR
for 1216 Å PHOTONS

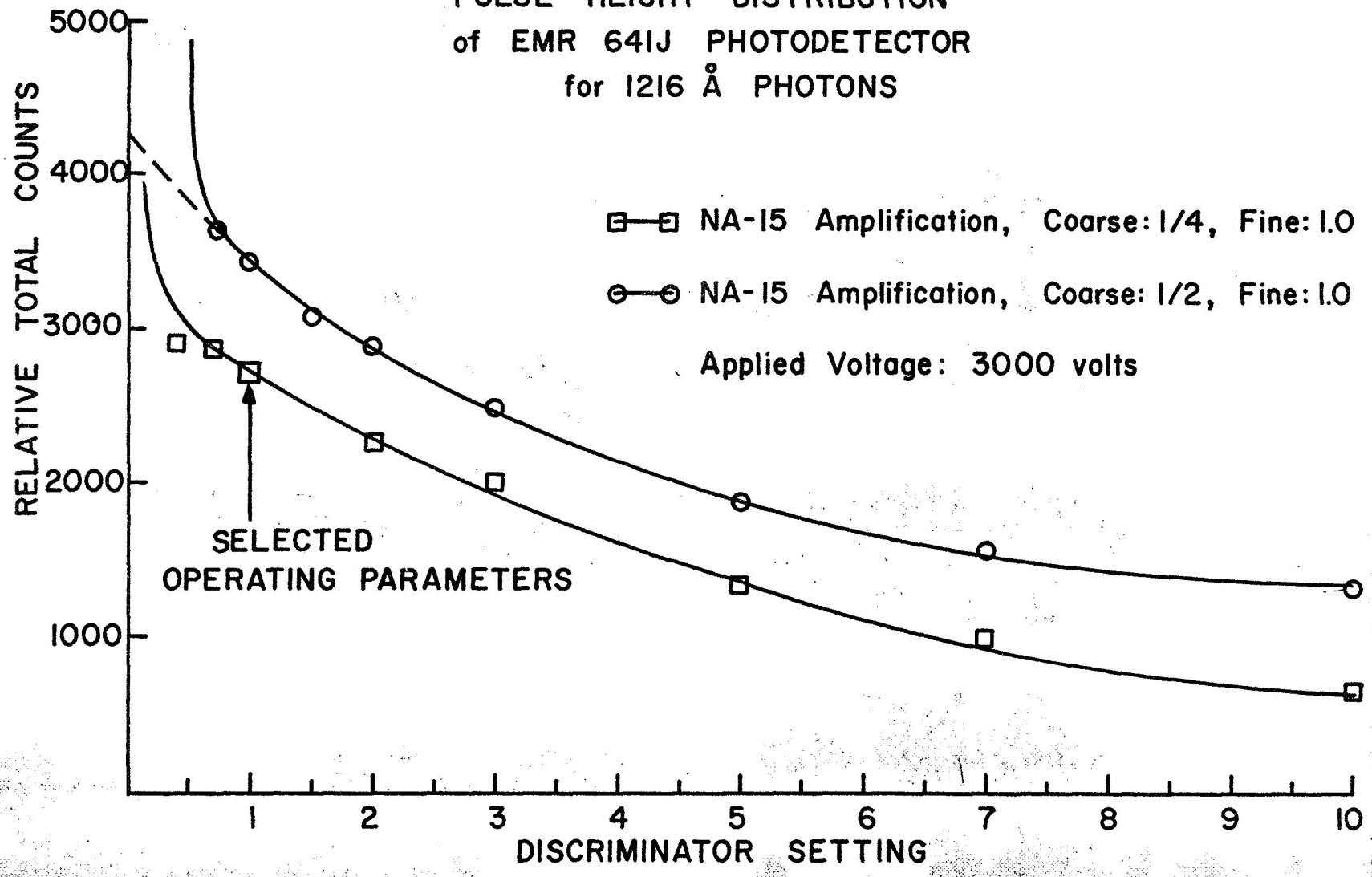

The electronics transmission factor is thus about 0.64.

Using this transmission factor along with (manufacturer's specified) photodetector quantum efficiency of 16%, the fraction of 4π solid angle viewed by the photodetector, and the 0.88 transmission factor for the tungsten wire screen between detector and the quenching region; it is possible to determine what fraction of the total available photons are counted. This factor is the ε_p defined in section III. The solid angle was taken to be the area of the specified photodetector effective opening (3/8 inch diameter) divided by the distance squared from this opening to the scattered particle beam (17/16 inch). The resulting valve for ε_p is 6.8×10^{-4}.

For several reasons, this value was not accepted as determining the quantity ε_p. The manufacturers specification of quantum efficiency is not considered satisfactory as it may change and the method and conditions of determination are not precisely known or controlled by the experimenter. In order to obtain as much of the available signal as possible the photodetector geometry is gross and not well defined. The determination of the electronics transmission factor is not precise.

2. Efficiency - Normalization to Previous Measured Total Cross Sections for Transfer to H(2s).

It was decided to establish a value for ε_p by measuring the total (all angles) cross section for charge

transfer to the 2s state of hydrogen in proton-helium collisions and normalizing the result to previously published cross sections.

This measurement was accomplished, as mentioned, by setting the detector assembly at the zero angle position, and measuring the number of forward scattered H(2s) atoms. The proton beam at the collection cup which was in place of the particle multiplier was taken as the incident beam. All atoms formed by charge transfer to the 2s state and not scattered out of this defined beam passed through the quenching region and could be detected. During these measurements the width of the first slit defining the assembly acceptance geometry was set at .040 inch.

The length of target gas, in which charge transfer takes place, must be specified for total transfer measurements. This length was measured to be 2.42 inches. Effusion of the gas through the incoming beam aperture and the opening into the detector assembly can result in an effective addition to this length. This effusion is not expected to extend beyond approximately the diameter of the openings[56,57]. This addition gives an effective length of 2.50 inches (6.30 cm).

The measured total cross section for 2s charge transfer for protons on helium was normalized to the results of Jaecks, et al[31] and Andreev, et al[33], at the incident

energy of 16 keV where the two published measurements are in best agreement. (Available results of Colli, et al[22] and Dose[58] have not been used due to questionable normalization and the results of Ryding, et al[59] are out of the present energy range.) The result is illustrated in Fig. 15. This single point normalization was chosen over a many point normalization which could have compensated for any systematic errors. The value obtained, by this normalization, for ε_p is 6.4×10^{-4} (within 6% of the value of 6.8×10^{-4} obtained using quoted quantum efficiency for the detector and other measured quantities).

The cross section for transfer to the 2s state of hydrogen from proton-argon collisions was also measured. Using the normalization determined from the helium measurement, the argon results are compared to other published results (including those of Bayfield[60]) in Fig. 16. The results show favorable consistency, since all of the present data are within the absolute errors quoted by the previous investigators.

In both helium and argon cases the slope of the cross section as a function of impact energy appears slightly greater for the present data than for other measurements. The present data has been corrected for the changing with particle velocity of the fraction of total 2s atoms decaying within the length of quenching region viewed by the photodetector. This correction has an adverse effect on the slope disagreement (Appendix A).

Fig. 15

TOTAL CHARGE TRANSFER TO H(2s)

$H_1^+ + He \rightarrow H(2s) + He^+$

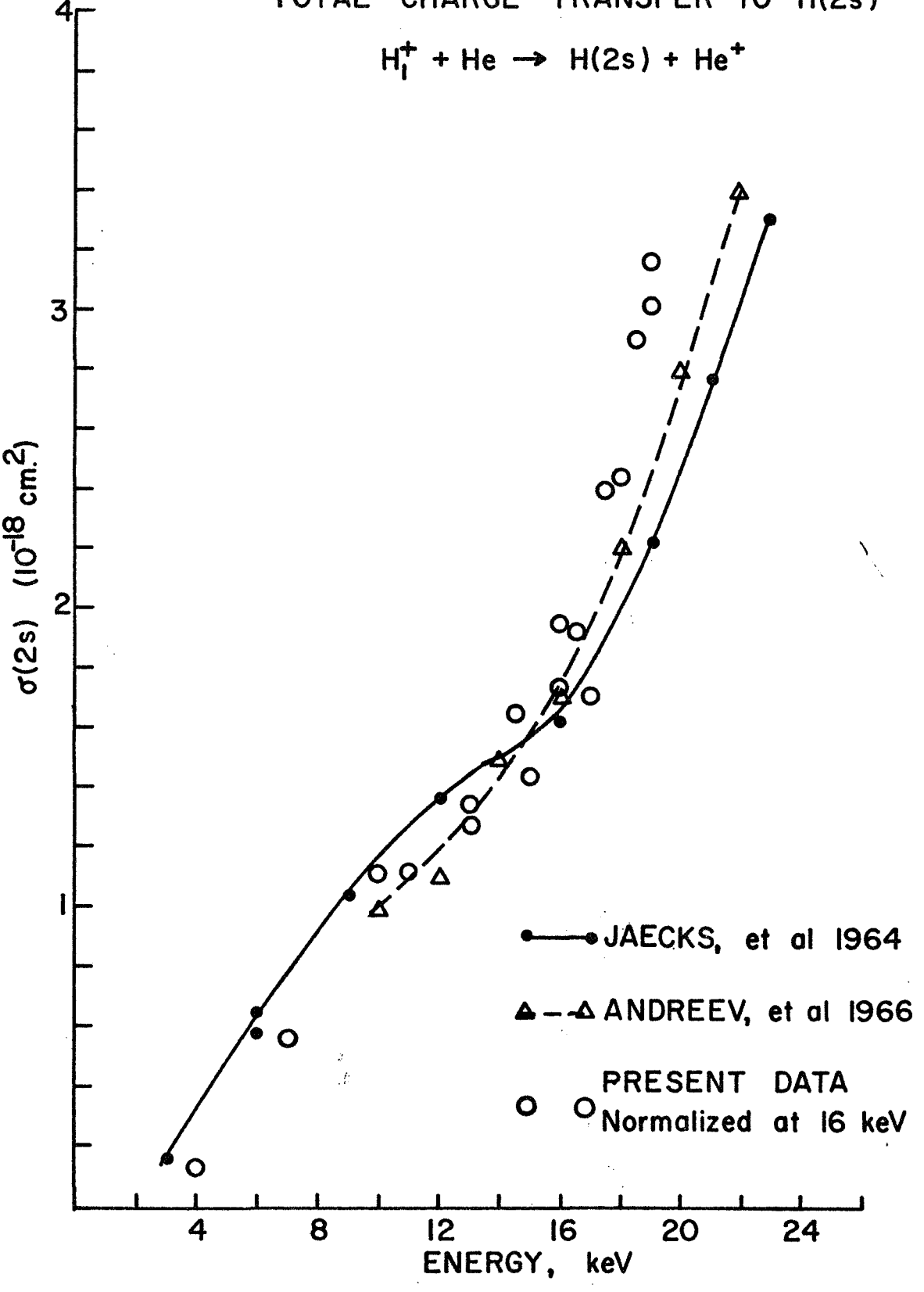

Fig. 16

TOTAL CHARGE TRANSFER TO H(2s)

$H_1^+ + Ar \rightarrow H(2s) + Ar^+$

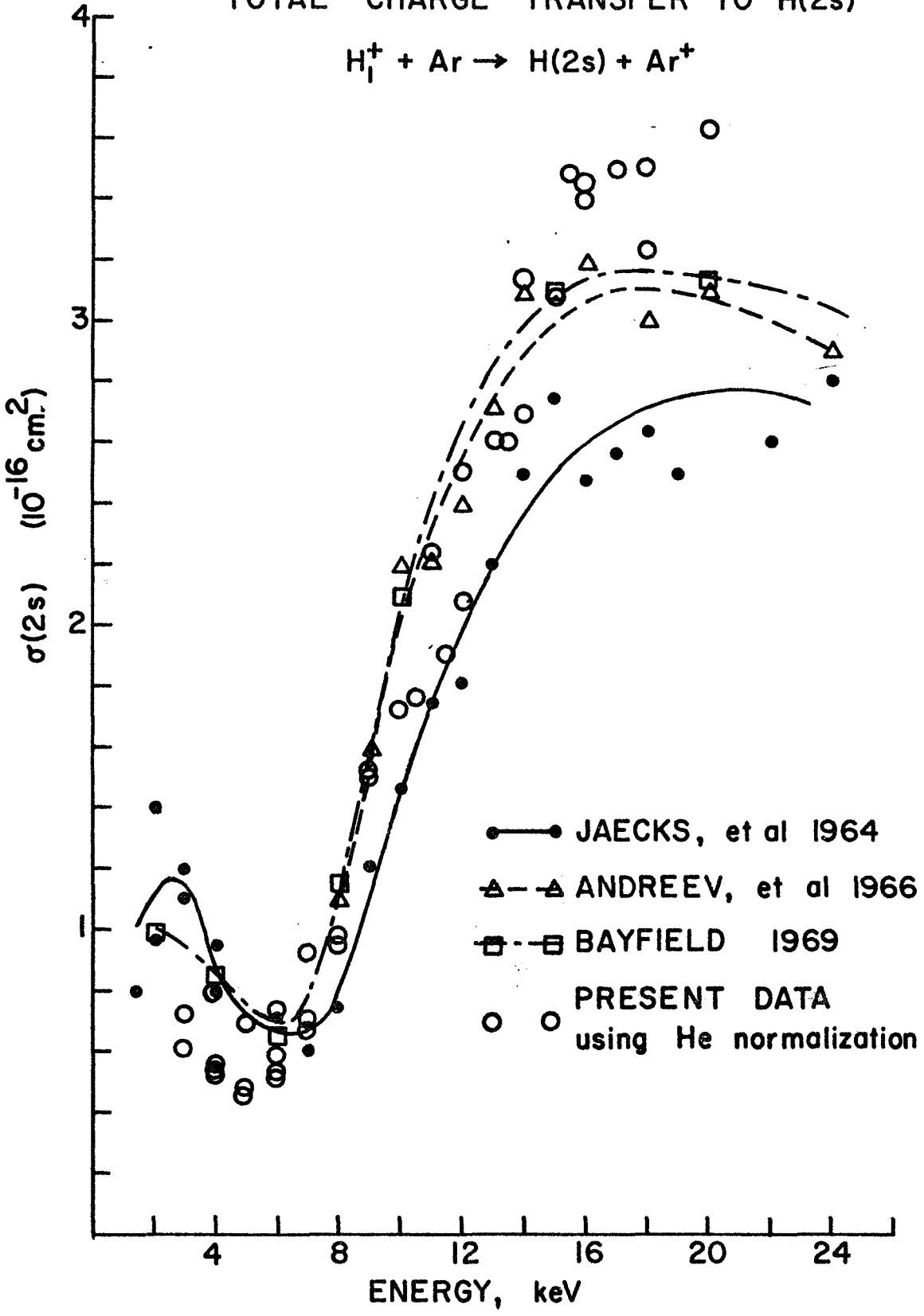

There are additional possible sources of systematic error in the normalization which are more ellusive and for which correction has not been made. These include: 1. differences between the several investigators in the polarization of the quench induced radiation (Appendix B), 2. quenching of radiation before the viewed region due to extension of the quench field through the scattered particle acceptance hole (Appendix A), 3. differences between present and previous investigators in contribution of cascade from higher hydrogen states to the 2s state (Appendix C), 4. the loss of atoms scattered out of the beam in the present experiment.

Because of normalization, any errors in the present data which do not change with energy or angle will not appear in the results for any measured quantities depending on photon detection. However, an error in measurement of total cross section for transfer to H(2s) which does not appear in the differential (in angle) measurements will lead to an error in the quoted magnitude for P_{2s} and $\frac{d\sigma_{2s}}{d\Omega}$. The error due to failure to count atoms which undergo transfer and are scattered out of the primary beam is such an error.

The fraction of hydrogen atoms formed in the 2s state by transfer and scattered out of the beam has been established to be about 7% for protons on argon at 4 keV.

As mentioned, this fraction is a maximum at low energies because of the $1/T^2$ (T is energy) dependence of the differential crsos section. Since the charge transfer fractions, P_o and P_{2s}, are smaller for helium than for argon, the fraction charge transfered and scattered out of the beam should be smaller for helium than for argon. Thus the fraction of atoms formed by charge transfer and scattered out of the beam is at most about 7%. Since the normalization of the total cross section for transfer to H(2s) is at 16 keV, the error in the photodetector normalization constant may be expected to be about 3 - 4%. This error has been neglected.

Two of the other sources of systematic error could have an influence on the magnitude of the photodetector normalization constant. The polarization of the quench induced radiation is discussed in Appendix B. This polarization will affect the measured values of cross sections. The polarization in the present data should be nearly the same as that of Andreev, et al[33] which was used for normalization. The polarization of the data of Jaecks, et al[31] has not been determined, but the normalization is at a point where the total cross section for transfer to H(2s) agrees with that of Andreev, et al. No correction of the normalization for polarization has been made. The calculations of appendix B indicate that there may be an overall error of 8% in the cross sections

of Andreev, et al used as normalization standards as well as in all of the present H(2s) data. The difference, between present work and that used for normalization in the contribution of cascade to the population of H(2s) at the detector is discussed in Appendix C. The estimated difference is about 2 to 3%. This error has also been neglected.

Some of the possible systematic error sources could have a small effect on the slope of the present data (as a function of Energy). The change with energy of the fraction of H(2s) scattered out of the primary beam could affect the slope of the total cross sections for transfer to H(2s), but only by about 3 - 4%. (The differential-in-angle measurements would not be affected.) The loss of H(2s) due to prequenching by the electric field extending through the entrance aperture of the quenching capacitor is estimated in Appendix A. Again the possible change in the fraction lost with varying energy, should only be about 4%. (In this case the differential measurements would be affected in the same way.) These small errors affect the slope of the total cross section for transfer to H(2s) in the same direction- greatest loss at lowest energies. However, the slope discrepancy introduced will not be quite as large as the apparent discrepancy between present and previous investigators (Figs. 15 and 16).

Even though this difference in slope of the cross sections may lead to similar error in the measurements of

differential transfer to the 2s state, the problem is not considered to be serious. The stated absolute value of the various measurements used for normalization and comparison are: ±40% by Jaecks, et al; ±20% by Andreev, et al; ±55% by Bayfield. The differences between present data and previous investigators are within these errors throughout the region. Further, the discrepancy between present data and that of other investigators is not significantly different from the discrepancies among the other investigators.

The absolute uncertanty of the value of ε_p is taken to be about 30% in accord with errors stated by the previous investigators.

Two different photodetectors, of the same model, were used in the course of the experiment. All of the total 2s transfer cross section measurements were made with the first detector and preliminary differential 2s cross sections were measured and reported[61] with this first detector. (These reported preliminary measurements were not corrected for any of the quench related errors.) After a loss of vacuum accident, this first detector deteriorated and had to be replaced. The second detector was used to take all of the differential measurements reported here and was normalized to the measurements made with the first detector. The values of ε_p mentioned above, are all for this second photodetector.

The efficiency of the photodetectors used was stable

throughout the data collection period except for an abrupt change in the apparent efficiency of the second photodetector. This change occurred suddenly and definitely appearing as an apparent change in ε_p from 6.4×10^{-4} to 4.8×10^{-4}. An attempt was made to trace this change to electronic failure in preamplifier, amplifier, or discriminator. It was finally decided that the change was a real change in the photodetector. The detector continued to operate in a consistent manner for several months after this change, and with the adjustment of ε_p gave results consistent with those previously obtained.

D. Particle Multiplier Characteristics.

1. General Operation.

The electronic arrangement for the particle multiplier was identical to that of the photodetector (Fig. 13). This multiplier has 13 stages with particles incident directly on the first dynode of the multiplier. The voltage divider resistors used were one megohm, but all other components in the particle detection channel were duplicates of those in the photon detection channel. The integrator controlled collection of data in both channels simultaneously.

The gain of the particle multiplier is not precisely known but was considerably less than that of the photodetector. The pulses from the particle multiplier were less favorably distributed in amplitude than the photon pulses, being grouped at small amplitudes. The pulse height dis-

tribution changed with time, as illustrated in Fig. 17. This change is indicated by the steeper slope of the pulse height curves, even with increased electronic amplification or increased applied voltage.

This deterioration may have been due to several factors. The bare multiplier was exposed to atmosphere for a total time of approximately 10 hours during installation and periods when the vacuum system was open for modifications. Prolonged exposure is known to alter the multiplier dynode surfaces. The bare multiplier in the chamber was exposed to minor changes in environment from use of various target gases, but it was in a vacuum of 1×10^{-4}mm of Hg or lower throughout the data collection period. The multiplier was continuously exposed to count rates near 50 kHz for periods of several days. For brief periods the multiplier was exposed to even more intense signal, for instance during checks of beam profile or zero angle position. Use of the multiplier was intermittent between June and October of 1969 when most of the change in pulse height distribution occurred. Between October 1969 and April 1970, when most of the presented data was collected, the multiplier was used approximately 60 hours per week. However, during this heavy use period the pulse characteristics were reasonably stable so that the apparent multiplier efficiency was constant.

The nuvistor preamp and model NA-15 amplifier were

Fig. 17

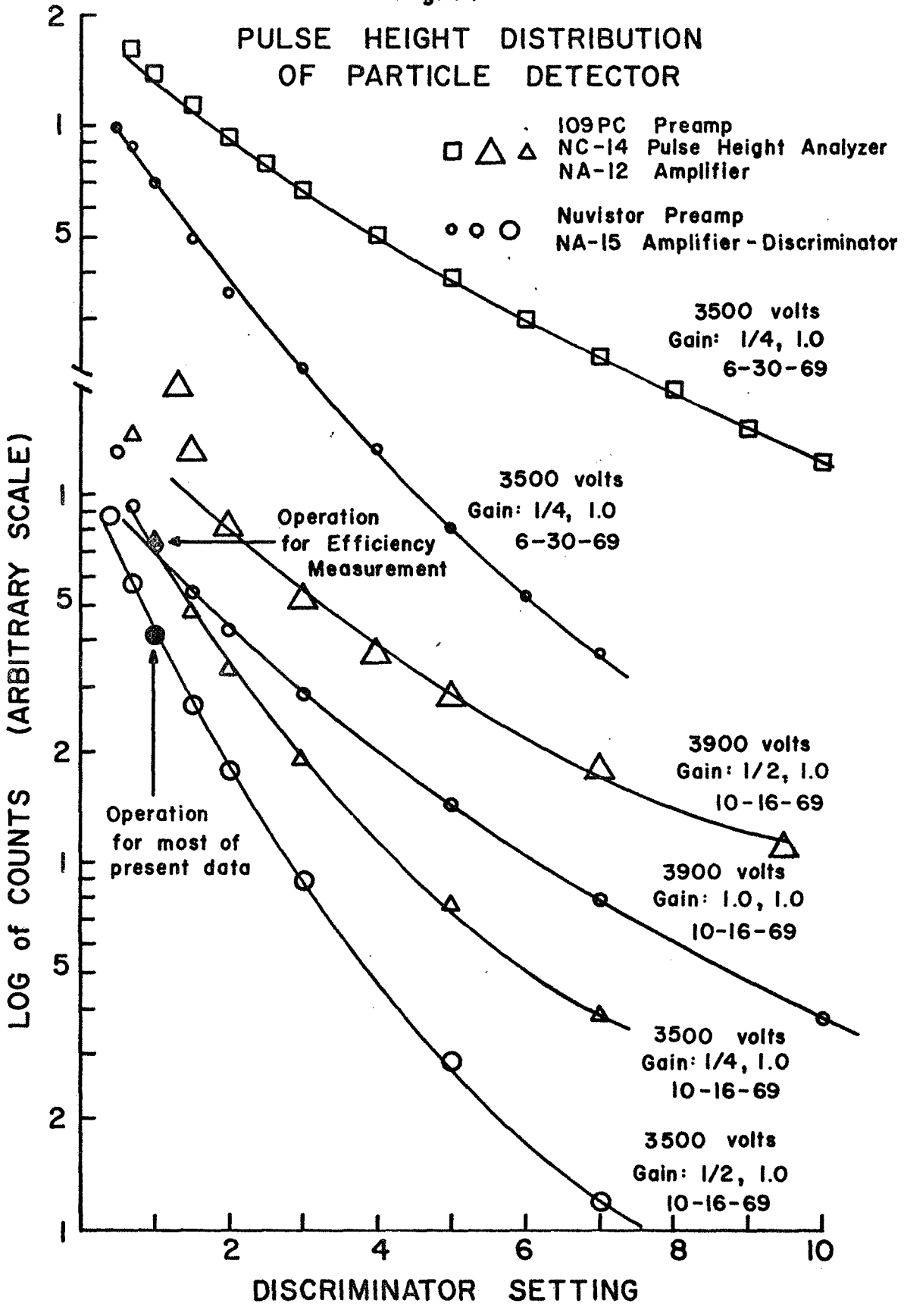
PULSE HEIGHT DISTRIBUTION
OF PARTICLE DETECTOR
109PC Preamp
NC-14 Pulse Height Analyzer
NA-12 Amplifier
Nuvistor Preamp
NA-15 Amplifier - Discriminator
3500 volts
Gain: 1/4, 1.0
6-30-69
3500 volts
Gain: 1/4, 1.0
6-30-69
Operation
for Efficiency
Measurement
3900 volts
Gain: 1/2, 1.0
10-16-69
3900 volts
Gain: 1.0, 1.0
10-16-69
3500 volts
Gain: 1/4, 1.0
10-16-69
3500 volts
Gain: 1/2, 1.0
10-16-69
Operation
for most of
present data
LOG of COUNTS (ARBITRARY SCALE)
DISCRIMINATOR SETTING
2
1
5
2
1
5
2
1
2
4
6
8
10

used for the present data. The operating parameters, applied voltage and selected amplification and discrimination, are indicated on Fig. 17.

During the entire period, the same multiplier with different pulse processing electronics was used by R. H. McKnight in measurement of the quantities P_{2p} and $\frac{d\sigma 2p}{d\Omega}$ for charge transfer to the 2p state of hydrogen as well as P_o and $\frac{d\sigma total}{d\Omega}$. This experiment required measurement of photons from the collision center in coincidence with the fast scattered atoms formed by charge transfer. The timing requirements of the coincidence technique dictated the nature of the pulse handling electronics (see ref. 50). Pulse height distribution with the electronics of this experiment are shown in Fig. 17, for comparison and because these electronics were used in the measurement of the particle multiplier efficiency.

2. Efficiency.

A unique method of measuring the particle multiplier efficiency was used[62]. The technique employs a coincidence measurement between the photons from the quenched 2s atom and resulting ground state hydrogen atoms. This technique is similar to that used by Christofori, et al[63] (generalized by Sheridan[64]) employing photon-photon coincidence to measure efficiency of photodetectors. For the present apparatus arrangement (Fig. 8), all of the particles passing through the quenching region strike the particle multiplier. Those atoms in the 2s state which emit a detected photon

must also strike the particle multiplier. If an atom which emitted a detected photon is counted by the multiplier, the two pulses will have a definite time relationship and can drive a standard coincidence module. The ratio of coincidence counts to total photon counts for the same collection period is a direct measure of the efficiency of the particle multiplier for detection of hydrogen atoms.

Using this coincidence technique, the efficiency of the particle multiplier was measured as a function of incident proton energy. The schematic arrangement of the coincidence circuitry is shown in Fig. 18. The pulse processing electronics used were those of the coincidence experiment for measurements of the 2p state. The electronic parameters were set as indicated in Fig. 17. The number of photons from the 2s state was determined from the difference of two runs, one with the quench capacitator at high voltage and one with it grounded. The numbers of accidental and accidental plus real coincidences were also appropriately subtracted. (The accidental rate was quite small since the total signal in the photon channel was small.) Several angles of scatter were used, but the variation of multiplier efficiency was found to be a function of particle velocity only, as expected.

The results are presented in Fig. 19. The coincidence measurement of efficiency is, naturally, for neutral hydrogen atoms only. As a check, the efficiency was determined by a separate technique. From the total particle

Fig. 18

SCHEMATIC FOR COINCIDENCE MEASUREMENT OF PARTICLE MULTIPLIER EFFICIENCY

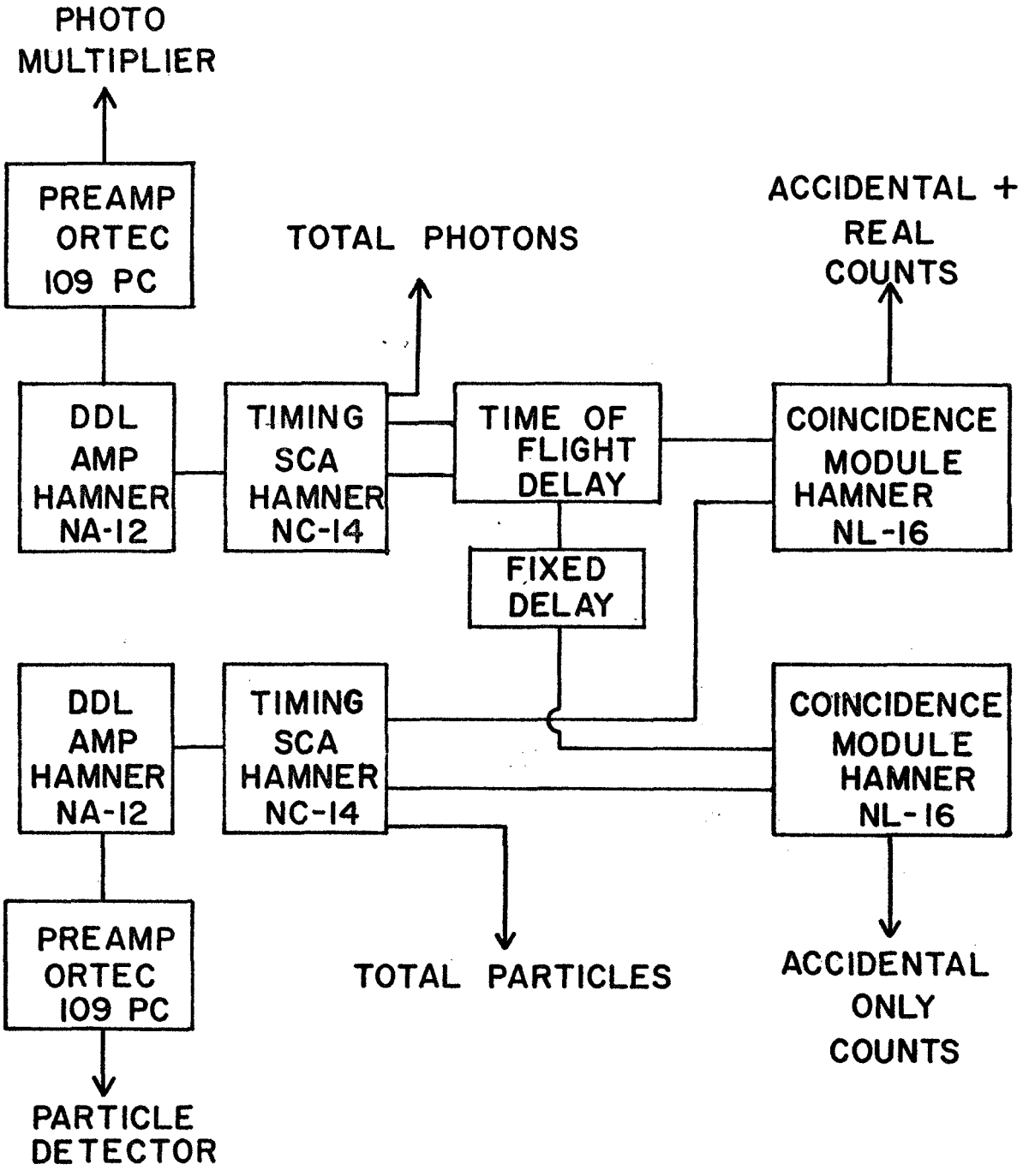

Fig. 19

EFFICIENCY OF MULTIPLIER

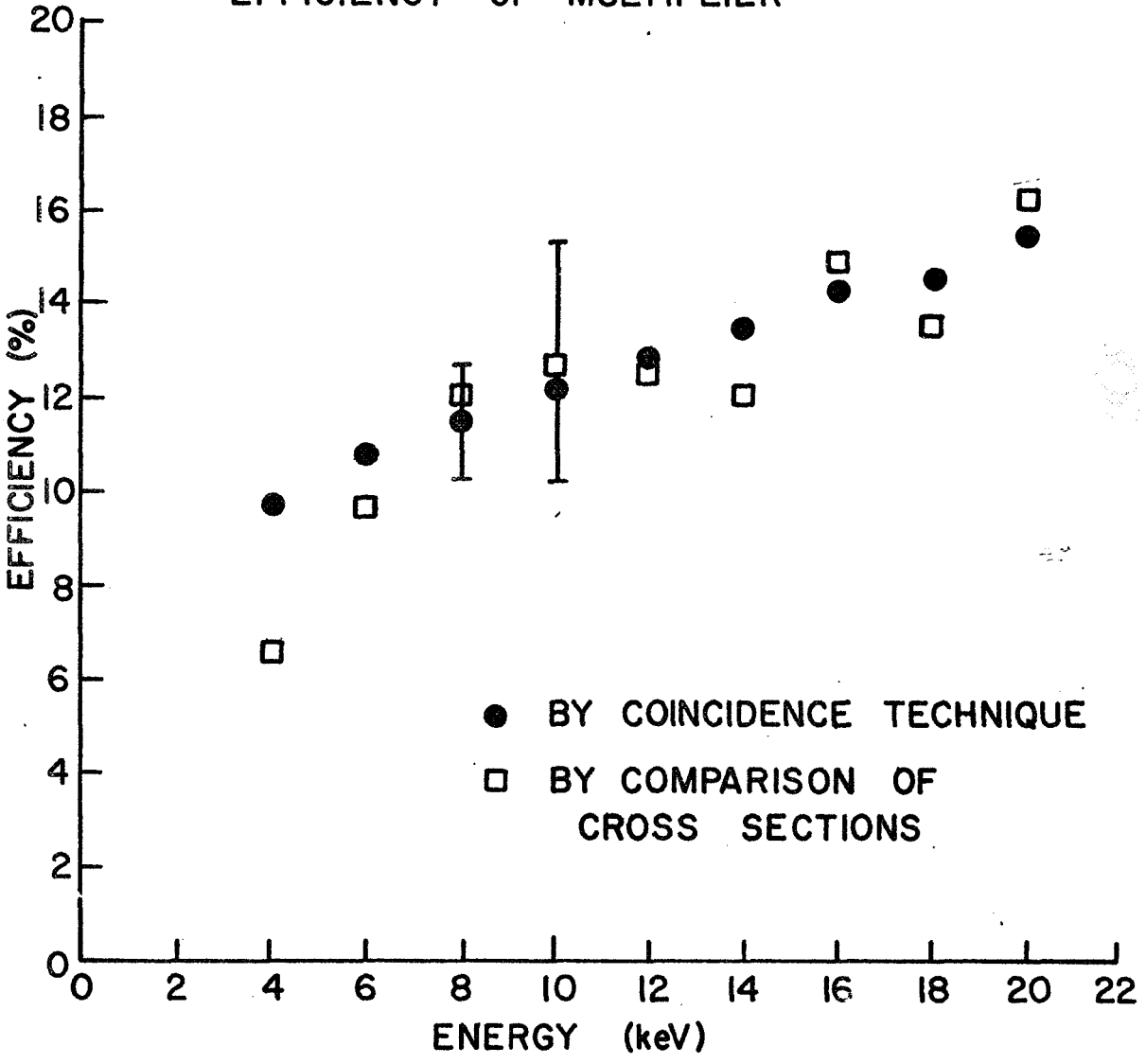

counts (protons plus hydrogen atoms) which were collected during the efficiency measurements, the total scattering differential cross section can be obtained for each angle and energy. This cross section can also be obtained from classical scattering theory such as presented in section II. Using the calculated cross section obtained from the work of Dose[10], the apparent particle detector efficiency for detecting the mixture of protons and hydrogen atoms (scattered from protons on argon) was obtained from the ratio of measured to calculated differential cross sections. These results are also shown on Fig. 19.

Experimental error is represented by the error bars. In the coincidence measurement of the efficiency the only errors are in the electronic losses and statistical uncertainty of the subtraction process. The coincidence measurement has been corrected by 15% for pulse losses due to pile up of counts at the high count rates used (near 100 kH_z), and for "flattopping" of pulses which destroys the cross over timing fidelity. The efficiency determined by comparing the scattered particle intensity with that predicted by classical theory involves experimental errors in target gas pressure, beam collection, and geometry. No error for the classically calculated cross section has been included. The value of the coincidence measurement of efficiency is its independence of any other measured or calculated quantity.

The excellent agreement of the two independent measurements gives credence to the coincidence technique. The agreement also supports the assumption that the efficiency of such detectors is the same for hydrogen atoms and protons of the same velocity, since the measurement by comparison of cross sections is for detection of a mixture which averages slightly more protons than atoms. This equality of detection efficiency has been assumed and substantiated in experiments such as those by Everhart, et al[65] and is supported by other investigations of surface quantum efficiency for production of secondary electrons by atoms and ions in various charge states[66].

The efficiency results for this particular multiplier are considerably lower than the 80 - 100% values frequently assumed or measured for such detectors. The values obtained may be influenced by the peculiar construction and history of this particular detector.

The problem in the present experiment was not to obtain high efficiency, but rather to limit the particle channel count rates to levels which could be handled by the electronics. The electronics used for measurement of primary quantities (P_o, P_{2s}, $\frac{d\sigma_{2s}}{d\Omega}$, $\frac{d\sigma_{total}}{d\Omega}$) began to drop counts due to pile up at a counting rate of about 50 kH_z; all data reported is for count rates lower than 40 kH_z. The coincidence electronics began to drop significant numbers of counts near 70 - 80kH_z, but could be operated

with corrections at rates up to 100kHz.

A conflict arises in the measurement of P_{2s} by the method employed. When the count rate in the photon channel is sufficiently high for ease of measurement, the count rate in the total scattered particle channel is too high to be handled by the electronics. An electronically manageable particle count rate will correspond to a higher photon count rate for lower particle counting efficiency. Thus the conflict is reduced by low counting efficiency, such as that for the multiplier used. Low counting efficiency is desirable in this experiment, as long as that efficiency is well known.

Since different preamplifiers, amplifiers, and discriminators were used for measurement of primary quantities (P_o, P_{2s}, $\frac{d\sigma_{total}}{d\Omega}$) than for measurement of the particle multiplier efficiency, it was necessary to determine the relationship between the two sets of electronics for the number of pulses transmitted. In order to find this relationship, the number of scattered particles was measured with the multiplier supplying pulses to each set of electronics. All other experimental parameters (pressure, number of incident protons, etc.) were held as nearly constant as possible between trials with the two different sets of electronics. With this procedure, the efficiency of the multiplier with the electronics used in measurement of primary quantities was established to be

0.486 of the efficiency determined by the coincidence technique. The accuracy of the final efficiency values used to calculate P_{2s} and $\frac{d\sigma_{total}}{d\Omega}$ is estimated to be ±10%.

V. RESULTS AND DISCUSSION.

A. Total Differential Scattering.

Figures 20 - 24 show comparisons of present experimental results and classical calculations from work of Bingham[7] and Dose[10] for total differential scattering of protons from helium and argon. These cross sections are for the total scattering including elastic, inelastic and charge changing processes.

The measurements were made in three different modes; with the scattering angle fixed, with the incident energy fixed, and with the product of incident energy and scattering angle fixed. With the scattering angle fixed, the impact parameter varies with changing incident energy. With the impact energy fixed, the impact parameter varies with scattering angle (for this mode the values of impact parameter displayed are obtained from the work of Dose[10]). With the product of scattering angle and incident energy (θT) fixed, the impact parameter is nearly constant. This last mode is best suited for analysis of the physical problem.

The background (gas-out of chamber) signals for total scattering were typical of background signals of all measured quantities. Background signals were relatively higher for helium cross sections than for argon, since the actual (gas-in) scattering is much smaller due to the smaller cross sections. For argon the gas-out signal was

usually less than 2% of the measured signal and always less than 5% for data collected as described at the end of section III. For helium at angles less than 2.5° the total scattering background was frequently as high as 10 - 15% and varied somewhat with beam focusing. As previously mentioned much of this background was attributed to scattering from the first geometry defining slit. For helium at angles less than 2.5°, background was always subtracted.

The accuracy of the total differential scattering cross sections are influenced by the following factors: target gas pressure, particle multiplier efficiency, solid angle of acceptance geometry, beam collection efficiency, angle setting accuracy. These factors have all been discussed in sections III. and IV. The square root of the sum of the squares of these contributing factors gives an estimate of ±15% for the absolute error in these cross sections for scattering angles greater than 2.0°. Below 2.0° the angle setting and beam collection become more sensitive. At these small angles additional problems of scattering of direct beam from the first geometry defining slit and large variation of the cross section over the range of acceptance angles contribute to the error (see section III.). The absolute accuracy of these total scattering cross sections is estimated to be ±30% for scattering angles between 1 and 2 degrees. The error bars displayed on the figures are standard deviations of six or more trials of a particular data point and thus

represent reproducibility only.

Figure 20 displays the differential cross section for transfer to H(2s) as well as the total differential scattering cross section from protons on argon at θT = 20 keV·Deg. Measurements for both positive (left of zero) and negative (right of zero) scattering angles are shown. The consistent positive to negative difference in measured cross section was used to construct a correction factor for the remainder of the data which was taken at positive scattering angles only (see section III.).

The values for both of the classical calculations shown on the figures required graphing the published results and extrapolating between calculated points to obtain cross sections for the particular values of θ and T desired. The accuracy of this process is estimated to be ±5%.

The cross sections calculated from the work of Bingham and Dose have been transformed from the center of mass reference to laboratory system in the case of helium. In the argon case, the difference in the cross sections between laboratory and center of mass systems is less than 3% and has been neglected.

For the argon target, there is a substantial difference between the classical calculations assuming a single exponential screening factor (Bingham) and the calculation assuming several shells of electronic charge and separate

screening factors for each (Dose). In every case, for argon, the data is in better agreement with the calculation assuming electronic shells than with the calculation with one screening factor (Bingham). This is particularly apparent in the data taken at a constant angle, 3^{o}, (Fig. 22).

For helium, with only one shell, it is expected that the two classical calculations should be in close agreement. Figures 23 and 24 show this to be the case and the agreement with the present experiment is also good except at largest impact parameter (smallest θT). For Fig. 24 the values of impact parameter are .450, .255, .138, .094, and .057 atomic units for the corresponding θT values of 5, 10, 20, 30, and 50 keV·deg. displayed.

Surprisingly no other experimental results were found for protons on helium or argon in this range of energy and scattering angle. Similar work for other projectiles and energies has been done (e.g. see references 67, 68, and 69) and with proton projectile, some work has been done at other energies and angles (e.g. see references 70, 71).

Fig. 20

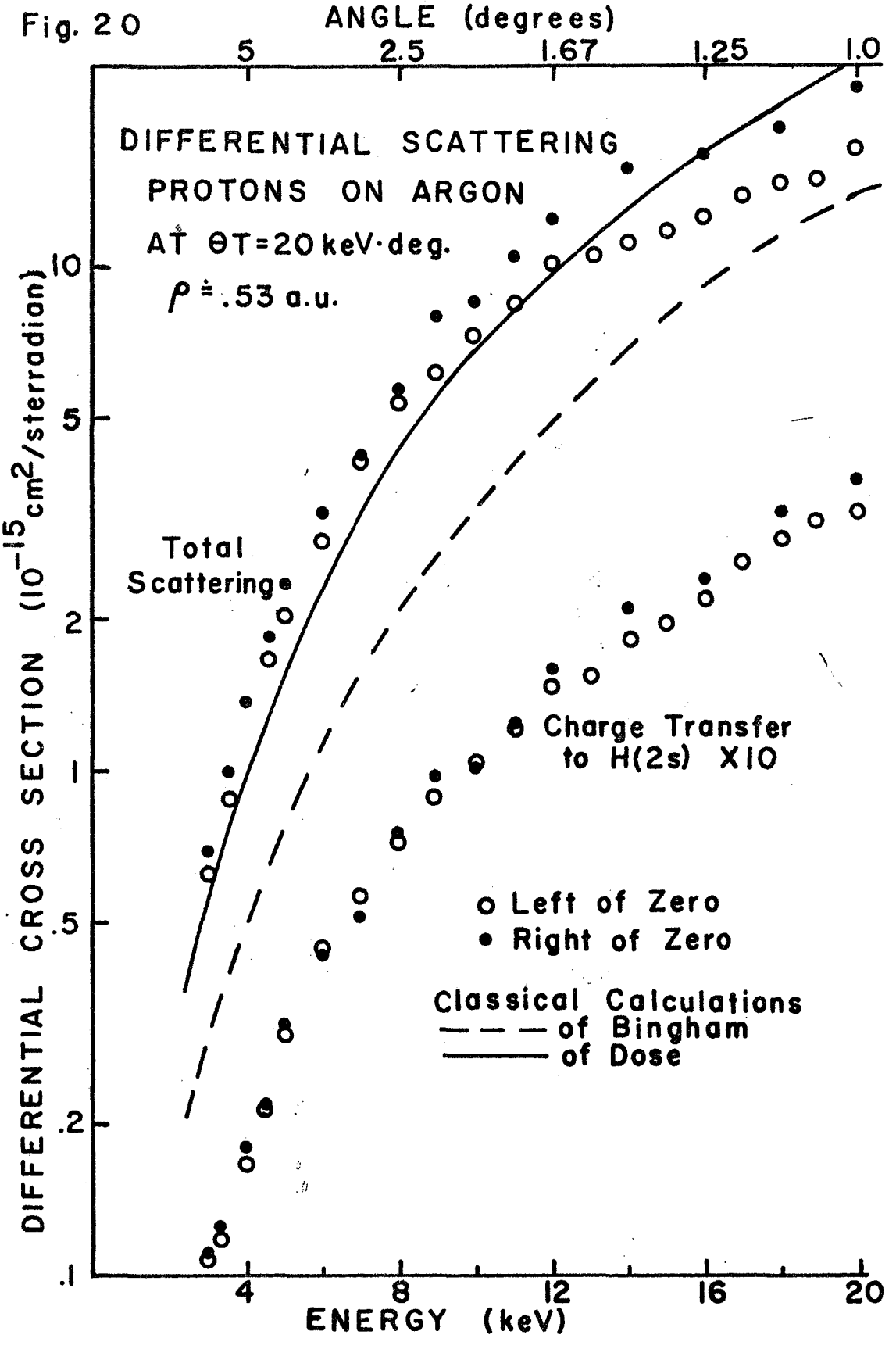
ANGLE (degrees)
5
2.5
1.67
1.25
1.0
DIFFERENTIAL SCATTERING
PROTONS ON ARGON
AT θT=20 keV·deg.
ρ ≐ .53 a.u.
Total Scattering
Charge Transfer to H(2s) X10
Left of Zero
Right of Zero
Classical Calculations
of Bingham
of Dose
DIFFERENTIAL CROSS SECTION (10⁻¹⁵ cm²/sterradian)
10
5
2
1
.5
.2
.1
4
8
12
16
20
ENERGY (keV)

Fig. 21

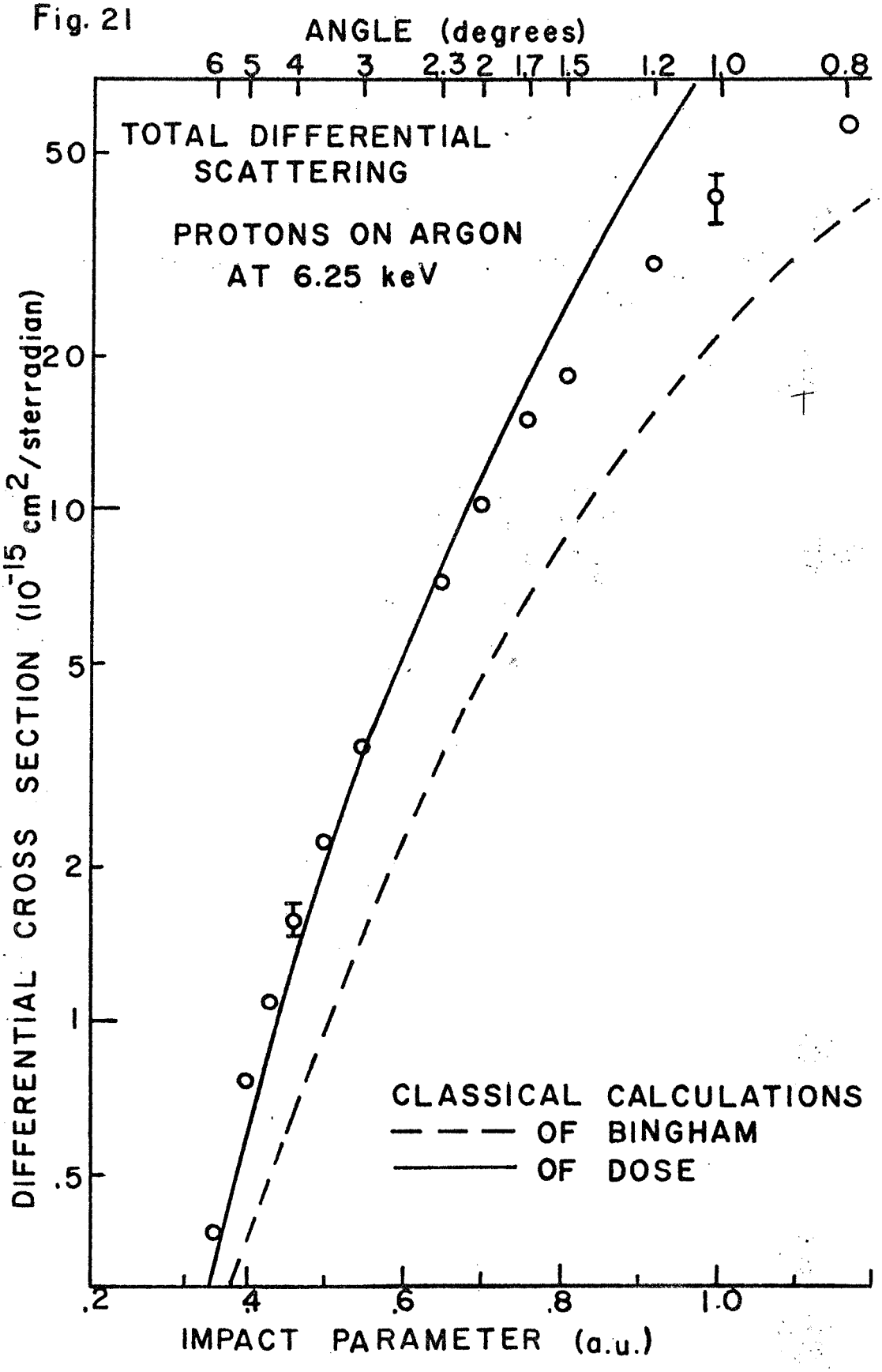
ANGLE (degrees)
6 5 4 3 2.3 2 1.7 1.5 1.2 1.0 0.8
TOTAL DIFFERENTIAL SCATTERING
PROTONS ON ARGON AT 6.25 keV
DIFFERENTIAL CROSS SECTION (10^{-15} cm^2/sterradian)
50
20
10
5
2
1
.5
CLASSICAL CALCULATIONS
— — — OF BINGHAM
——— OF DOSE
.2 .4 .6 .8 1.0
IMPACT PARAMETER (a.u.)

Fig. 22 TOTAL DIFFERENTIAL SCATTERING
PROTONS ON ARGON
AT 3.0° LABORATORY

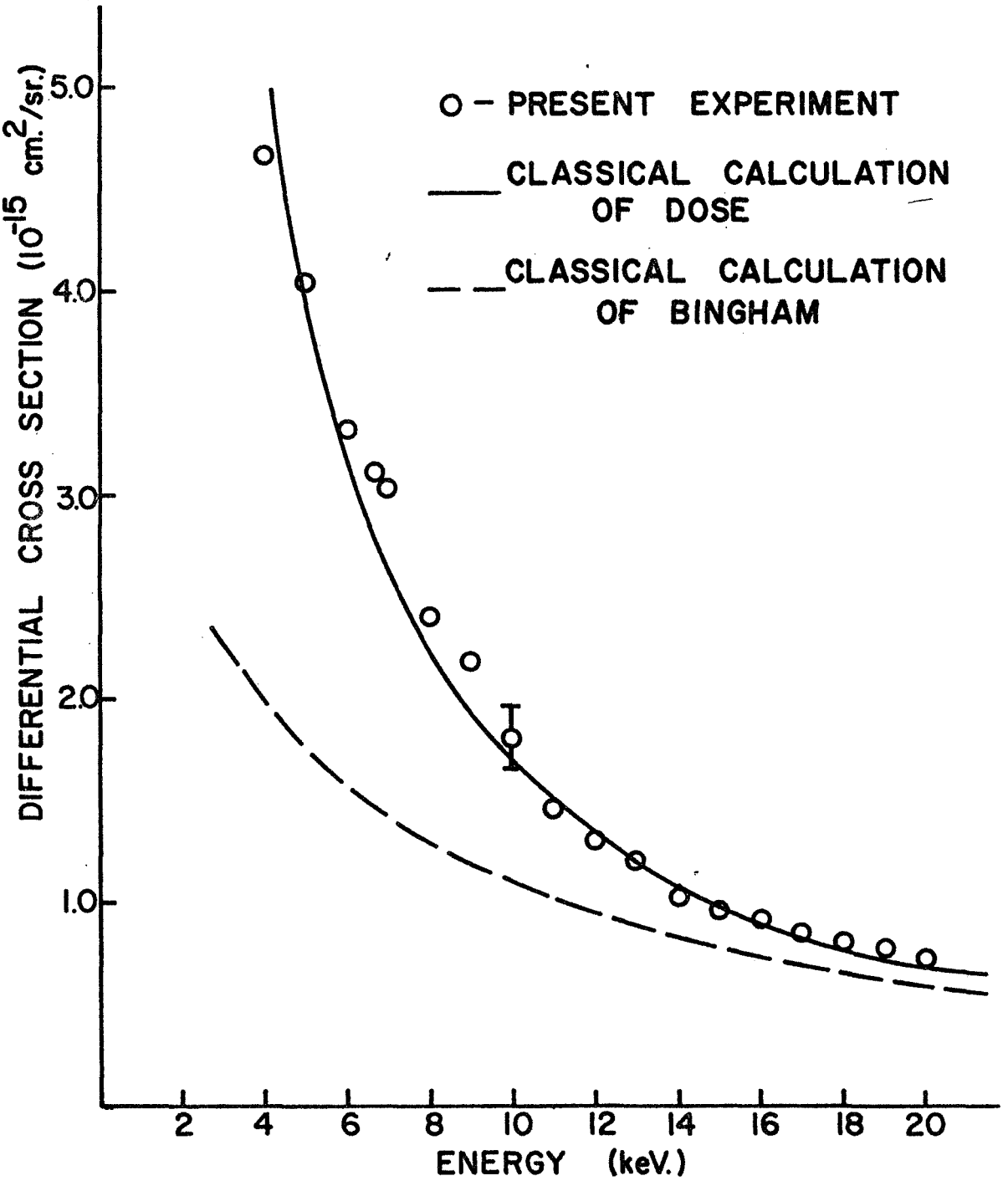

Fig. 23

TOTAL DIFFERENTIAL SCATTERING
PROTONS ON HELIUM
AT 6.25 keV.

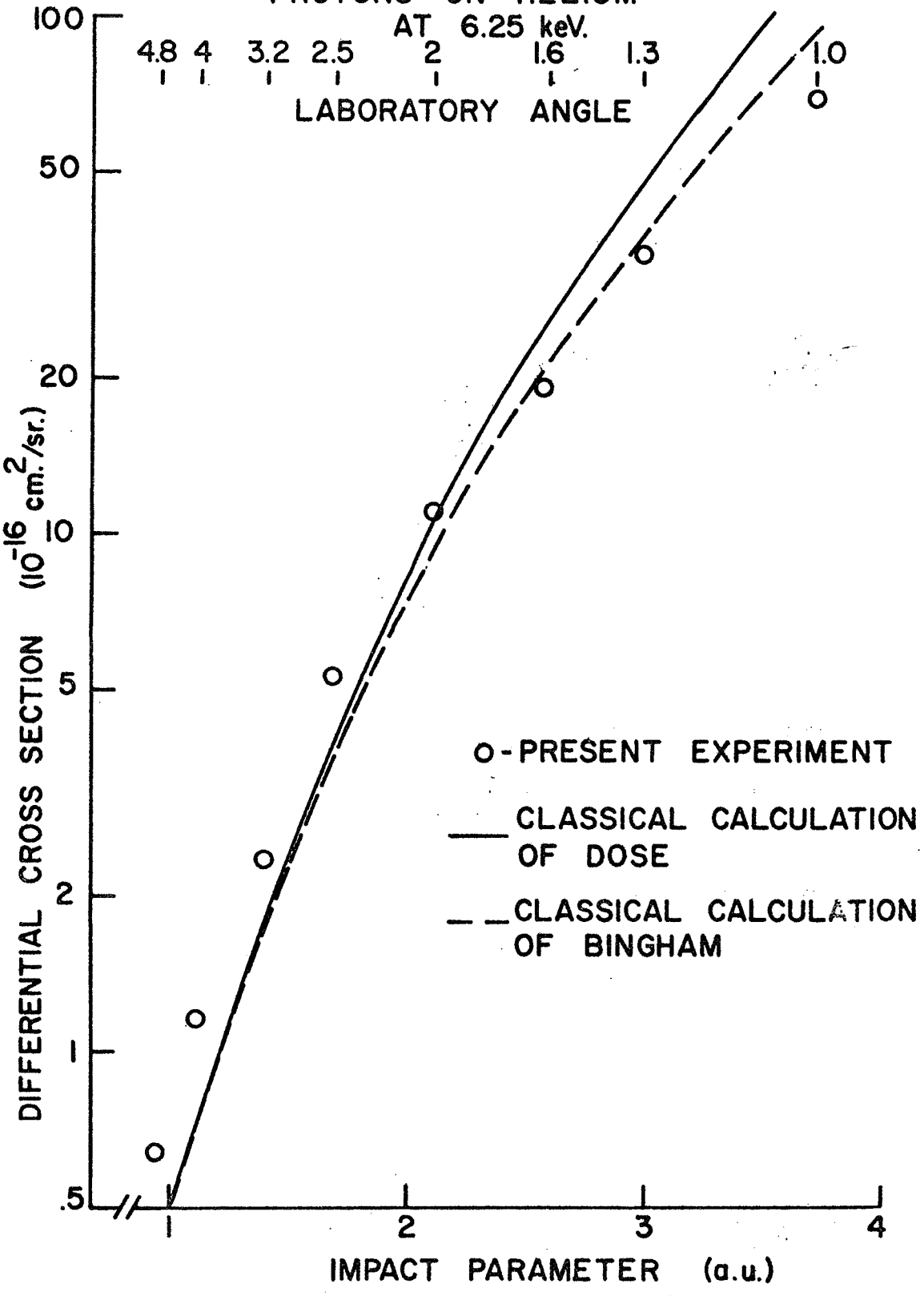

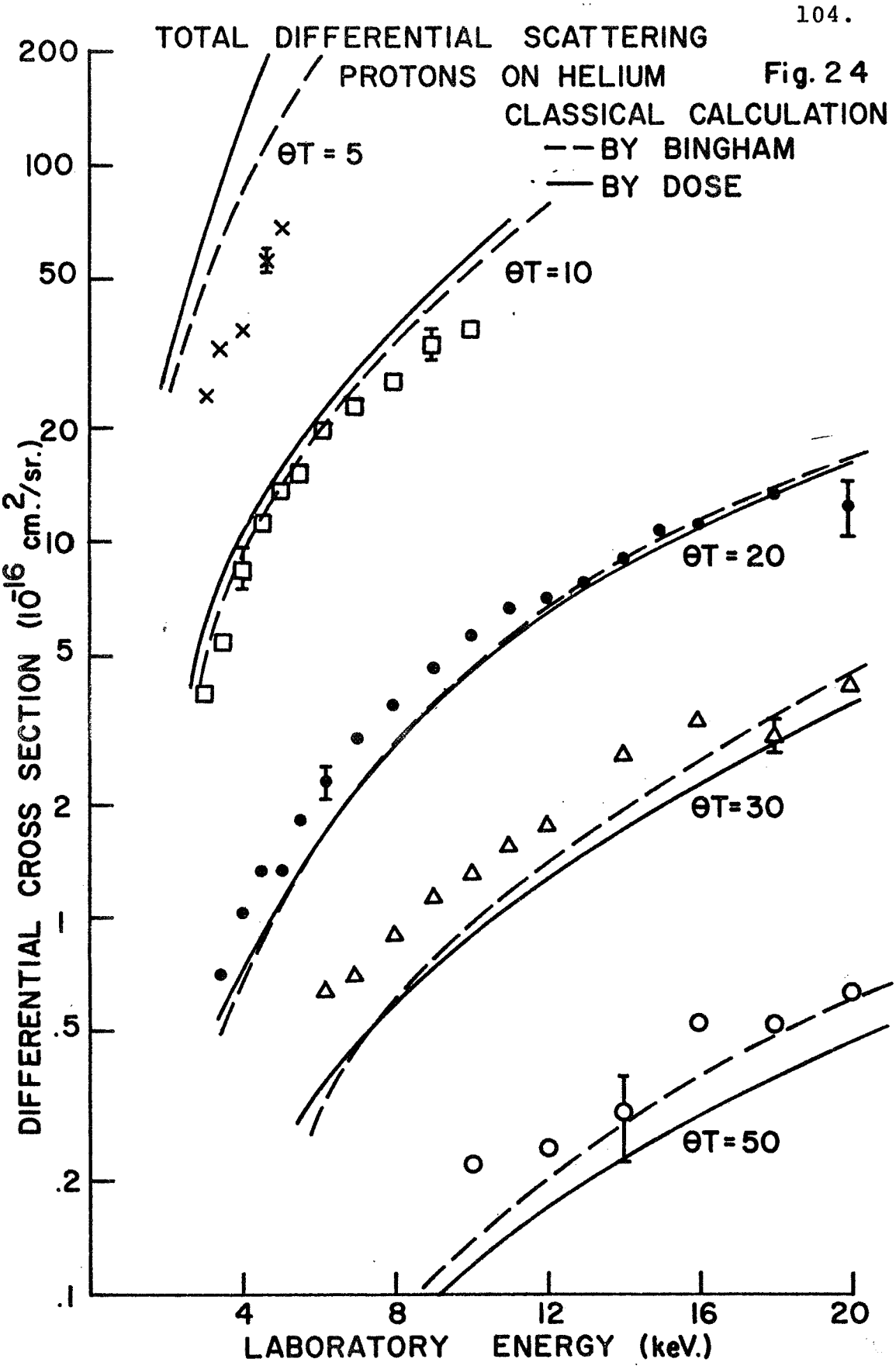
TOTAL DIFFERENTIAL SCATTERING
PROTONS ON HELIUM
CLASSICAL CALCULATION
--BY BINGHAM
—BY DOSE
θT = 5
θT=10
θT = 20
θT=30
θT=50
DIFFERENTIAL CROSS SECTION (10^{-16} cm.^{2}/sr.)
LABORATORY ENERGY (keV.)
200
100
50
20
10
5
2
1
.5
.2
.1
4
8
12
16
20

Fig. 24

B. Charge Transfer Probabilities from Protons on Argon.

The measured charge transfer probabilities for transfer to all states of hydrogen, P_o, and for transfer to the 2s state of hydrogen, P_{2s}, are shown for protons incident on argon in Figs. 25, 26, and 27.

For the data of Fig. 25, taken at constant scattering angle, both the impact parameter and relative velocity change for each data point. The values of P_o show excellent agreement with those obtained by Everhart, et al[65]. The data of Fig. 26 and 27 was taken at constant impact parameter and constant relative velocity respectively to investigate the dependence of observed oscillations on impact parameter and collision time (inverse velocity). As before, the values of impact parameter used for these graphs are obtained from the work of Dose[10].

Even though no appropriate theoretical considerations of charge transfer for this system are available, some comparisons to the qualitative ideas about the general behavior of charge transfer probabilities (from secion II.) can be made.

Figs. 26 and 27 show that the oscillation of P_o is definitely a function of the relative velocity, or collision time. Fig. 26 shows the regularity of the oscillations as a function of collision time. For these close collisions, P_o is shown by Fig. 27 to be nearly independent of impact

parameter at 6.25 keV. This behavior is characteristic of what has been referred to as resonant transfer in which many oscillations of the electron charge probability occur between the initial and final states during the collision. The oscillation in observed charge transfer probability for the collision then depends upon the time of collision. As the collision time changes (with changing velocity) the electron is first left in one state, then the other with continuing periodic variation.

Probability of transfer to all states, P_o, should be dominated by transfer to H(1s). The transfer to H(2s) and H(2p) (reference 50) together are about 10% of the total transfer. Transfer to n=3 levels is less likely[85] and higher levels should be even less probable. It is reasonable to assume that P_o should be approximately 80% transfer to H(1s).

Inspection of the lowest energy levels of the united (K^+) and separated $(Ar + H)^+$ atom limits (Fig. 28) shows that transfer to H(1s) satisfies the conditions for "quasi-resonance" given in section II. That is, (in atomic units) $E_2(0) - E_1(0) >> \frac{1}{\tau} >> E_2(\infty) - E_1(\infty)$ where τ is the collision time and 0 and ∞ denote the separation of the colliding nuclei. In Fig. 28 no attempt has been made to correlate states or to show the relationship of united and separated atom energies. However, the $Ar^+ + H(1s)$ transfer will connect the lowest K^+ state with

one of the excited states separated by at least 20 volts so that $E_2(0) - E_1(0) \simeq$ 1a.u. The collision time can be estimated by taking $\tau = v \times$ (interaction length). For the present experiment v is between .4 and 1.0a.u. and the interaction length can be estimated to be about 3a.u., so that $1/\tau$ is between 0.3 and 0.8a.u. Thus $E_2(0) - E_1(0) >> \frac{1}{\tau}$ is approximately satisfied. The energy separation of the separated atom states connected by transfer to H(1s), leaving the argon ion in its lowest state, is 2.1 ev - less than 0.1a.u. - so that $\frac{1}{\tau} >> E_2(\infty) - E_1(\infty)$ is satisfied. Since there are not many nearby energy levels to interfere with the resonant transfer the "quasi-resonance" conditions are satisfied and the observed behavior of P_o is expected.

The transfer to the 2s state, P_{2s}, does not exhibit such positive "quasi-resonant" oscillations as a function of collision time. The variation of the transfer probability is of small magnitude and is not a regular function of collision time (Fig. 26). At a constant velocity (Fig. 27) there appear to be small variations with impact parameter not expected for "quasi-resonance".

Referring to Fig. 28, the energy separation for transfer to H(2s), $E_2(\infty) - E_1(\infty)$, is 12.3ev (.46a.u.) so that $E_2(\infty) - E_1(\infty)$ is not $<< \frac{1}{\tau}$. This means that charge transfer to H(2s) will be small (as observed) and may not be "quasi-resonant". The resonance may also be destroyed by interference with the other nearby energy levels.

The results presented for both P_o and P_{2s} are independent of some of the error sources influencing cross section measurements. Because they are ratios of cross sections these probabilities are independent of the absolute value of pressure, beam collection efficiency, and scattering geometry. The values of P_o are even expected to be independent of particle detector efficiency. The only affect of these quantities on P_{2s} and P_o will be from variations between individual data collections.

The error bars exhibited for P_{2s} results represent the standard deviation of five or more separate determinations. The typical relative error is ±10% and arises primarily from the statistical uncertainty in the subtraction of data with quench field applied and with the field off.

The absolute error of P_{2s} is estimated to be ±40%. The primary source of this error is the uncertainty in the efficiency of the photodetector (±30%). The ratio, P_{2s}, may be subject to the systematic errors due to polarization, prequenching loss, and quenching length change with velocity; which were mentioned in section IV. and are discussed in the Appendicies. The fraction "f" describing the fraction of the 2s states decaying within the quenching length viewed by the photodetector has been applied, but other less well defined corrections have not. The maximum error in the overall slope of the results of P_{2s} is

estimated to be ±15% due to the combination of these possible sources of systematic error.

The relative error and absolute error of P_o are the same. The only errors in this case arise from possible change in pressure or beam collection between data collections and from background corrections (generally about 2%). The P_o values should be accurate to ±5% for protons on argon.

Fig. 25

TRANSFER PROBABILITIES
FROM PROTONS ON ARGON
AT 3° LABORATORY

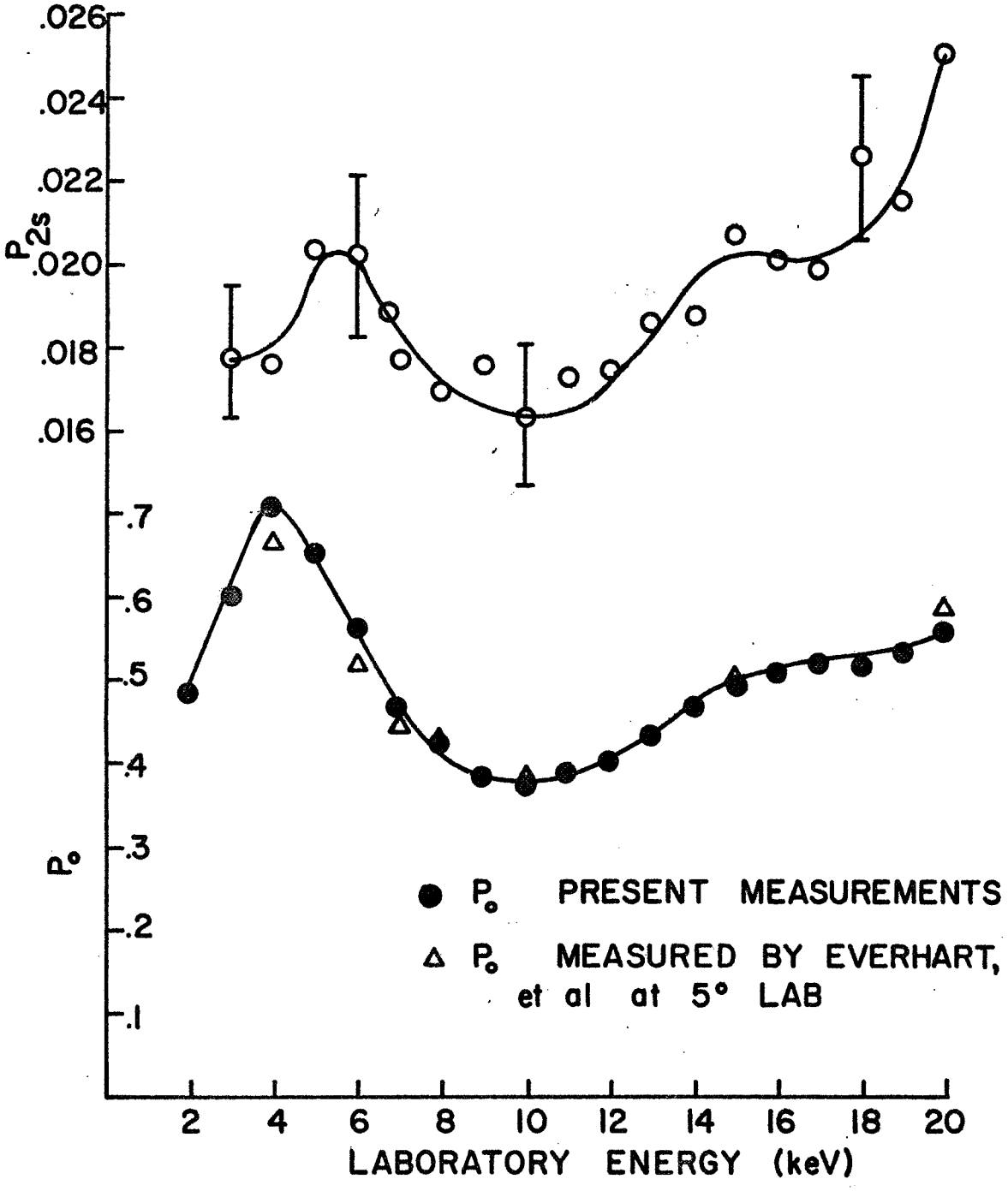

Fig. 26

TRANSFER PROBABILITIES
FROM PROTONS ON ARGON
AT $\theta T = 20$ keV-deg. $\rho \doteq .526$ a.u.

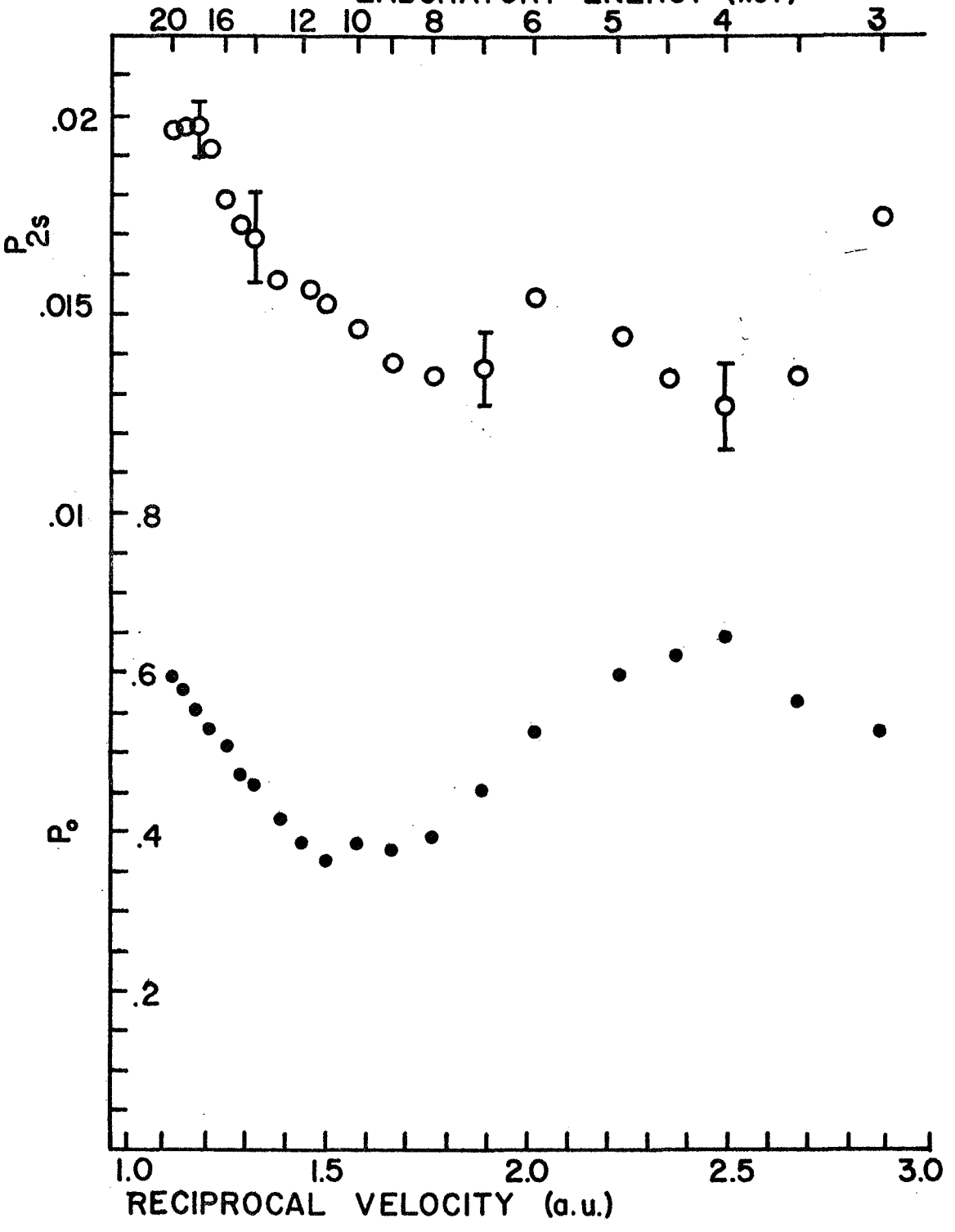

Fig. 27

TRANSFER PROBABILITIES
FROM PROTONS ON ARGON
AT 6.25 keV

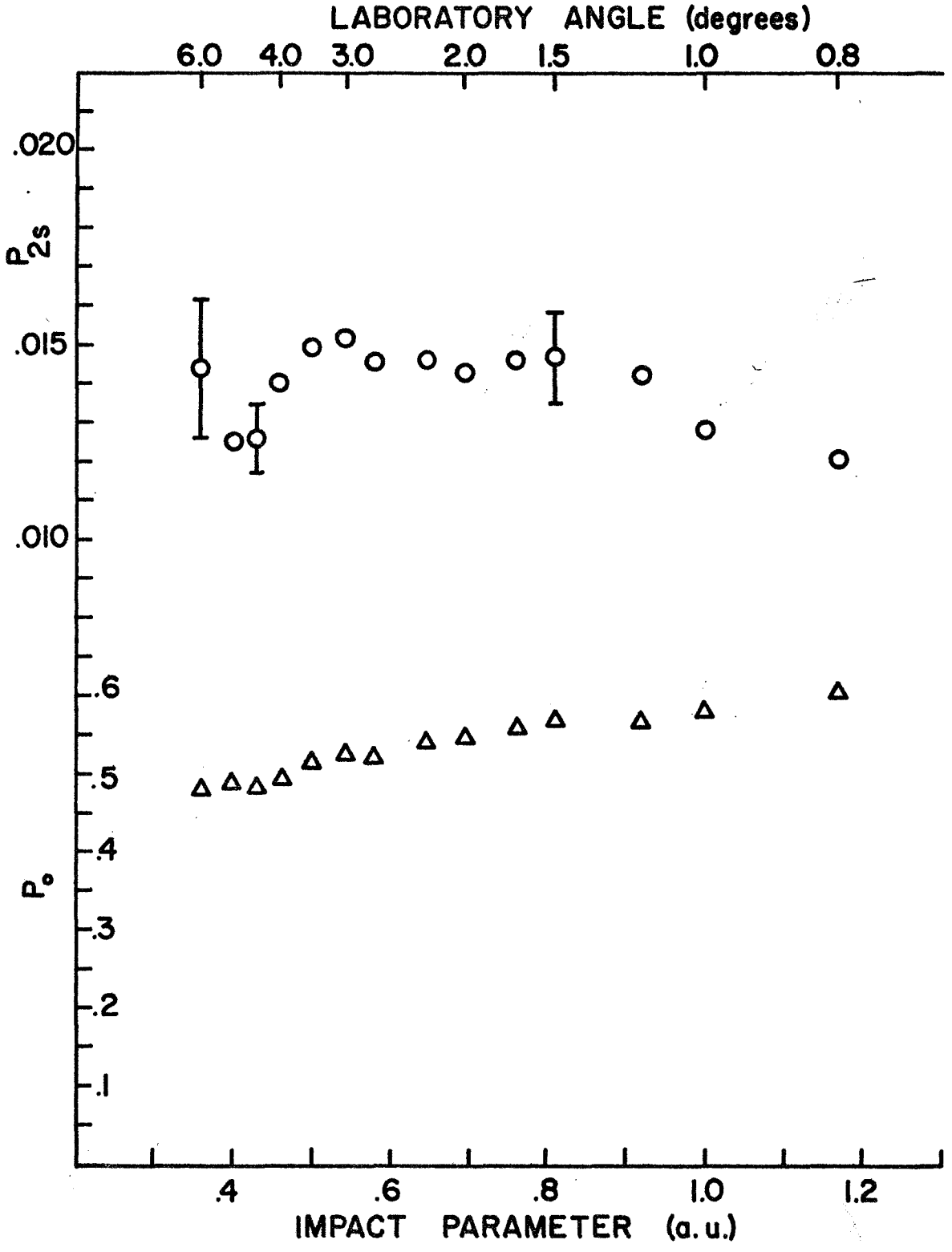

Fig. 28

LOWEST ENERGY LEVELS OF $(Ar+H)^+$ AND K^+
(Constructed using Ref. 72)

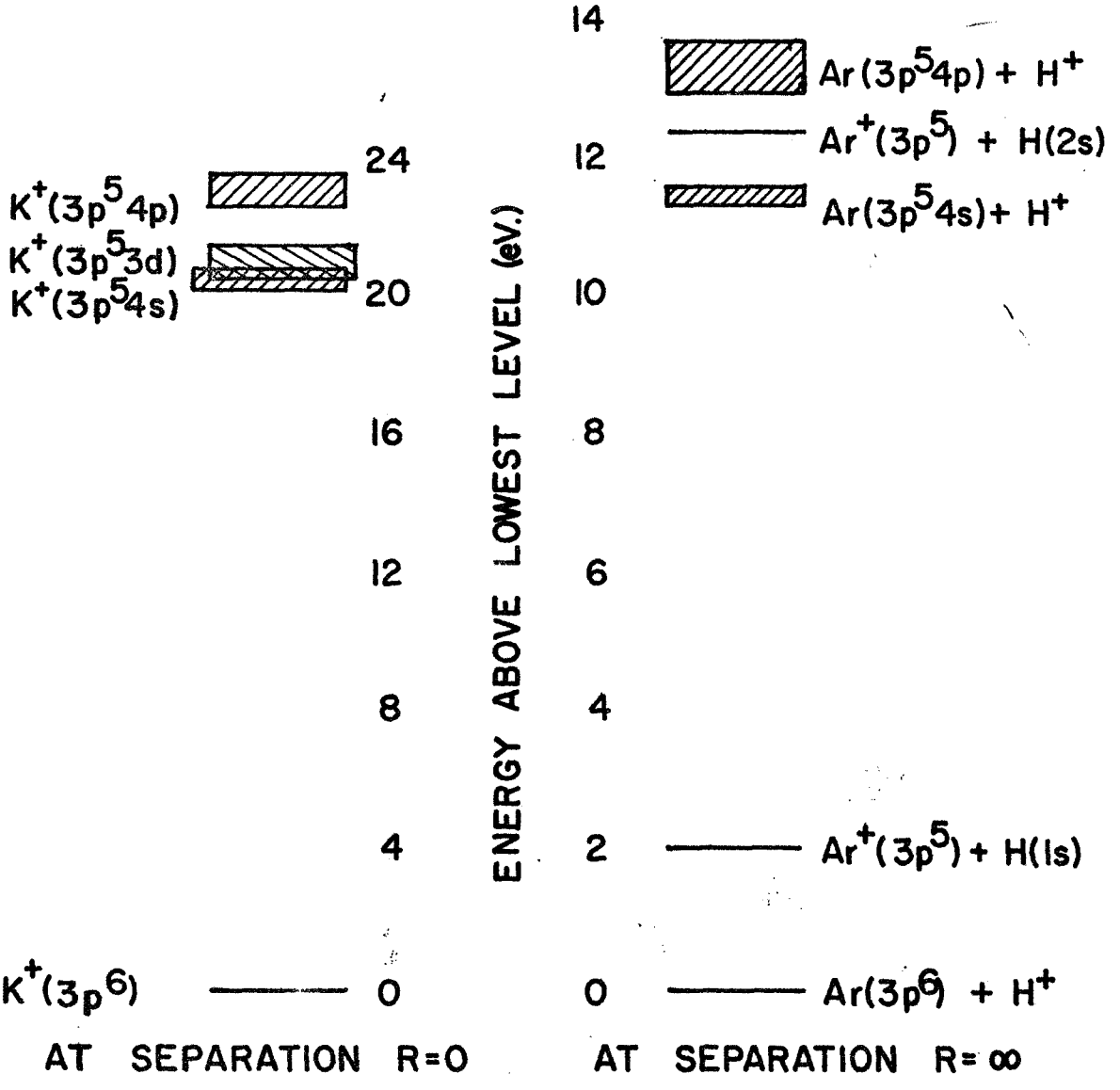

C. Charge Transfer Probabilities From Protons on Helium.

The measurements of charge transfer probabilities, P_o and P_{2s} from protons on helium are displayed in Figs. 29 - 33.

The results for P_o show the "quasi-resonant" behavior described earlier. Fig. 29 shows the regular oscillation of P_o with reciprocal velocity for several values of impact parameter. The agreement with the earlier results of Everhart is excellent except for a small discrepancy near 10 keV. (Values from Helbig and Everhart for θT = 5, 50, and 100 keV·deg. have been omitted for clarity.) Fig. 30 demonstrates the lack of any oscillation of P_o with impact parameter for a constant incident proton velocity of about 1.10×10^8cm/sec. The accuracy of present values of P_o is about ±10%. This is larger than the error in the argon data partly due to the necessity of correcting for background scattering with gas removed from the chamber (as high as 15%).

The oscillating behavior of P_o is qualitatively as predicted by theory given in section II. Comparison of Helbig and Everhart results to the impact parameter calculations of Green for transfer to the 1s state and of Sin Fai Lam for transfer to 1s, 2s and 2p states has already been shown (Fig. 3). The failure of these calculations to give quantitatively correct results is apparently due to

failure of the impact parameter formulation to represent adequately these close collisions. This failure may be partly due to neglecting the screening of the target nucleus by its electrons. This screening has an effect on the nuclear trajectories and, perhaps more importantly, on the energy levels of the quasi-molecules formed during the collision. Additionally, the constructed wave functions employing atomic eigenstates may not be adequate for these relatively slow close collisions.

Fig. 30 shows that, for a constant velocity, P_{2s} does not oscillate as a function of impact parameter. Since, for the entire range, the impact parameter is much smaller than the distance over which the collision occurs, the time of the collision is independent of the change in impact parameter. No oscillations are then expected. Unlike the more complicated proton-argon system, the transfer to the 2s state of hydrogen does show oscillations of the "quasi-resonant" type with varying collision time. In the energy range tested, two distinct maxima appear as a function of reciprocal velocity for a constant impact parameter (Fig. 31). This behavior is independent of impact parameter for the range of close collisions tested, but only values for θT = 20 keV·deg. (ρ = 0.26 a.u.) cover the entire range.

The data displayed in Fig. 31 are in good agreement with the preliminary data for θT = 20 keV·deg. previously

reported from this same experiment[61]. The preliminary data for P_{2s} was based on calculation of the total scattering rather than actual measurement and was not corrected for the fraction "f" describing the change with energy in the fraction of 2s states decaying in view of the photodetector. With such correction, this preliminary data is in good agreement with the present results, but has not been included here.

The P_{2s} error bars shown are standard deviations of five or more independent trials of the particular data point and thus represent relative error. This typical relative error is ±12%. As in the argon data, the absolute accuracy is not expected to be greater than about ±40% because of the uncertainty in photodetector calibration. There is also a possible overall error in slope of about ±15% due to the systematic errors mentioned earlier. Most data points are the average of four or more trials, with a few points being the average of only 2 trials (primarily values for θT = 50 keV·deg.).

Comparison to earlier measurements of P_{2s} at a constant laboratory angle, 2.2°, by Dose and Meyer[73] is shown in Fig. 32. Since it has already been demonstrated that P_{2s} is nearly independent of impact parameter in the range tested, good agreement between this constant angle (varying impact parameter) data and the present constant impact parameter is expected. The agreement in shape is good, as

demonstrated, but the absolute magnitude is quite different.

The normalization procedure of Dose and Meyer involves measuring charge transfer between scattered protons at 12 keV and residual gas between the scattering center and the detector. At 12 keV nearly all of the particles scattered to 2.2^{o} are protons (see Fig. 29). Thus Dose and Meyer have used these scattered protons as an incident beam and have measured the total charge transfer to the 2s state between these scattered protons and the helium gas in the path between the scattering center and their fixed-position detector. This background signal is normalized to the total 2s transfer cross section measured by Colli, et al[22], to obtain the efficiency of the photodetector. The normalization of the data of Colli, et al is to the Born approximation at 40 keV, which is dubious. Thus the factor of 3 disagreement in magnitude between present results and those of Dose and Meyer probably results from the difficulty of obtaining good normalization by their technique as well as the questionable magnitude of the results they use as a standard.

The shape of the portion of Dose and Meyers results below 20 keV is substantiated by the present work. Their results indicate a third maximum should be expected in P_{2s} at an energy greater than 60 keV.

The charge transfer probability to the 2s state of

hydrogen has been calculated in the impact parameter formulation by Sin Fai Lam[34] for $\theta T = 20$ keV·deg. as previously described. Fig. 33 shows the comparison of this calculation and the present results. This theory provided qualitative agreement with the results for P_o, failing in that case only in describing the magnitude of the maxima. The calculated results for P_{2s} not only disagree with present results by a factor of 10 in magnitude but further, disagree dramatically in relative shape.

Some possible weaknesses of this theory have already been discussed. For the collision time at these energies, the uncertainty principle dictates an uncertainty of a few eV in the electronic energies of the system during collision. Thus excitation of any of the states (shown in Fig. 5) which are near in electronic energy to the state tending to $He^+(1s) + H(2s)$ should be taken into account in the theory. For example, electronic states tending to $He\,^1S(1s2s) + H^+$ have not been included in the expansion which describes the wave function of the collision system.

The "quasi-resonant" behavior of P_{2s} may appear somewhat surprising. Apparently the competition of the above mentioned group of states may have considerable effect on P_{2s}, but it has not destroyed the "quasi-resonant" behavior. The criterion set forth for such behavior, in section II. was $E_2(0)-E_1(0) >> \frac{1}{\tau} >> E_2(\infty)-E_1(\infty)$. For transfer to the 2s state the collision time is approxi-

mately given by, $\tau = v \times$ (interaction length). The velocity varies from .4 to 1 a.u. and the interaction length is estimated to be about 2a.u. Referring to Fig. 5 (the correlation diagram for HeH^+) we find that in the united atom limit, $E_2(0)-E_1(0) \simeq 2.2$ a.u. (60 eV) which is greater than the approximate value of $1/\tau$ between 0.5 and 1.2 a.u. as required for "quasi-resonance". The other part of the criterion is not well satisfied since $E_2(\infty)-E_1(\infty)$ is about .73 a.u. However, the implication of this failure is primarily that the charge transfer to H(2s) will be small, as indeed it is observed to be.

The empirical formula of Everhart (see section II.) representing oscillating charge transfer, P_o, for $H^+ + H$ and $H^+ + He$ might represent at least positions of maxima and minima in the P_{2s} measurements. In that case, P_{2s} will be represented by

$$P_{2s} = A \sin^2 \left[\frac{\langle Ea \rangle}{2v} - B\right], \quad \text{(see sec. II p. 27)}$$

in atomic units, where A, the amplitude of the peaks, is not given by the empirical model in the case of the 2s state. From the two observed peaks in P_{2s}, with $\langle Ea \rangle = \dfrac{h}{\frac{1}{v_{n+2}} - \frac{1}{v_n}}$, where $1/v_{n+2}$ is for one peak and $1/v_n$ is for the other, $\langle Ea \rangle$ is found to be about 9 a.u. Using Everhart's value of $B = \pi/4$ we find that $\sin^2 \left[\frac{\langle Ea \rangle}{2v} - \frac{\pi}{4}\right]$ is a minimum at approximately 10 keV and 30 keV and a maximum at 6.3 keV,

16 keV, and 85 keV. These results are in good agreement with experiment and predict that the third maximum is around 85 keV. Of course, the peaks should be correctly separated by the empirical equation, but the result would be out of phase without $B = \pi/4$, as it has been observed to be for the other experiments.

There may be alternative models for the structure of P_{2s}. Some of the structure may arise from coupling to the ground state transfer. For example the minimum at 11 keV is coincident with the minimum of P_o. This minimum may be associated with the shoulder at about 11 keV in the total cross section for transfer to the 2s state (Fig. 15). Such coupling to the ground state should be accounted for by coupled state calculations. However, Sin Fai Lam's results do not exhibit the 11 keV shoulder in the cross section for transfer to 2s. According to the suggestion of Polvektov and Presnyakov[30], this shoulder may be due to coupling to the ground state; thus the ground state coupling idea is qualitatively supported.

In general the behavior of P_{2s} from protons on helium is observed to be similar to the behavior of P_o for protons on helium. The same empirical formula seems to fit both cases, at least qualitatively. It would be interesting to extend the measurement of P_{2s} for protons on helium to higher energies in order to check for the peak at 85 keV predicted by the empirical formula.

Fig. 29

CHARGE TRANSFER PROBABILITY
FROM PROTONS ON HELIUM

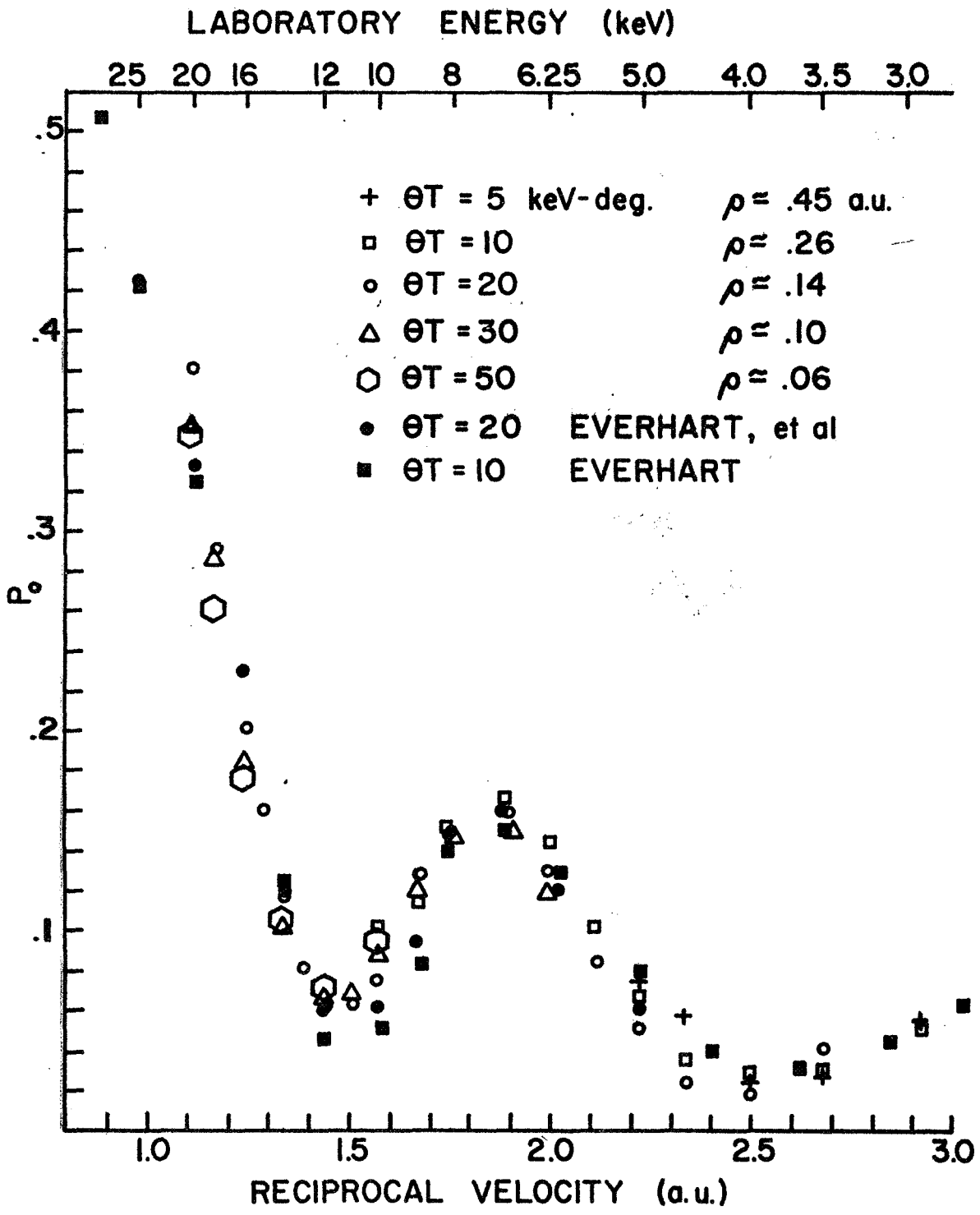

Fig. 30
CHARGE TRANSFER PROBABILITIES
FROM PROTONS ON HELIUM
AT 6.25 keV (laboratory)

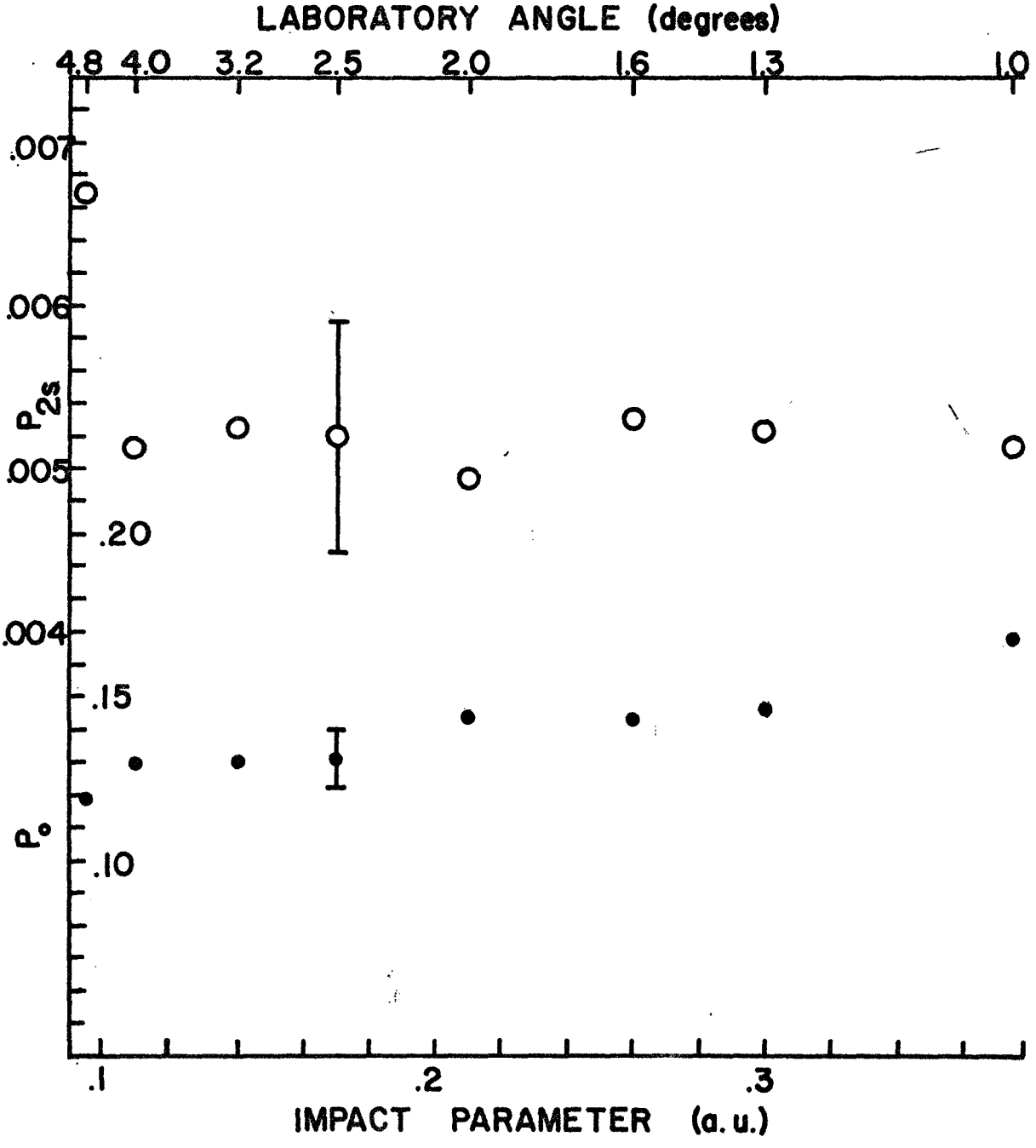

Fig. 31
CHARGE TRANSFER PROBABILITY
TO 2s HYDROGEN
FROM PROTONS ON HELIUM

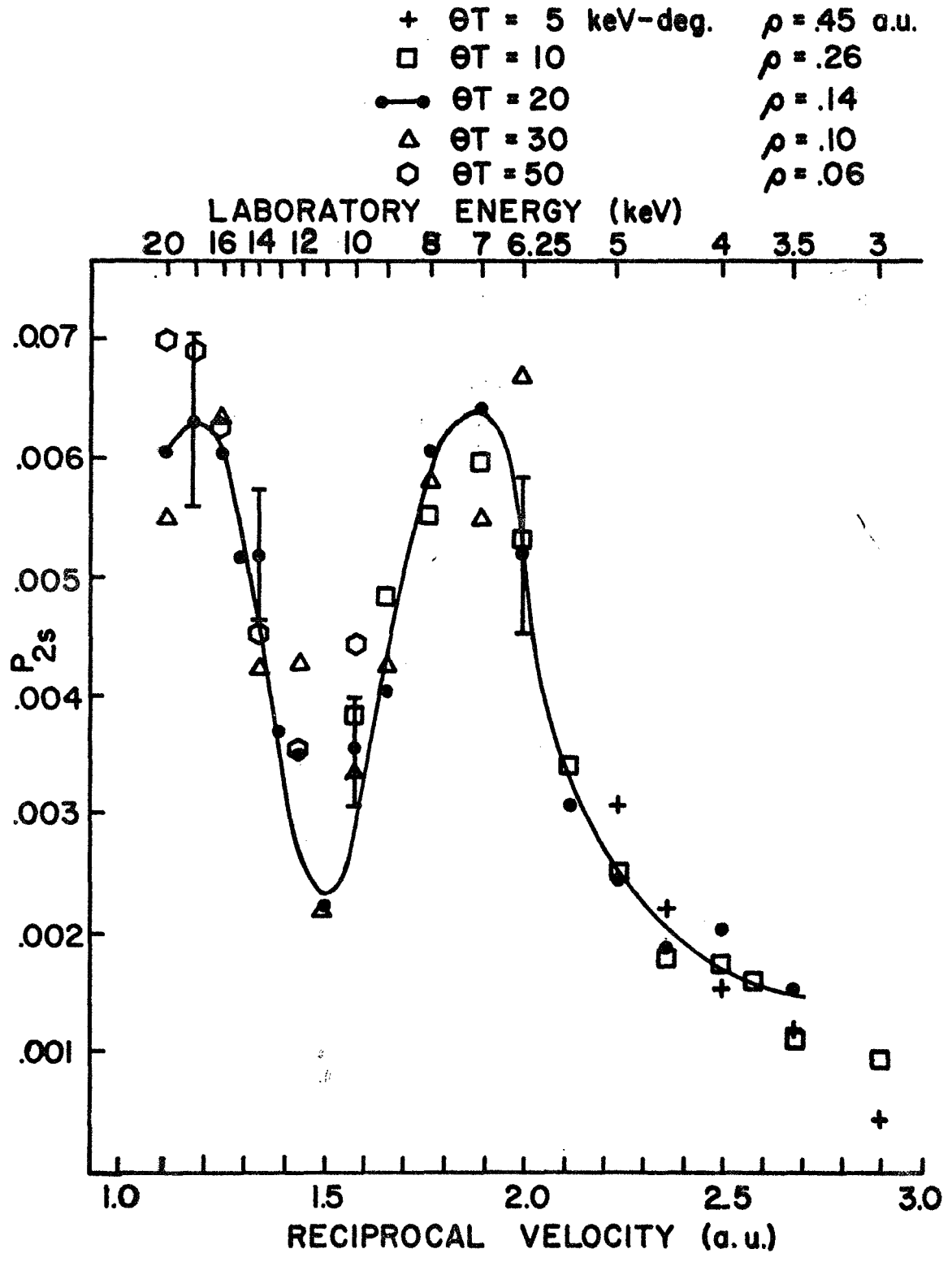

Fig. 32
PROBABILITY FOR CAPTURE INTO H(2s)
FROM PROTONS ON HELIUM

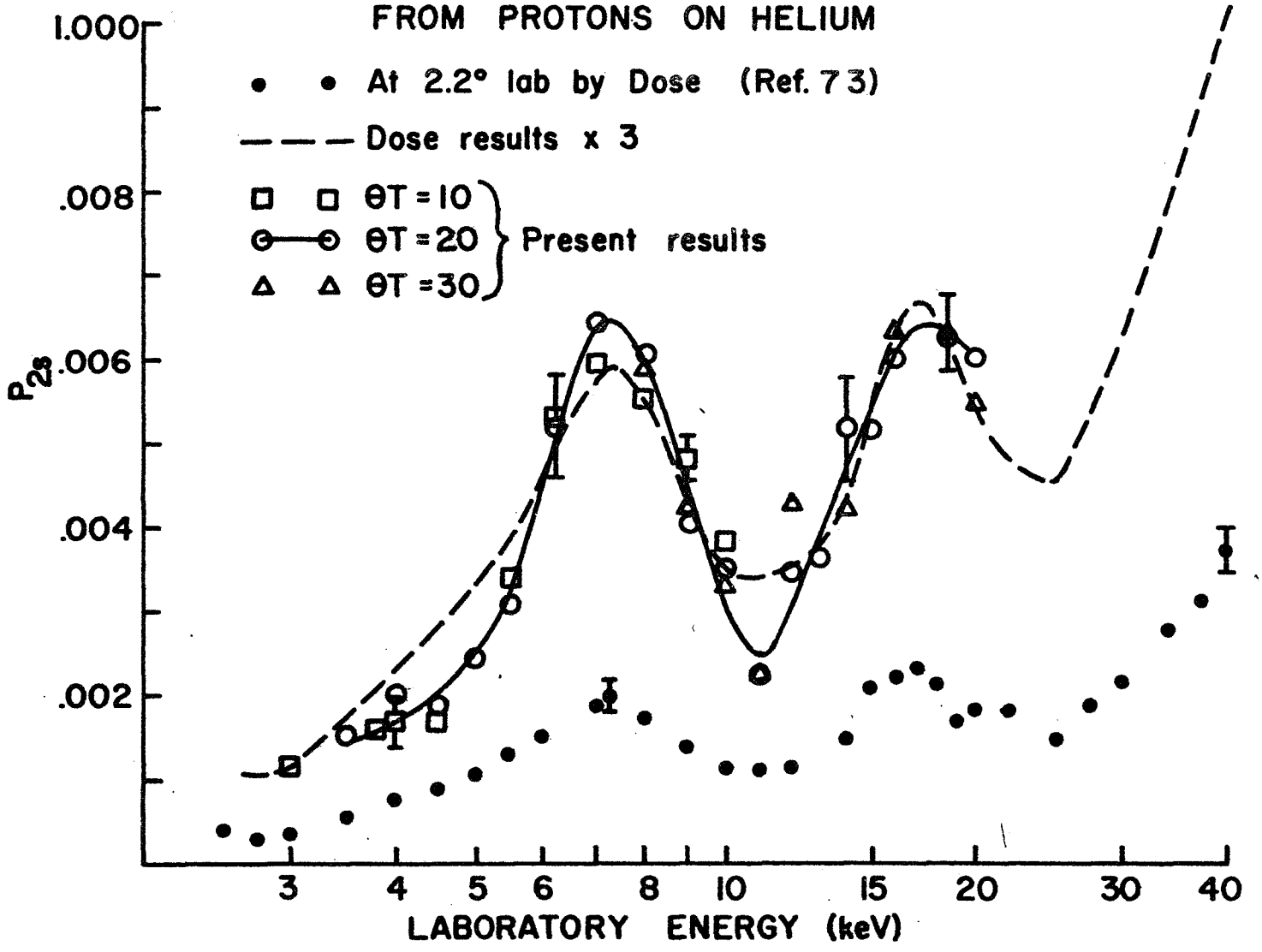

Fig. 33

PROBABILITY FOR CAPTURE INTO H(2s) FROM PROTONS ON HELIUM

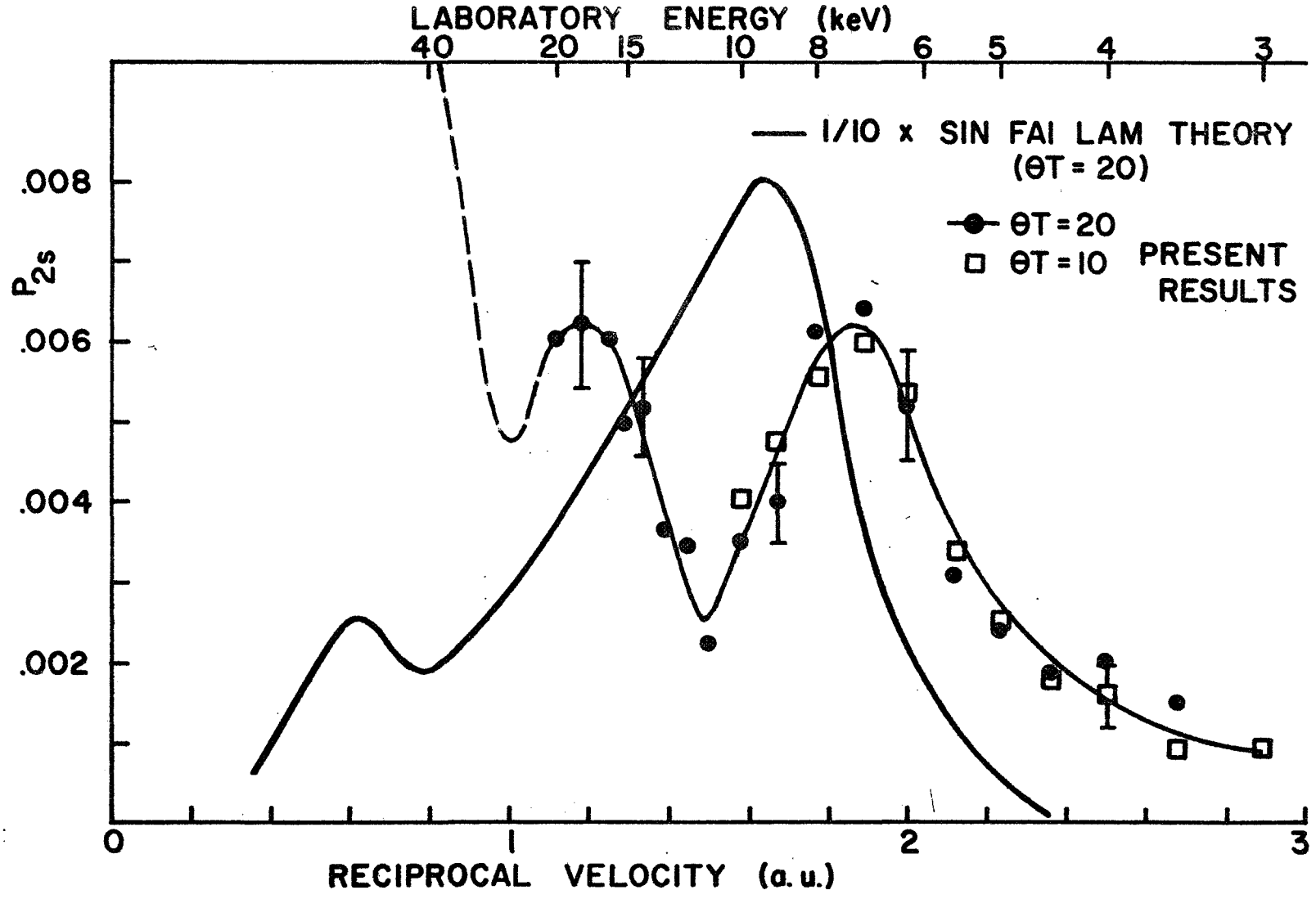

APPENDIX

A. Quenching of the 2s State and Related Errors.

1. Quenching of Metastables.

As in many previous experiments, the present work relies on the lifetime of the 2s state of hydrogen in a field free region, and the extreme shortening of this lifetime through Stark mixing of the 2s and 2p states in an electric field.

Decay of the 2s state is optically forbidden because photons require one unit of angular momentum which cannot be provided. The primary decay mode of the 2s state is double photon emission, so that the lifetime of the 2s state is quite long (0.14 sec.).

Application of an electric field provides an interaction which connects states of quantum number ℓ differing by ±1 and with the same quantum number M_J[74]. Thus in the presence of an electric field the 2s state of hydrogen is mixed with the 2p state. The 2p state decays by photon emission to the 1s state with a lifetime of 1.6×10^{-9}sec. Thus through this coupling the apparent lifetime of the 2s state can be drastically reduced by a field. The lifetime can be calculated quantum mechanically[74]. I. A. Sellin[75] has measured the apparent 2s lifetime and found excellent agreement with these calculations. The minimum 2s lifetime, for fields in excess of 600 volts/cm is approximately 4.5×10^{-9}sec. The expression representing

the 2s lifetime is[75]

$$\tau_{2s} = \tau_{2p}\left\{1 + \frac{M^2}{[1-(1+M^2)1/2]^2}\right\}$$

where τ_{2p} is the 2p lifetime and the field interaction, M, is $M = \frac{2\sqrt{3}\,Eea_o}{L}$ where E is field strength, L is the Lamb shift, a_o is the Bohr radius, and e is the electronic charge.

For the present experimental situation, where hydrogen atoms in the 2s state move through a field region, the number of photons emitted from the region will depend on the lifetime and thus on the applied field. In the present case, increasing the voltage applied to the quenching capacitor should increase the number of photons emitted in the region viewed by the photodetector until the lifetime is sufficiently short that all 2s atoms decay in the viewed region; or, for faster atoms, the number emitted will increase until the lifetime reaches a minimum (around 600 volts/cm applied field). In this latter case some 2s atoms possibly will not decay in the region viewed. This behavior is observed as shown (Fig. 34). At 15 keV and above an appreciable fraction of the 2s atoms do not decay in the region viewed by the photodetector so that the yield curve saturates only because minimum lifetime is reached at around 1000 volts applied to the capacitor plates.

Fig. 34

PHOTON YIELD FOR QUENCHING
OF H(2s) METASTABLES
Produced by charge transfer of
protons in argon

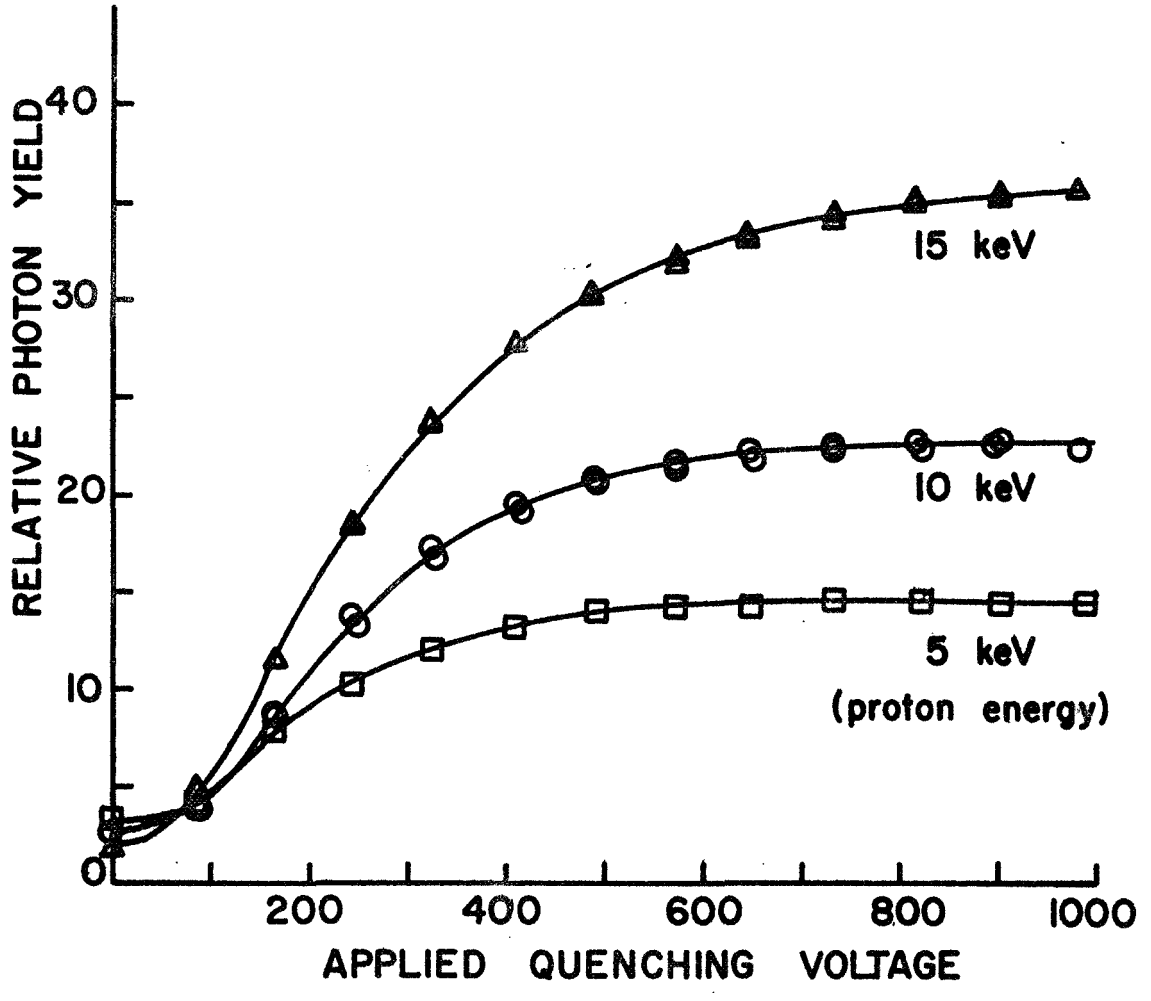

2. Correction For Finite Length of Quenching Region.

For a simple parallel plate capacitor, the field strength would be nearly uniform. However, the peculiar construction of the present capacitor leads to a nonuniform field strength. The high voltage end of the capacitor is a closed shallow tube, with provision for photodetector to view the entire quenching region. The capacitor was constructed in the peculiar shape (shown in Fig. 35) in order to help contain the field and in order to shield the quenching region from stray electrons or photons in the detector assembly.

The field within this capacitor was calculated by a simple numerical technique employing a standard computer. A two dimensional array of points representing the capacitor shape was constructed. The potential was set at zero at all points except on the surface of the tube end (box in two dimensions) of the capacitor. Holes in the capacitor were assumed sufficiently small to be ignored. The tube was set at -905 volts which was the applied voltage throughout the experiment, and the front plate was held at zero potential. The potential at each point on the array due to the nearest neighbor points was then calculated employing Laplace's equation. This calculation was repeated iteratively until a steady state was attained for the potential at each point on the array inside the capacitor. The field along the beam axis

Fig. 35
QUENCH CAPACITOR

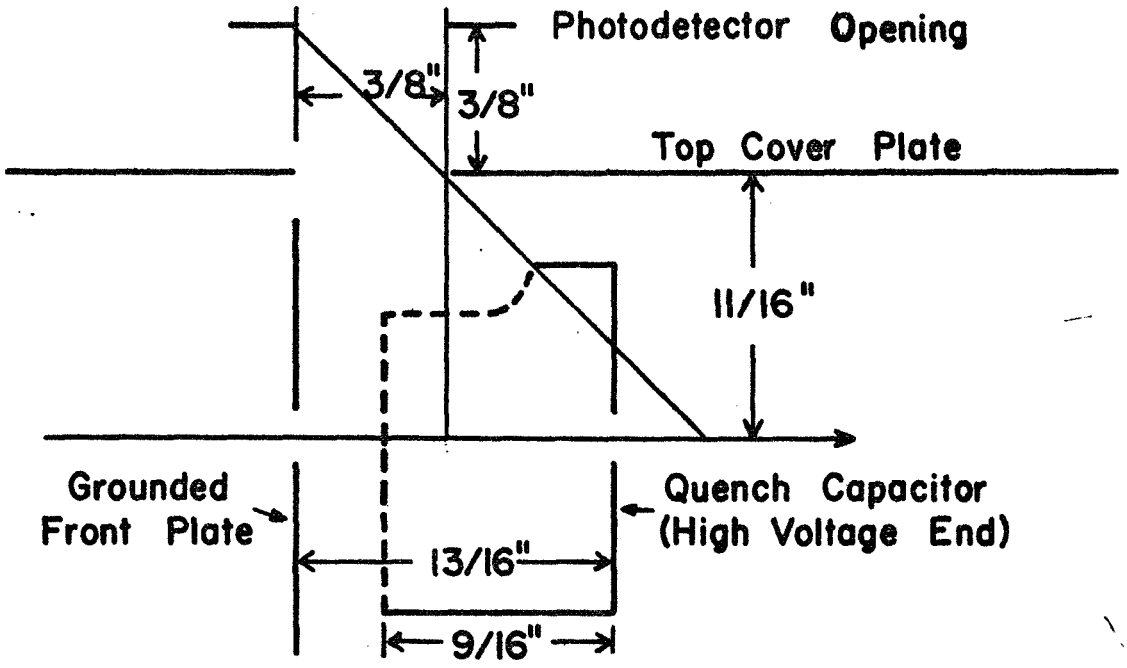

SCHEMATIC DECAY OF METASTABLES

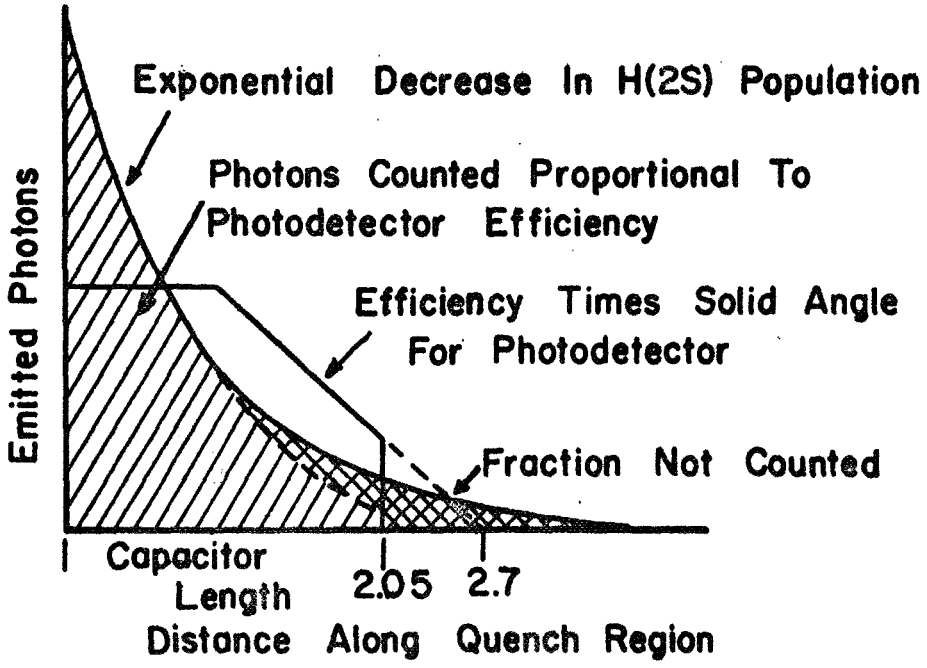

was then obtained from the potential of array points along the axis. The potential dropped by approximately 1% at points a distance of 3/16 inch off the axis. Thus the field perpendicular to the axis was taken to be uniform within the dimensions of the scattered beam. The field strength along the axis for -905 volts applied is shown in Fig. 36.

The decay of the 2s state atoms is shown schematically in Fig. 35. As indicated, an appreciable fraction of sufficiently fast atoms can travel the length of the quench region without decaying. Further, all parts of the quenching region are not viewed equally by the photodetector because of changing solid angle, so that photons from the back part of the capacitor will not be counted directly proportional to the detector efficiency. It is necessary to determine what fraction of photons are counted for each energy.

The fraction to be determined, will be independent of photodetector efficiency and number of incident atoms, so that normalization of the decay curve is arbitrary. Take the total number of available photons, for total quenching, to be $N = \int_0^\infty e^{-t/\tau} dt$ where τ is the lifetime and t is the time in the quench field. Then for a finite quenching length, the fraction of photons which are counted, will be

$$f = \frac{\int_0^{\ell} e^{-x/v\tau}\, dx}{\int_0^{\infty} e^{-x/v\tau} dx}$$

Fig. 36

QUENCHING FIELD

for 905 volts applied

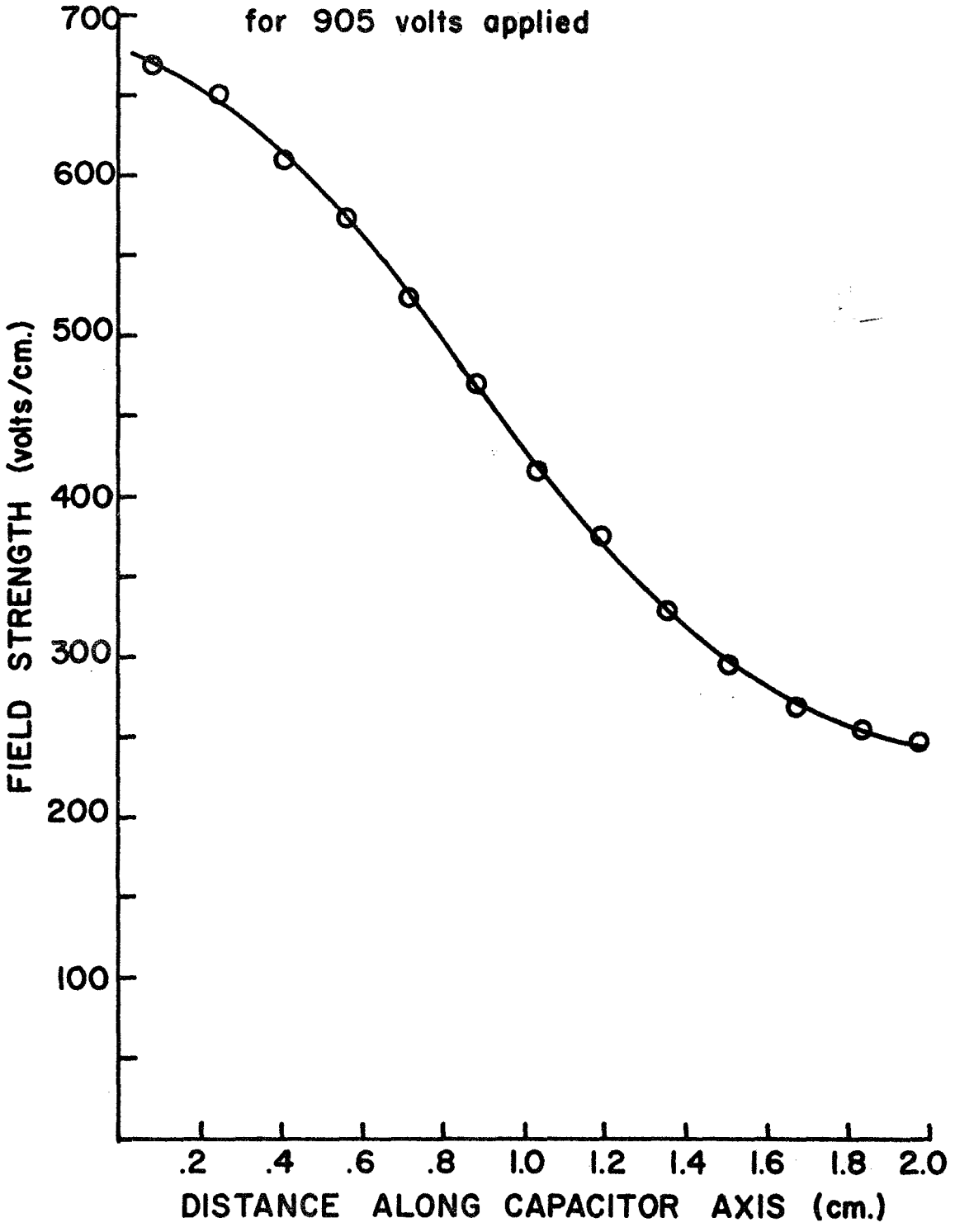

where ℓ is the length of the quench region and the time in this region (for a fixed velocity, v) is given by $t = x/v$.

For the present geometrical situation, the first centimeter of the quenching region is viewed by the entire photodetector opening. The last 1.05 cm is viewed by a decreasing portion of this opening. Assuming this decrease in effective solid angle to be linear, we can express it as a multiplier to the exponential decay. (The assumption of linear decrease of effective solid angle is essentially the same assumption employed in the Jordan and Brode approximation which was found to be adequate for much more sensitive geometry.) This factor will then be a straight line of the form $y(x) = mx + b$ with the conditions that at $x = 1$ cm, $y(1) = 1$, and that at $x = 2.7$ cm, where this line intersects the scattered particle beam axis, $y(2.7) = 0$. For these conditions, $y(x) = -0.588\,x + 1.588$ for x in cm. Thus the fraction of photons counted for the present experimental arrangement is

$$f = \frac{\int_0^1 e^{-x/v\tau}dx + R\int_1^{2.05} y(x)\, e^{-x/v\tau}dx}{\int_0^\infty e^{-x/v\tau}dx}$$

Where R is the fraction of metastables which remain after traversing the first 1 cm of quenching length, i.e.

$$R = \frac{\int_0^\infty e^{-x/v\tau}dx - \int_0^1 e^{-x/v\tau}dx}{\int_0^\infty e^{-x/v\tau}dx}$$

For a constant lifetime, τ, the expression for f can be evaluated in closed form for each velocity used. In the

present case, however, τ changes with the changing field strength in the capacitor region. However, most of the decay is induced in the first 1 cm where the field strength is highest and τ is nearly constant. The evaluation can also be carried out in closed form for τ of different value for the two regions of the quenching capacitor. For the -905 volts applied the field strength in the first centimeter varies from 675 volts/cm to 425 volts/cm, with corresponding values of τ about 4.8×10^{-9}sec. and 6.3×10^{-9}sec.

Evaluation of the fraction f was carried out assuming $\tau_1 = 5.31 \times 10^{-9}$sec., corresponding to a constant field of 550 volts/cm in the first region. By similar approximation the lifetime in the second capacitor region was assumed constant at 8.46×10^{-9}sec. The results are given in Table 1, where for each energy the appropriate velocity was used in the evaluation. The results show 99% of the atoms decay and are counted proportional to the detector efficiency for 1 keV energy and 69% are counted for 20 keV energy. For comparision, f was also evaluated for a simple parallel plate capacitor of 2.05 cm plate separation,i.e. assuming a constant field of 442 volts/cm giving a constant lifetime of 6.10×10^{-9}sec. The maximum discrepancy between the two approximations was 4% at 20 keV. It was concluded that the two region approximation would be a sufficient approximation to the continuous field variation expected for the apparatus.

Table 1. Fraction of Metastables Decaying Within Viewing Length of Photodetector

Energy of Particle	Fraction, "f"
1 keV	.987
2	.957
3	.927
4	.901
5	.878
6	.856
7	.838
8	.821
9	.806
10	.792
11	.778
12	.766
13	.754
14	.743
15	.733
16	.723
17	.714
18	.704
19	.697
20	.689
21	.681

The values of f obtained have been used to correct all of the data in this report for the change with energy of the number of metastable, H(2s), atoms decaying within view of the photodetector. The correction is applied so that the cross sections and probabilities at 16 keV (normalization point) are unchanged.

3. Prequenching Loss.

A further source of error may arise from the quenching process. The quenching field can extend through the entrance hole in the capacitor and induce some quenching of metastables before the region viewed by the multiplier. The hole in the capacitor plate leads to weakening of the field immediately inside the quenching region as well as extension of the field beyond the region viewed by the photodetector. The exact form of the field and length of extension out of the viewed region will depend on the details of the slit structure. Smythe[76] obtains an expression for the field near an ideal slit in a thin conducting sheet. Using this result as a guide the extension of the field and its strength can be qualitatively estimated.

A rough estimate of the loss of photons due to prequenching by the field extending through the slit is obtained by calculating the fraction of metastables quenched in a distance of one half the slit width by a field of one half the maximum value inside the quench region. Assuming

a constant field and with the appropriate 0.1 cm slit width, the fraction of metastables lost is

$$\text{fraction lost} = \frac{\int_0^{.05} e^{-x/v\tau} dx}{\int_0^{\infty} e^{-x/v\tau} dx} = 1 - e^{-\frac{.05}{v\tau}}$$

For a field of 330 volts/cm the lifetime is about 8.0×10^{-9} sec. Using the appropriate velocities the calculated values of the fraction lost varies from 7.2% at 4 keV to 3% at 20 keV.

Only the change in this fraction lost with changing velocity is important, as the loss at 16 keV is included in the normalization factor for the photodetector efficiency. The change of this loss fraction over the energy range studied should be about 4% according to the preceding estimate. The effect on the slope of the total 2s cross section measurements used for photodetector normalization (sec. IV. C.) would be to improve the slope agreement between present data and previous investigators. However, the slope disagreement would not be eliminated by a correction as small as that estimated.

No correction of the data for this prequenching loss of photons has been attempted because the estimated change of slope over the energy range is quite small and because the estimate is tenuous. Thus, this possible source of error remains in the data for the probabilities, P_{2s}, and for the differential cross sections for transfer to the 2s state.

The total cross sections for transfer to the 2s state as measured by Jaecks, et al[31] and Andreev, et al[33] are not subject to any of the errors discussed in this appendix section. These experiments were performed with quenching fields in the target gas region so that a steady state of production of H(2s) and decay through the 2p states occured. These cross sections as measured by Bayfield[60] should be subject to the preceding considerations, but he makes no mention of any corrections and does not describe his quenching field strength in detail.

An additional source of error in 2s cross sections associated with the quenching by electric fields is the polarization of the quench induced radiation. This is discussed in the next section.

B. Polarization of Quench Induced Radiation From H(2s)

1. Previous Investigations.

In the earlier measurements[31,33] of total transfer to H(2s), the radiation induced by electrostatic quenching was assumed to be iootropic. This assumption was based on the relative values of the fine structure splitting, between $2P_{3/2}$ and $2P_{1/2}$; and the Lamb shift, between $2S_{1/2}$ and $2P_{1/2}$ states of hydrogen. Since the Lamb shift is only about 10% of the fine structure splitting, (Fig. 37), it was assumed that the $2S_{1/2}$ state coupled primarily to the $2P_{1/2}$ state. The radiation from the $2P_{1/2}$ to $1S_{1/2}$ transition should be isotropic, so that it was assumed that radiation induced by the quench field would be nearly isotropic.

In 1968, Fite, et al[77] reported measurements of polarization of weak-field quench induced radiation from H(2s) atoms which were formed by electron impact on H(1s) atoms. Using electric fields of 3 to 15 volts/cm, they found that radiation intensity polarized parallel to the electric field (I_{11}) was weaker than the intensity polarized perpendicular to the field (I_1). The polarization measured at 90° with respect to the field direction was observed to be

$$P = \frac{I_{11} - I_1}{I_{11} + I_1}\Bigg|_{90^\circ} = -.30 \pm .02$$

Following the suggestion of Fano; Fite, et al, calculated the polarization retaining the $2P_{3/2}$ component of

Fig. 37

ENERGY SPLITTING OF N=2
STATES OF HYDROGEN

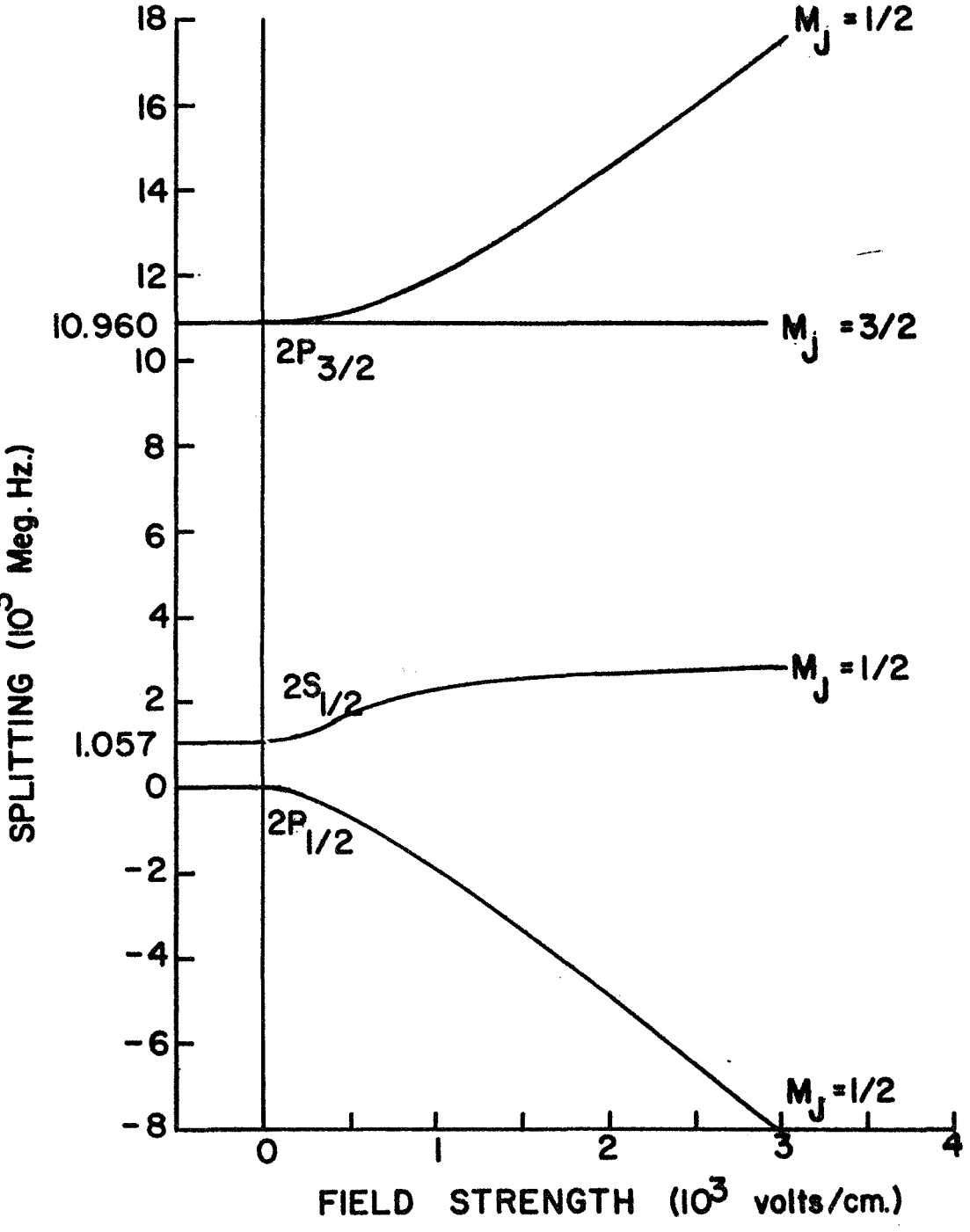

the weak-field mixing. The wave function of the atom in the field was expressed as

$$\psi_M = U(2S_{1/2,M}) + a\ U(2P_{1/2,M}) + b\ U(2P_{3/2,M})$$

where only M of ±1/2 were included since the stark mixing is only for states of the same m quantum number. The coefficients a and b for admixture of $2P_{1/2}$ and $2P_{3/2}$ states were obtained from a time-independent perturbation expansion. The dipole matrix element for radiation from the mixed state, ψ_M, to the ground state $1S_{1/2}$ now included terms for both $2P_{1/2}$ and $2P_{3/2}$. The intensity of the radiation is obtained by squaring this dipole matrix element. The contribution of the square of the $2P_{3/2}$ term was indeed small, but the cross product term was not negligible. The polarization predicted by this calculation was -.329 in reasonable agreement with the experiment. A similar calculation for a wide range of field strengths is to be outlined in this section.

An attempt to improve the above calculation for weak fields has been reported by Casalese and Gerjuoy[78] who include the effects of the hyperfine splitting of the n=2 states (between 24 and 180MHz). Their result, polarization of -.323, does not substantially improve the agreement between experiment and theory. The inclusion of the width of the P states (about 100 MHz) might have more effect on the polarization than the hyperfine splitting.

For fields above about 100 volts/cm, the shift of energy levels of the hydrogen states in the applied field will have an effect on the polarization of the radiation. The shift of the n=2 states in an electric field is shown in Fig. 37 from reference 79. For sufficiently high fields the shift of energy levels is so great that the original splitting has no influence and transitions are expected to take place only between states for which $\Delta m = 0$. This is just the component of radiation along the field, I_{11}, so that the polarization should become +1.0.

2. Calculation of the Polarization as a Function of Field Strength.

The procedure for the following calculation of the polarization of quench induced radiation from H(2s) was suggested by Dr. J. Macek. Part of the calculation is similar to the work of Lüders[79] for the calculation of lifetime of the $2S_{1/2}$ state in an electric field.

In order to calculate the polarization of the radiation from H(2s) atoms in an electric field, it is necessary to construct the time dependent wave function for the atom in the field. As previously mentioned, the electric field will connect those unperturbed states with ℓ differing by ±1 but which have the same M_J. Since the initial state is $2S_{1/2}$ with $M_J = +1/2$ or $-1/2$, the unperturbed states mixed by the field will be $2S_{1/2}$, $2P_{1/2}$, $2P_{3/2}$ with $M_J = +1/2$ or $-1/2$. The complete calculation will be carried out for

$M_J = +1/2$; the same results hold for $M_J = -1/2$. Thus for the present case, the eigenfunctions ϕ_1, ϕ_2, ϕ_3, representing unperturbed states $2P_{3/2}$, $2S_{1/2}$, and $2P_{1/2}$ respectively, provide a complete set of eigenfunctions for describing the atom. Following Schiff[80], we can relate these eigenfunctions of the unperturbed atom to the eigenfunctions, ψ_j, of the atom in the field.

In an electric field, the atom is described by

$$H\psi_j = E_j\psi_j \tag{1}$$

where H includes the operator, $\vec{E}\cdot\vec{r}$, for the electric field. It is permissible to define a matrix form of H with the unperturbed eigenfunctions, ϕ_i, but this matrix will not be diagonal. Since the basis set, ϕ_i, chosen has only three eigenfunctions the matrix definition of H will be three by three. Let the matrix definition of H be given by, $H_M = (\phi_v|H|\phi_u)$ where v and u are 1, 2, or 3. The matrix then becomes

$$H_M = \begin{pmatrix} E_3 & M & 0 \\ M & E_2 & V \\ 0 & V & 0 \end{pmatrix} \tag{2}$$

where $$M = (\phi_1|eE\cdot r|\phi_2) \tag{3a}$$

$$V = (\phi_3|eE\cdot r|\phi_2) \tag{3b}$$

and where the energy of the unperturbed $2P_{1/2}$ state, E_1, has been taken to be zero.

According to transformation theory[80] the unitary matrix U, which diagonalizes H_M, provides the coefficients U_{ji} which describe the expansion of the new eigenfunction, ψ_j,

(for which H_M is diagonal) in terms of the previous basis set ϕ_i. That is,

$$\psi_j = \sum_{i=1}^{3} U_{ji}\phi_i. \qquad (4)$$

There will be three indepent eigenfunctions, ψ_j. The matrix U which will diagonalize H_M is obtained by solving the eigenvector problem,

$$\begin{pmatrix} E_3 & M & 0 \\ M & E_2 & V \\ 0 & V & 0 \end{pmatrix} \begin{pmatrix} U^j{}_1 \\ U^j{}_2 \\ U^j{}_3 \end{pmatrix} = \lambda^j \begin{pmatrix} U^j{}_1 \\ U^j{}_2 \\ U^j{}_3 \end{pmatrix} .$$

The eigenvectors, $\vec{U}^j$, together form the desired matrix U. Thus solution of the eigenvector problem provides the expansion coefficients needed in (4) to define the eigenfunctions, ψ_j, of the atom in the field in terms of the known eigenfunctions ϕ_i, of the unperturbed atom.

The H(2s) atom will evolve, in time, in an electric field because the eigenfunctions, ψ_j, contain ϕ_1 and ϕ_3 which decay to the ground state of hydrogen, $1S_{1/2}$, (to be represented as ϕ_o). Thus the time dependent wave function for the atom in the field is

$$\Psi = \sum_j a_j \psi_j e^{-iE_j t - \gamma_j t} .$$

The coefficients a_j can be determined from the initial condition that all atoms enter the field in the unperturbed state, ϕ_2. That is,

$$\Psi\Big|_{t=0} = \sum_j a_j \psi_j = \sum_j a_j \sum_{i=1}^{3} U_{ji}\phi_i = \phi_2 ,$$

from which $\sum_j a_j U_{ji} = \delta_{i2}$

so that for a unitary matrix, U; $a_j = U_{j2}^*$. The wave function representing a hydrogen atom in an electric field which was initially in the $2S_{1/2}$ state is thus

$$\Psi = \sum_{j=1}^{3} U_{j2}^* \sum_{i=1}^{3} U_{ji} \phi_i e^{-iE_j t - \gamma_j t} \tag{5}$$

Ignoring the widths of the P levels and the hyperfine structure, the radiation from the atom represented by (5) to the ground state, ϕ_o, is given by

$$I_{total} \propto \int d\Omega \int_0^{\infty} \sum_{q=-1}^{1} (\phi_o | X_q | \Psi)^* (\phi_o | X_q | \Psi) \, dt \tag{6}$$

where $(\phi_o | X_q | \Psi)$ is the usual dipole matrix element for a radiative transition and X_q is the component of the X along polarization direction q. Taking the field along the z axis, the components of X are

$$X_o = r \cos\theta = r(4\pi/3)^{1/2} Y_{10}$$

$$X_{-1} = \frac{r \sin\theta}{2} e^{-i\phi} = r(r\pi/3)^{1/2} Y_{1-1}$$

$$X_{+1} = \frac{r \sin\theta}{2} e^{+i\phi} = r(4\pi/3)^{1/2} Y_{1+1}$$

where the Y_{1q} are the spherical harmonics. The integration over all time implies that all of the original H(2s) atoms decay.

After putting (5) into (6) the relationship can be written,

$$I_{total} \propto \int d\Omega \sum_{q=-1}^{1} \sum_{j} \sum_{j'} |U_{j2}|^2 (\phi_o|Xq|\psi_j)^*(\phi_o|Xq|\psi_{j'})$$

$$x \int_o^\infty e^{-[i(E_{j'}-E_j) + \gamma_j + \gamma_{j'}]}dt$$

The integration over time yields

$$\int_o^\infty e^{-[i(E_{j'}-E_j) + \gamma_j + \gamma_{j'}]t}dt = \frac{1}{i(E_{j'}-E_j)+\gamma_j+\gamma_{j'}}$$

However, for $j' \neq j$, $(E_{j'}-E_j)$ is large so that the integral is negligible compared to its value with $j' = j$. Thus in the summation $j' \neq j$ can be neglected. This gives,

$$\int_o^\infty e^{-[i(E_{j'}-E_j) + \gamma_j + \gamma_{j'}]t}\, dt = \frac{\delta_{jj'}}{2\gamma_j} .$$

Using this result,

$$I_{total} \propto \int d\Omega \sum_{q=-1}^{1} \sum_{j} \frac{|U_{j2}|^2}{2\gamma_j} \left| (\phi_o|Xq|\psi_j) \right|^2$$

The width γ_j is for one of the eigenfunctions of the atom in the field, that is for a particular mixture of ϕ_3, ϕ_2, ϕ_1, (representing $2P_{3/2}$, $2S_{1/2}$, $2P_{1/2}$). The value of γ_j depends on the relative mixture of P states with the S state. That is

$$\gamma_j \propto |U_{j1}|^2 \gamma_{P3/2} + |U_{j2}|^2 \gamma_{S1/2} + |U_{j3}|^2 \gamma_{P1/2} .$$

But $\gamma_{P3/2} = \gamma_{P1/2} \equiv \gamma$ whereas $\gamma_{S1/2} = 0$, so that

$$\gamma_j \propto (|U_{j1}|^2 + |U_{j3}|^2) \quad \gamma .$$

Thus the expression for the total radiation is

$$I_{total} \propto \int \frac{d\Omega}{\gamma} \sum_q \sum_j \frac{|U_{j2}|^2}{|U_{j1}|^2+|U_{j3}|^2} \left| (\phi_o|X_q|\psi) \right|^2$$

The part of the dipole matrix elements involving $r(4\pi/3)^{1/2}$ is common to all of the intensity expressions and thus can be included in the proportionality factor. The same is true for $1/\gamma$. Then,

$$I_{total} \propto \int d\Omega \sum_q \sum_j \frac{|U_{j2}|^2}{|U_{j1}|+|U_{j3}|^2} (\phi_o|Y_{1q}|\psi_j) .$$

The component of I_{total} along the field direction is

$$I_{11} \propto \sum_j \frac{(U_{j2})^2}{(U_{j1})^2+(U_{j3})^3} |(\psi_j|Y_{10}|\phi_o|^2 \quad \text{where} \qquad (7)$$

where $\psi_j = \sum_{i=1}^{3} U_{ji}\phi_i$. The other two similar components (for $q = \pm 1$) are perpendicular to the field direction so that $I_{total} = I_{11} + 2I_1$.

In an experiment with radiation viewed at 90^0 to the field direction, the detector will be along one of the perpendicular component directions, so that this component is not seen. Thus the usual definition of polarization is

$$P = \frac{I_{11}-I_1}{I_{11}+I_1} \Big|_{90^0}$$

Employing $I_{total} = I_{11}+2I_1$, the expression for polarization

can be put into the form, $$P = \frac{3I_{11}-I_{total}}{I_{11}+I_{total}}\Big|_{90^0}. \qquad (8)$$

Further, since total quenching has been assumed, $I_{total} \propto 1$, so that only I_{11} must be calculated.

To complete the calculation the matrix elements V and M (3a and 3b) must be calculated so that the matrix(2) describing the atom in a field can be diagonalized and the expansion coefficients, U_{ji}, obtained. These matrix elements

$$M = (\phi_1|eE\cdot r|\phi_2) = eE(\phi_1|r\cos\theta|\phi_2) = eE(4\pi/3)^{1/2} \cdot(\phi_1|rY_{10}|\phi_2)$$

and $$V = (\phi_3|eE\cdot r|\phi_2) = eE(4\pi/3)^{1/2}\ (\phi_3|rY_{10}|\phi_2)$$

are of the same form as the dipole matrix elements, $(\phi_i|Y_{10}|\phi_o)$, which appear in expression (7).

These elements are most easily evaluated by using the Wigner-Eckhardt theorem. The elements are in the form

$$(\phi_i|Y_{10}|\phi_o) = (LSJM_J|Y_{10}|L_oS_oJ_oM_{Jo})$$

In order to apply the theorem we need to recouple to the LM_LSM_S scheme. This recoupling gives

$$(LSJM_J|Y_{10}|L_oS_oJ_oM_{Jo}) = \sum_{\substack{M_{Lo}\\ M_L\\ M_{So}}} (LS_oJM_J|LM_LSM_{So})\,(LM_L|Y_{10}|L_oM_{Lo})\,(L_oM_{Lo}S_oM_{So}|L_oS_oJ_oM_{Jo})$$

where the recoupling coefficients can be evaluated using standard tables[81]. Also, use has been made of the information $M_S=M_{So}$ and $S=S_o$ for this transition. The Wigner-Eckhardt theorem,

$$(LM_L|T_{kq}\ L_oM_{Lo}) = \frac{(-1)^{k-L_o-L}}{2L+1}\ (kqL_oM_{Lo}|kL_oLM_L)$$

$$(L||T_k||L_o)^{82}$$

(where T_{kq} is a tensor operator such as Y_{10}) can now be applied to $(LM_L|Y_{10}|L_oM_{Lo})$ and the evaluation can be performed. (The reduced matrix element $(L||Y_1||L_o)$ is evaluated in ref. 82 for the spherical harmonics).

Applying all the quantities thus determined gives the value of the matrix elements

$(\phi_1|Y_{10}|\phi_o) = \frac{+\sqrt{2}}{\sqrt{3}}$ for radiation from $^2P_{3/2}$ to $^1S_{1/2}$

$(\phi_2|Y_{10}|\phi_o) = 0$ for radiation from $^2S_{1/2}$ to $^1S_{1/2}$

$(\phi_3|Y_{10}|\phi_o) = -\frac{1}{\sqrt{3}}$ for radiation from $^2P_{1/2}$ to $^1S_{1/2}$

Since ϕ_o and ϕ_2 have identical angular components, evaluation of M and V is carried out by including integration over r with the radial components of the wave functions ϕ_2. Then,

$M = (\phi_1|eE\cdot r|\phi_2) = -\sqrt{6}\ Eea_o$ for the mixing of $^2P_{3/2}$ and $^2S_{1/2}$

and $V = (\phi_3|eE\cdot r|\phi_2) = \sqrt{3}\ Eea_o$ for the mixing of $^2P_{1/2}$ and $^2S_{1/2}$.

(which is the same as other investigators have obtained for these matrix elements[79].)

All of the information necessary is now available to calculate (7)

$$I_{11} = \sum_j \frac{U_{j2}^2}{U_{j1}^2 + U_{j3}^2} \Big| \sum_i U_{ji} (\phi_i | Y_{10} | \phi_o) \Big|^2 .$$

The diagonalization of the matrix (2) giving U_{ji} was accomplished for each value of field strength E, by a standard computer program[83]. The intensity, I_{11} (7) and the polarization, (8), were then evaluated for each set of U_{ji} obtained.

The results are shown in Fig. 38. For weak fields (10 volts/cm) the value obtained is P = -.329 in agreement with the result calculated by Fite, et al[77]. For the present experimental arrangement most of the radiation comes from the first part of the capacitor where the field strength averages about 550 volts/cm. The predicted polarization at this field strength is -.20.

3. Application to the Experiment.

The intensity measured by the photodetector has been assumed to be proportional to the total intensity which determines the measured cross section (or probability P_{2s}). Since the radiation is not isotropic this proportionality will not be direct. A standard analysis[84] employs the polarization, as defined, to relate the intensity observed at any angle to the total intensity. The result can be expressed in the form

$$I(\theta) = \frac{I_{total}}{4\pi} \cdot \frac{3(1 - P\cos^2\theta)}{3 - P} \qquad (9)$$

Fig. 38

POLARIZATION OF QUENCH INDUCED RADIATION FROM H(2s)

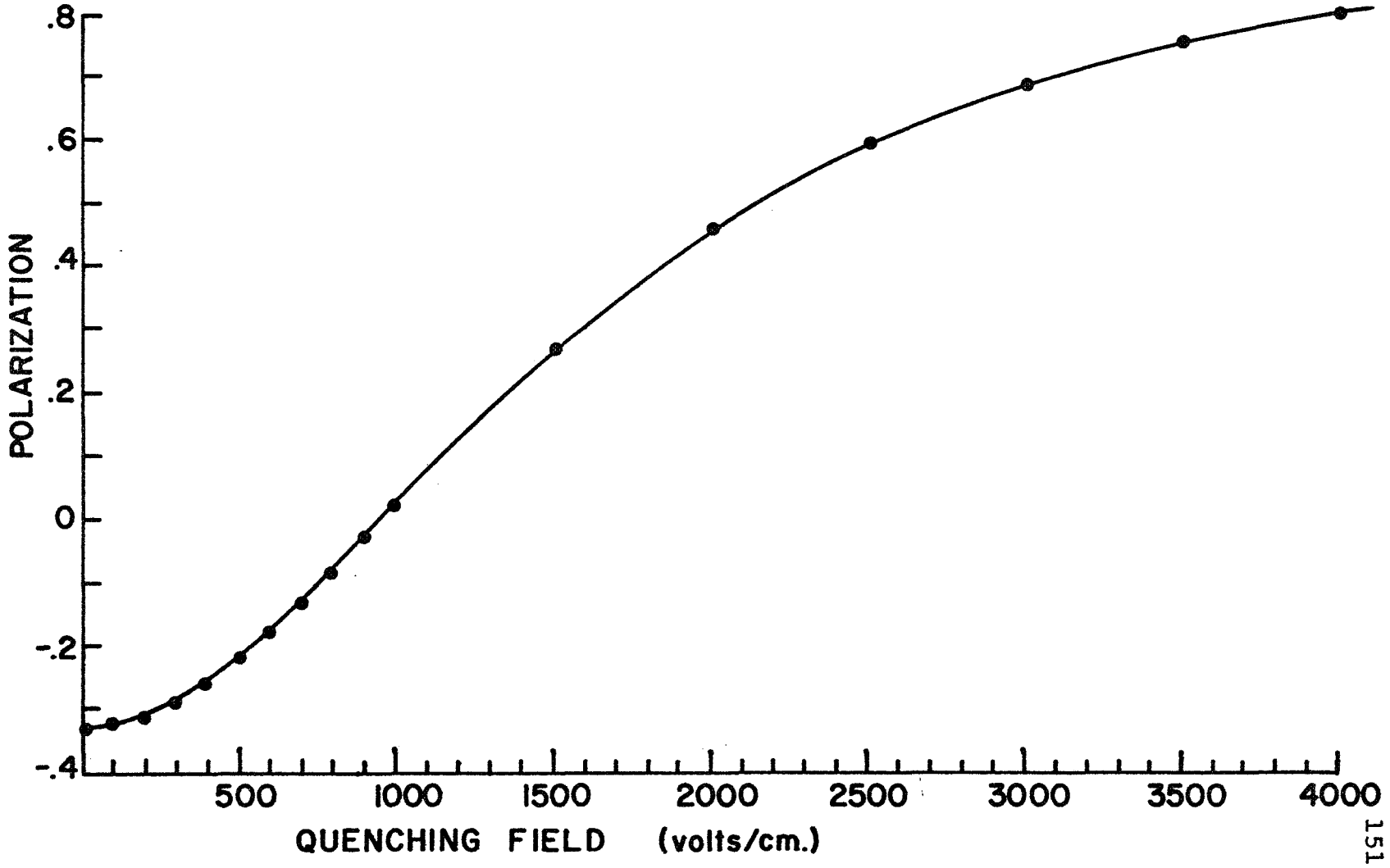

For the present experimental situation θ is approximately 90^0, so that for the predicted polarization of -.20,

$$I(\theta) = \frac{I_{total}}{4\pi} \left(\frac{3}{3+.2} \right) = \frac{I_{total}}{4\pi} (.94)$$

Since the previous assumption was that the intensity at the detector was $I_{total}/4\pi$ times the solid angle viewed by the detector, the error is about 6%; the measured intensity being about 6% lower than assumed.

This predicted error is for radiation detected at 90^0. The actual apparatus arrangement allows the detector to accept radiation from a large spread of angles around 90^0. The effect of the polarization is thus reduced as seen by inspection of the expression (8).

The measurements used for normalization of the photo-detector are expected to contain similar errors. The polarization of the measurements of Andreev, et al[33], with the detector at 90^0 to a field of 600 volts/cm, should be about P = -.18. The error then being about the same as for present measurements. The polarization of the measurements of Jaecks, et al[31] is not directly predicted by the present-ed theory due to the alternating of field direction.

No correction has been applied to the data for the predicted polarization. No attempt has been made to predict possible variation of the polarization with velocity of H(2s) atom in the field. Any such affect is expected to be secondary. Thus the predicted correction is an overall

factor, and should be applied before normalization. Since it is a +6% correction to the absolute values that are only accurate to about ±40%, neglect of the polarization is not considered to be a serious error.

Experimental measurement of the polarization of quench induced radiation from H(2s) as a function of applied field would provide interesting comparison to the predicted values.

C. Cascade Contributions to the H(2s) Population.

Some of the H(2s) atoms detected in the quenching region may be due to transfer to the n=3,4,5... states of hydrogen with subsequent transition to the 2s state. Such a contribution to the H(2s) population should not be counted as charge transfer to the 2s state.

The approximate contribution from n=3 and n=4 states to the H(2s) population can be estimated using the measurements of Hughes, et al[85]. These measurements report the total (all angles) cross sections for transfer to 3s, 3p, and 4s states of hydrogen from collisions of protons and various gas atoms, and compare the magnitude of these cross sections to the magnitude of the 2s and 2p transfer cross sections. The 3p and 4p states can decay to the 2s state. The magnitude of the 3p state is given, but the magnitude of the 4p state must be estimated from the behavior of the other cross sections.

Since for the present apparatus the path from the collision center to the detection region is quite long (about 15 cm), any atoms formed in 3p or 4p states decay before reaching the detector region. The fraction of the H(2s) population at the detector contributed by atoms formed in the 3p state is given by.

$$\text{Cont. (2s) from (3p)} = \frac{\sigma_{3p}}{\sigma_{2s}} \left(\frac{A_{3p-2s}}{A_{3p}}\right)$$

where A_{3p-2s} is the transition probability 3p-2s and A_{3p} is the total transition probability 3p to all other states. The same relationship holds for the contribution of 4p-2s and each of the higher states. Using the measurements of Hughes, et al[85] and the appropriate transition probabilities (from ref. 74 p. 266) the contribution from the 3p state for helium is

$$\text{Cont. 2s from 3p} = (.25)\ (.12) = .03$$

The contribution from the atoms formed in the 4p state is obtained, after estimating σ_{4p}, to be approximately

$$\text{Cont. 2s from 4p} = (.08)\ (.12) = .01$$

The contribution of each of the higher states should be less. It is reasonable to assume the contribution from all higher states is approximately .01. Thus the total cascade contribution to the population of H(2s) at the detector is estimated to be 5% for protons on helium. The estimated cascade contribution for argon is 3%.

The estimate is for an overall contribution to the magnitude of the total charge cross section for transfer to the 2s state. It is assumed that this fractional contribution will be approximately the same for the differential cross sections and probabilities measured. It is possible for the contribution to change as a function of angle or energy because of different behavior of 3p (or higher states) and the 2s cross sections as a function of these quantities. However, any such change should be considerably less than

5% overall correction. Thus the slope of any of the P_{2s} measurements should be affected by less than 5%.

It should be noted that the contribution of cascade to the total crsos section for transfer to the 2s state measured by other investigators will not be the same as that estimated for the present case. The measurements of Jaecks, et al[31] and Andreev, et al[33] were made with quenching in the collision region. The decay times of the upper states are sufficiently long that part of the hydrogen atoms formed by transfer to these upper states do not decay until after passing the region viewed by the photodetector. In addition, the presence of the electric field in the collision region modifies the transition probabilities making transition to the 1s state more probable (transition to the 2s state less probable) than in the field free case. Both of these considerations decrease the contribution of cascade to the population of H(2s) at the detector. The magnitude of the cascade contribution to transfer cross sections is thus expected to be slightly less for these measurements than for the present measurements. The measurements of Bayfield[60] were made with apparatus arrangement similar to that of the present measurements so that cascade contribution would be similar to that estimated. The difference between measurements with quenching in the collision region (Jaecks and Andreev) and measurements with quenching after the collision

region (Bayfield and present), due to contribution of cascade, is estimated to be 2-3%.

Again the correction for cascade has not been applied to the present measurements. The estimate is a -5% correction to be absolute value of 2s probabilities and cross sections (estimated accuracy ±40%) and has thus been considered negligible.

It might be noted that the estimated overall correction for prequenching of H(2s) and cascade contribution to H(2s) are opposite and of approximately the same magnitude. The variation of these two contributions with energy, affecting the slope of all data, will not necessarily cancel, but should be quite small.

Several corrections have been estimated but not applied to the data. These estimates were made in order to determine the approximate magnitude of the effect which the various error sources might have. The estimated corrections are all small and somewhat tenous, so that actual correction of the data was not carried out.

D. Tabulation of Differential Cross Sections and Charge Transfer Probabilities.

Tables 2 through 12 present the tabulated results of all the measurements discussed in this thesis. The listed individual errors represent standard deviations of at least 5 (usually more) trials of that particular data point and thus represent relative error only. Estimates of overall accuracy are listed with each set of data. These estimates are discussed in the main body of the thesis, where data is presented, with some details discussed in the other appendix sections.

Table 2: PROTONS ON ARGON AT θT = 20 keV·deg.

Energy	Total Differential Scattering, $\frac{d\sigma_{total}}{d\Omega}$	Charge Transfer Probability, P_o
3.5 keV	0.892 x 10^{-15} $\frac{cm^2}{sterradian}$	0.564
4.0	1.333 ±.122	.646
4.5	1.657	.622
5.0	2.06	.600
6.0	2.86 ±.16	.529
7.0	4.15	.454
8.0	5.29	.393
9.0	6.12	.378
10.0	7.23	.387
11.0	8.51	.365
12.0	10.37	.388
13.0	11.03	.415
14.0	17.79 ±.70	.462
15.0	12.85	.476
16.0	13.24	.511
17.0	14.90	.532
18.0	15.62	.555
19.0	16.01	.580
20.0	18.83	.594

Estimated absolute error of $\frac{d\sigma_{total}}{d\Omega}$, ±15%, except near 1° (20keV), ±30%; of P_o, ±5%.

Table 3: PROTONS ON ARGON AT θT = 20 keV·deg.

Energy	Probability of Transfer to 2s, P_{2s}	Differential Cross Section $\frac{d\sigma_{(2s)}}{d\Omega}$
3.0 keV	1.743×10^{-2}	0.105×10^{-16} $\frac{cm^2}{sterradian}$
3.5 keV	1.351	0.119
4.0	1.272 ±.108	0.168 ±.014
4.5	1.345	0.226
5.0	1.446 ±.118	0.298 ±.030
6.0	1.542	0.442
7.0	1.362	0.570
8.0	1.353 ±.091	0.731 ±.061
9.0	1.381	0.870
10.0	1.468	1.051
11.0	1.534	1.248
12.0	1.556 ±.058	1.485 ±.144
13.0	1.585	1.581
14.0	1.694 ±.114	1.860 ±.228
15.0	1.726	2.05
16.0	1.794	2.25
17.0	1.916	2.73
18.0	1.968 ±.076	3.06 ±.31
19.0	1.960	3.20
20.0	1.961	3.48

Estimated Absolute Error ±40%.

Table 4: PROTONS ON ARGON AT 6.25 keV.

Angle	Impact Parameter	Total Differential Scattering, $\frac{d\sigma_{total}}{d\Omega}$	Charge Transfer, P_o
6.0°	0.36 a.u.	$0.382 \times 10^{-15} \frac{cm^2}{sr}$	.480
5.0	0.40	0.769 ±.010	.490
4.5	0.43	1.093	.482
4.0	0.46	1.578	.495
3.5	0.50	2.23	.515
3.0	0.55	3.45	.526
2.7	0.58	4.97 ±.13	.523
2.3	0.65	7.21	.544
2.0	0.70	9.80	.548
1.7	0.76	14.24	.560
1.5	0.81	16.77	.571
1.2	0.92	27.6	.571
1.0	1.01	36.9	.588
0.8	1.17	50.3	.611

Values of impact parameter taken from Dose[10].

Estimated absolute error of $\frac{d\sigma_{total}}{d\Omega}$, ±15%; except near 1°, ±30%.

Estimated absolute error of P_o, ±5%.

Table 5: PROTONS ON ARGON AT 6.25 keV.

Angle	Impact Parameter	Probability of Transfer, P_{2s}	Differential Cross Section, $\frac{d\sigma_{(2s)}}{d\Omega}$
6.0^0	0.36 a.u.	1.444×10^{-2}	$0.0563 \times 10^{-16} \frac{cm^2}{sr}$
5.0	0.40	1.248	0.0968
4.5	0.43	1.263 ±.080	0.1394 ±.0040
4.0	0.46	1.409	0.2236
3.5	0.50	1.491	0.3332
3.0	0.55	1.517	0.5281
2.7	0.58	1.458 ±.060	0.7306 ±.0400
2.3	0.65	1.462	1.064
2.0	0.70	1.437	1.463
1.7	0.76	1.461	2.205
1.5	0.81	1.468 ±.113	2.720 ±.120
1.2	0.92	1.422	4.358
1.0	1.01	1.288	5.288
0.8	1.17	1.213	6.938

Estimated absolute error, ±40%.

Table 6: PROTONS ON ARGON AT 3.0^0.

Energy	Total Differential Scattering, $\frac{d\sigma_{total}}{d\Omega}$	Charge Transfer Probability, P_o
3 keV		.602
4	$4.66 \times 10^{-15} \frac{cm^2}{sterradian}$	.709
5	4.06	.657
6	3.33	.564
6.67	3.11	
7	3.00	.470
8	2.41	.427
9	2.19	.385
10	1.81 ±.10	.375
11	1.45	.391
12	1.31	.403
13	1.21	.436
14	1.02	.472
15	0.971 ±.015	.494
16	0.938	.512
17	0.846	.525
18	0.805	.520
19	0.793	.537
20	0.735	.561

Estimated absolute error of $\frac{d\sigma_{total}}{d\Omega}$, ±15% of P_o, ±5%.

Table 7: PROTONS ON ARGON AT 3.0^0.

Energy	Probability of Transfer, P_{2s}	Differential Cross Section, $\frac{d\sigma_{(2s)}}{d\Omega}$
3 keV	$(1.81 \pm .12) \times 10^{-2}$	0.726×10^{-16} $\frac{cm^2}{sterradian}$
4	1.77×10^{-2}	.827
5	2.04	.820
6	2.03	.682
6.67	1.89	.592
7	1.77	.539
8	1.70	.401
9	1.77	.393
10	1.64 ±.17	.304 ±.032
11	1.74	.254
12	1.76	.232
13	1.87	.228
14	1.88	.198
15	2.08	.204
16	2.02	.185
17	1.92	.174
18	2.27 ±.13	.181 ±.010
19	2.16	.177
20	2.51	.187

Estimated absolute error, ±40%.

Table 8: PROTONS ON HELIUM, TOTAL DIFFERENTIAL SCATTERING CROSS SECTIONS, $\frac{d\sigma_{total}}{d\Omega}$

(in units of 10^{-16} $\frac{cm^2}{sterradian}$)

Energy	θT=5keV·Deg. ρ=0.45a.u.	θT=10 ρ=0.26a.u.	θT=20 ρ=0.14a.u.	θT=30 ρ=0.09a.u.	θT=50 ρ=0.05a.u.
3 keV	24.6	3.99			
3.5	34.8	5.55	0.723		
4	36.6	8.52 ±.95	1.03		
4.5	56.8 ±4.8	11.36	1.35		
5	67.6	13.78	1.36 ±.10		
5.5		15.52	1.85		
6.25		20.0 ±1.0	2.36 ±.18	0.644±.040	
7		23.1	303	0.701	
8		26.9	3.69	0.915	
9		24.4	4.66	1.17	
10		37.1	5.35	1.32	0.223
12			7.13±.15	1.79	0.247
14			9.04	2.80	0.308 ±.083
16			11.14±.93	3.39	0.536
18			13.37	3.07±.25	0.535
20			12.36	4.43	0.645

Estimated absolute error ±15% except near 1 degree ±30%.

Table 9: PROTONS ON HELIUM, CHARGE TRANSFER PROBABILITY, P_o.

Energy	θT=5 keV·Deg.	θT=10	θT=20	θT=30	θT=50
3 keV	.056	.053			
3.5	.028	.031	.040		
4	.023	.026	.019		
4.5	.058	.034	.022		
5	.074	.068	.046		
5.5		.103	.082		
6.25		.144	.130	.119	
7		.165	.160	.150	
8		.152	.153	.148	
9		.115	.128	.119	
10		.106	.175	.086	.097
12			.062	.066	.071
14			.118	.107	.105
16			.203	.185	.178
18			.293	.288	.262
20			.381	.355	.348

Estimated absolute error, ±10%.

Table 10: PROTONS ON HELIUM; CHARGE TRANSFER TO THE 2s STATE, P_{2s}.

Energy	θT=5 keV·Deg.	θT=10	θT=20	θT=30	θT=50
3 keV	$.043 \times 10^{-2}$	$.160 \times 10^{-2}$			
3.5	.121	.095	$.153 \times 10^{-2}$		
4	.155	.113	.202		
4.5	.220±.032	.175	.187		
5	.310	.178±.032	.243		
5.5		.250	.310		
6.25		.340±.051	.521±.071	$.670 \pm .057 \times 10^{-2}$	
7		.532	.644	.517	
8		.599	.608	.588	
9		.554	.403±.050	.425	
10		.485±.022	.355	.334	.444
12			.349	.428	.360
14			.520±.062	.424	.463
16			.605	.635	.623
18			.627±.079	.630±.044	.692
20			.607	.551	.701

Estimated absolute error, ±40%.

Table 11: PROTONS ON HELIUM, DIFFERENTIAL CROSS SECTIONS FOR TRANSFER TO 2s STATE, $\frac{d\sigma(2s)}{d\Omega}$ (in units of 10^{-18} $\frac{cm^2}{sterradian}$)

Energy	θT=5 keV·Deg.	θT=10	θT=20	θT=30	θT=50
3 keV	1.06	0.638			
3.5	4.21	0.527	0.111		
4	5.67	0.963	0.208		
4.5	12.50	1.99	0.252		
5	20.96	2.45	0.330		
5.5		3.88	0.574		
6.25		6.80	1.23	0.431	
7		12.29	1.95	0.362	
8		16.11	2.24	0.538	
9		19.06	1.88	0.497	
10		17.99	1.90	0.440	.099
12			2.49	0.766	.089
14			4.70	1.19	.143
16			6.74	2.15	.334
18			8.38	1.93	.370
20			7.50	2.44	.452

Estimated absolute error, ±40 - 50%.

Table 12: PROTONS ON HELIUM AT 6.25 keV.

Angle	Impact Parameter	Charge Transfer, P_o	Total Differential Scattering, $\frac{d\sigma_{total}}{d\Omega}$
1.0^0	.095 a.u.	.169	$(71.4\pm7.0)\times10^{-16}$ $\frac{cm^2}{sr}$
1.3	.110	.147	35.3
1.6	.140	.143	20.0
2.0	.170	.144	11.1
2.5	.110	.131	5.44
3.2	.260	.130	2.36±.18
4.0	.300	.130	1.19
4.8	.375	.119	.644±.042

	Charge Transfer, P_{2s}	Differential Cross Section $\frac{d\sigma_{(2s)}}{d\Omega}$
1.0^0	$.515\pm.085\times10^{-2}$	36.8×10^{-18} $\frac{cm^2}{sr}$
1.3	$.523\times10^{-2}$	18.4
1.6	.532	10.6
2.0	.494	5.48
2.5	.520	2.82
3.2	.525±.071	1.24
4.0	.514	.612
4.8	.670±.050	.431

Estimated absolute errors: P_o, ±10%; $\frac{d\sigma_{total}}{d\Omega}$, ±15% except near 1 degree ±30%; P_{2s}, ±40%; $\frac{d\sigma_{(2s)}}{d\Omega}$ ± 40 - 50%.

BIBLIOGRAPHY

1. N. Bohr, Kgl. Danske Videnskab Selskab, Mat-fys. Medd., 18, 8 (1948).

2. H. A. Bethe, Intermediate Quantum Mechanics, (W. A. Benjamin, Inc., New York and Amsterdam, 1964) p.63.

3. J. Lindhard, Vibeke Nielsen, and M. Scharff, Kgl. Danske Videnskab Selskab, Mat-fys. Medd. 36, 10 (1968).

4. O. B. Firsov, Sov. Phys. JETP, 6, 534 (1958).

5. N. F. Mott and H. S. W. Massey, The Theory of Atomic Scattering, (Oxford University Press, London, 1965), Third edition, Chapt. V, Secs. 5 and 6.

6. E. Everhart , G. Stone, and R. J. Carbone, Phys. Rev., 99, 1287 (1955).

7. F. W. Bingham, J. Chem. Phys., 46, 2003 (1967).

8. F. T. Smith, Abstracts of Papers of V. International Conference on the Physics of Electronic and Atomic Collisions, (Publishing House Nauka, Leningrad, 1964) p. 181.; also, F. T. Smith, R. P. Marchi, and O. Heinz, Phys. Rev., 161, 31 (1967).

9. L. D. Landau and E. M. Lifshitz, Mechanics, (Addison-Wesley Publishing Company Inc., 1960), Chap. IV.

10. V. Dose, Helv. Phys. Acta, 41, 261 (1968).

11. W. S. Wilson and R. B. Lindsay, Phys. Rev., 47, 681 (1935); also H. A. Bethe and E. E. Salpeter, Quantum Mechanics of One and Two Electron Atoms (Springer-Verlag, Berlin 1957) p. 145.

12. D. R. Bates and R. McCarroll, Advances in Physics, supplement of Phil. Mag., 11, 39 (1962).

13. B. H. Bransden, Advances in Atomic and Molecular Physics, Vol. I, (Academic Press, 1965), Chapt. 3.

14. D. R. Bates, Atomic and Molecular Processes, D. R. Bates, Editor (Academic Press, New York and London, 1962), Chapt. 14.

15. N. F. Mott and H. S. W. Massey, The Theory of Atomic Scattering (Oxford University Press, London, 1965), third edition, Chapt. XV sec. 2 and Chapt. XIX sec. 5.

16. M. R. C. McDowell, Lectures on Ion-Atom Collisions, (National Bureau of Standards, Technical Note 185 1963).

17. R. A. Mapleton, Phys. Rev., 122, 528 (1961); and ibid, 130, 1839, (1963).

18. L. Wilets and D. F. Gallaher, Phys. Rev., 147, 13 (1966).

19. S. E. Lovell and M. B. McElroy, Proc. Roy. Soc. (London), A283, 100 (1965).

20. G. W. McLure, Phys. Rev., 148, 47 (1966).

21. James E. Bayfield, Phys. Rev. Letters, 20, 1223, (1968).

22. L. Colli, F. Christofori, G. E. Frigerio, and P. G. Sona, Phys. Letters, 3, 62 (1962).

23. R. F. Stebbings, R. A. Young, C. L. Oxley, and H. Ehrhardt, Phys. Rev., 138, A1312 (1965).

24. G. J. Lockwood and E. Everhart, Phys. Rev., 125, 567 (1962); G. J. Lockwood, H. F. Helbig and E. Everhart, ibid, 132, 2078 (1963); H. F. Helbig and E. Everhart, ibid, 136, A674 (1964); H. F. Helbig and E. Everhart, ibid, 140, A715 (1965).

25. I. M. Cheshire, J. Phys. B (Proc. Phys. Soc.) 1, 428 (1968).

26. T. A. Green, H. E. Stanley, and You-Chien Chiang, Helv. Phys. Acta, 38, 109 (1965).

27. T. A. Green, Phys. Rev., 152, 18 (1966).

28. S. K. Allison and M. Garcia-Monoz, Atomic and Molecular Processes, D. R. Bates, Editor (Academic Press, New York and London, 1962) p. 753.
(The results recorded here are compiled from work by Hasted (1952), Stedeford (1955), and Stier and Barnett (1956)).

29. Helbig and Everhart, Phys. Rev., 136, 141 (1964); also Keever and Everhart, Phys. Rev. A, 1, 1083 (1970).

30. I. A. Poluektov and L. P. Presnyakov, Abstracts of Papers of V International Conference on the Physics of Electronic and Atomic Collisions, (Publishing House Nauka, Leningrad, 1967), p. 71.

31. D. Jaecks, B. Van Zyl, and R. Geballe, Phys. Rev., 137, A340 (1965).

32. D. Pretzer, B. Van Zyl and R. Geballe, Proceedings of III International Conference on the Physics of Electronic and Atomic Collisions (North-Holland Publishing Company, Amsterdam, 1964), p. 618.

33. E. P. Andreev, V. A. Ankudinov, and S. V. Bobashev, JETP, translation 23, 375 (1966).

34. L. T. Sin Fai Lam, Proc. Phys. Soc., 92, 67 (1967).

35. T. Dean Gaily, Phys. Rev., 178, 207 (1969).

36. W. Heizenberg, Z. Physik, 39, 499 (1926).

37. L. Pauling, Chem. Rev., 5, 173 (1928); also L. Pauling and E. B. Wilson, Introduction to Quantum Mechanics, (McGraw-Hill Book Company, Inc., New York and London, 1935) pp. 314-331.

38. B. N. Finkelstein and G. E. Horowitz, Z. Physik, 48, 118 (1928).

39. N. F. Mott, Proc. Cambridge Phil. Soc., 27, 523 (1931).

40. D. R. Bates, H. S. W. Massey, and A. L. Stewart, Proc. Roy Soc. (London), A216, 437 (1953).

41. Francis J. Smith, Proc. Phys. Soc., 84, 889 (1964).

42. G. J. Lockwood and E. Everhart, Phys. Rev., 125, 567 (1962).

43. W. Lichten, Phys. Rev., 131, 229 (1963).

44. W. Lichten, Phys. Rev., 139, A27 (1965).

45. H. H. Michels, J. Chem. Phys., 44, 3834 (1966).

46. Manfred Von Ardenne, Tabellen der Electrone physik Ionphysic and Ubermikroskopie (Deutscher Verlag der Wissenshaften, Berlin, 1956).

47. Lawrence, Beauchamp, and McKibben, NIM, 32, 357 (1965).

48. Moak, Banta, Thurston, Johnson, and King, Rev. Sci. Inst., 30, 694 (1959).

49. E. B. Jordan and R. B. Brode, Phys. Rev., 43, 112 (1933).

50. R. H. McKnight, Ph.D. Thesis, University of Nebraska (unpublished, 1970). Appendix

51. W. Gaede, Annalen der Physik, 46, 357 (1915).

52. H. Ishi and K. Nakayama, Trans. 8 Nat. Vac. Symp., (Permagon Press, London, 1961) p. 519.

53. A. E. deVries and P. I. Rol, Vacuum, 15, 135 (1965).

54. P. Carr, Vacuum, 14, 37 (1964).

55. Alan Edwards and M. E. Rudd, Autoionizing Levels Of Neon Produced by H^+, He^+ and Ne^+ Beam, Ph.D. Thesis, University of Nebraska (unpublished, 1967) p. 15.

56. R. D. Present, Kinetic Theory of Gases, (McGraw-Hill Book Company, Inc., New York and London, 1958) p. 21.

57. L. H. Toburen, M. Y. Nakai, R. A. Langley, The Measurement of High Energy Charge Transfer Cross Sections for Incident Protons and Atomic Hydrogen in Various Gases., Ph.D. Thesis of Toburen, (Oak Ridge National Laboratory Report ORNL-TM-1988, 1967) p. 215.

58. V. Dose, Helv. Physica Acta, 39, 683 (1966).

59. G. Ryding, A. B. Wittkower, and H. G. Gilbody, Proc. Phys. Soc. (London), 89, 547 (1966).

60. J. E. Bayfield, Phys. Rev., 182, 115 (1969).

61. D. H. Jaecks, R. H. McKnight, D. H. Crandall, Abstracts of VI International Conference on Physics of Electronic and Atomic Collisions (The M.I.T. Press, Cambridge, Mass., 1969) p. 862.

62. R. H. McKnight, D. H. Crandall, D. H. Jaecks, Rev. Sci. Inst., (to be published about Sept. 1970); also Bulletin of APS, Jan. 1970, EI-12, p. 74.

63. F. Christofori, P. Fenici, G. E. Frigerio, N. Molho and P. G. Sona, Physics Letters, 6, 171 (1963).

64. J. R. Sheridan, Rev. Sci. Inst., 40, 358 (1969).

65. F. P. Ziemba, G. J. Lockwood, G. H. Morgan, and E. Everhart, Phys. Rev., 118, 1552 (1960).

66. B. L. Schram, A. J. H. Boerboom, W. Kleine, and J. Kistemaker, Physica, 32, 749 (1965).

67. E. N. Fuls, P. R. Jones, F. P. Ziemba, and E. Everhart, Phys. Rev., 107, 704 (1957).

68. G. O. Taylor, Jr., D. W. Martin, and E. W. Thomas, Scattering of He^+ Ions by Noble Gases at High Energies, (Thesis of Taylor) Technical Report to U. S. Atomic Energy Commission, Oak Ridge, Tenn. (USAEC Document Number ORO-2591-42, 1970).

69. W. Aberth,and D. C. Lorents, Phys. Rev., 139, A1017 (1965); ibid, Phys. Rev. 144, 109 (1966); ibid Phys. Rev., 182, 162 (1969); also D. Coffey, D. C. Lorents, and F. T. Smith, Phys. Rev., 187, 201 (1969).

70. G. D. Magnuson, J. W. Boring, C. E. Carlston, Abstracts of VI International Conference on Physics of Electronic and Atomic Collisions, (The M.I.T. Press, Cambridge, Mass., 1969), p. 524.

71. M. Barat and J. C. Houver, Comptes Rendus, 264B, 38 (1967).

72. C. E. Moore, Atomic Energy Levels, Vol. 1, (U.S. Government Printing Office, Bureau of Standards Circular 467, Washington D.C., 1949).

73. V. Dose and V. Meyer, Physics Letters, 23, 69 (1966).

74. H. A. Bethe and E. E. Salpeter, Quantum Mechanics of One and Two Electron Atoms (Academic Press Inc., New York, 1957), Sec. 51, 55 and 67.

75. I. A. Sellin, Phys. Rev., 136, A1245 (1964).

76. W. R. Smythe, Static and Dynamic Electricity, 2nd edition, (McGraw-Hill Book Company, Inc., New York and London, 1950), p. 91.

77. W. L. Fite, W. E. Kauppila, and W. R. Ott, Physical Review Letters, 20, 409 (1968); also W. R. Ott, W. E. Kauppila, and W. L. Fite, Phys. Rev. A, 1, 1089 (1970).

78. J. Casalese and E. Gerjuoy, Phys. Rev., 180, 327 (1969).

79. G. Lüders, Z. Naturforshg., 5a, 608 (1950).

80. L. I. Schiff, Quantum Mechanics, 3rd edition, (McGraw-Hill Book Company, New York, 1968), p. 155.

81. M. Abramowitz and I. A. Stegun, Handbook of Mathematical Functions, (Dover Publications, New York, 1965 or National Bureau of Standards, 1964) p. 1006.

82. A. R. Edmonds, Angular Momentum in Quantum Mechanics, (Princeton University Press, Princeton, 1960), p. 75-76.

83. System 360 Scientific Subroutine Package (360 A-CM-03X), Version II Programmers Manual (published by IBM).

84. J. A. Smit, Physica, 2, 104 (1935).

85. R. H. Hughes, C. A. Stigers, B. M. Coughty, and E. D. Stokes, Phys. Rev. A, 1, 1424 (1970).

VIII. ACKNOWLEDGEMENTS.

I wish to express my gratitude to several individuals and agencies for support during this project.

Dr. Duane H. Jaecks suggested the problem and provided encouragement and creative ideas throughout the investigation period. His ability to visualize problems and translate ideas into experimental arrangement have been an inspiration encouraging original thinking.

The apparatus, including accelerator, scattering chamber, and support equipment have been shared throughout the project with another student, Mr. Ronald H. McKnight. Because of his patience and abilities we have enjoyed fruitful cooperation while working on similar projects. Nearly all of our technical problems were pursued mutually so that his contributions were essential to the success of this project.

Dr. J. Macek has contributed valuable ideas and discussion on all aspects of the significance of the experiment. I wish to express particular gratitude for his suggestion of the technique for calculating the polarization of quench induced radiation and his guidance through this calculation.

Ideas and useful discussion have been provided by nearly all members of the University of Nebraska atomic collisions research group.

Technical assistance has been provided by [illegible] individuals. Mr. Don Fuehring was responsible for construction of the scattering chamber and related hardware. Mr. Peter Martin assisted with electronics problems. Mr. Bob Dubois helped with servicing of equipment and preparation of drawings.

Special thanks are extended to the National Science Foundation [illegible] which made this project possible [illegible] Research Council and the National [illegible] nistration for personal support, including [illegible] ellowship which has provided support [illegible] ure of the project.